

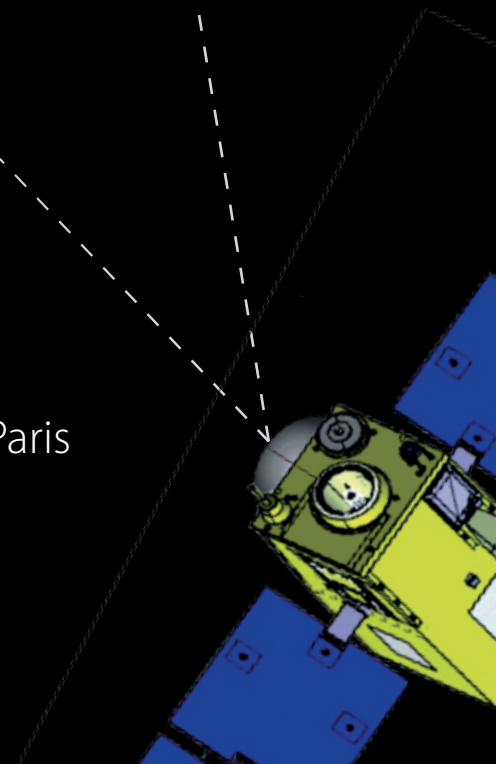
FARSIDE

A mission to the farside of the Moon



Mark Wieczorek Institut de Physique du Globe de Paris
Lead proposer

A proposal in response to the call for a medium-sized mission opportunity in ESA's science programme for a launch in 2025 (M4)



PROPOSING TEAM

Mark Wieczorek (lead proposer)

Institut de Physique du Globe de Paris

35 rue Hélène Brion, Case 7071, 75205 Paris Cedex 13, France

wieczor@ipgp.fr, +33 1 57 27 53 08

David Mimoun (technical lead)

Institut Supérieur de l'Aéronautique et de l'Espace, France

David Baratoux

University of Toulouse, France

Sylvain Bouley

Université Paris Sud, France

Baptiste Cecconi

LESIA, Observatoire de Paris, France

Gareth Collins

Imperial College London, London, United Kingdom

Anthony Cook

Aberystwyth University, United Kingdom

Ian Crawford

Birkbeck College London, United Kingdom

Véronique Dehant

Royal Observatory of Belgium, Belgium

Heino Falcke

Radbound Universiteit Nijmegen, The Netherlands

Raphaël Garcia

Institut Supérieur de l'Aéronautique et de l'Espace, France

Domenico Giardini

ETH Zürich, Switzerland

Robert Grimm

Southwest Research Institute, United States

Matthias Grott

German Aerospace Center, Germany

Jerzy Grygorczuk

Space Research Center, Polish Academy of Sciences, Poland

Leonid Gurtvis

Joint Institute for VLBI in Europe, Delft University of Technology, The Netherlands

Boris Ivanov

Russian Academy of Sciences, Russia

Ralf Jaumann

German Aerospace Center, Germany

Jean-Luc Josset

Space Exploration Institute, Switzerland

Marc Klein-Wolt

Radboud University Nijmegen, The Netherlands

Gunther Kletetschka

Charles University, Czech Republic

Leon Koopmans

Kapteyn Astronomical Institute, University of Groningen, The Netherlands

Benoît Langlais

University of Nantes, France

David Lawrence

Johns Hopkins University, Applied Physics Laboratory, United States

Philippe Lognonné

Institut de Physique du Globe de Paris, France

Anastasios Margonis

German Aerospace Center, Germany

Pierre-Yves Meslin

Institut de Recherche en Astrophysique et Planétologie, France

Clive Neal

University of Notre Dame, United States

Jürgen Oberst

German Aerospace Center, Germany

Pavel Ripka

Czech Technical University in Prague, Czech Republic

Nicole Schmitz

German Aerospace Center, Germany

Tilman Spohn

German Aerospace Center, Germany

Stephanie Werner

University of Oslo, Norway

Philippe Zarka

Observatoire de Paris-CNRS, France

This proposal is supported by *Airbus Defense and Space*.

FARSIDE

A mission to the farside of the Moon

SCIENCE

FARSIDE is a mission to the farside of the Moon that consists of a lander and an instrumented relay satellite. The lander will make pioneering radio astronomy, geophysical, and geochemical measurements from the interior of the 2000-km diameter South Pole-Aitken basin. From a relay satellite at the Earth-Moon L2 Lagrange point, the surface will be monitored for impact-generated light flashes, and synergistic radio and magnetic measurements will be obtained.

Why the farside of the Moon?

The farside hemisphere of the Moon is a unique scientific platform. The farside is shielded from terrestrial radio-frequency interference and has a very thin ionosphere.

The farside records the primary differentiation of the Moon and hosts the largest recognized impact basin in the Solar System. The farside surface is unpolluted by contaminating Earthshine.

Science objectives

Make the first radio-astronomy measurements from the most radio-quiet region of near-Earth space.

By combining simultaneous measurements from the lander and relay satellite, FARSIDE will perform the first sky mapping at low frequencies and make pathfinder measurements of the red-shifted neutral hydrogen line that originates from before the formation of the first stars in our Universe.

Determine the internal structure and thermal evolution of the Moon.

Using impact events with known coordinates and times with previously localized deep moonquake sources, the core size and state, mantle structure, and crustal thickness will be determined. Heat flow and magnetic sounding data will determine the temperature profile of the Moon, and radon monitoring will inform exosphere processes.

Quantify impact hazards in near-Earth space by the measurement of impact flashes.

By the detection of light flashes generated by impact events, the impact flux and size-frequency distribution of small near-Earth objects will be determined. Impact flashes will provide localized seismic sources, allowing seismic investigations with only a single station.

PAYOUT

Lander payload

Radio astronomy receiver - Dedicated low-frequency measurements from 16 kHz to 40 MHz.

Seismometer - Internal structure of the Moon from a modern broad-band seismometer.

Heat flow probe - Thermal evolution of the Moon from subsurface temperature measurements.

Electromagnetic sounder - Internal structure and thermal state of the Moon from electromagnetic impedances.

Gamma-ray spectrometer - Absolute elemental abundances for studies of the South Pole-Aitken basin.

Surface camera - Surface monitoring, regolith micro-structure, and safe deployment of instruments on the surface.

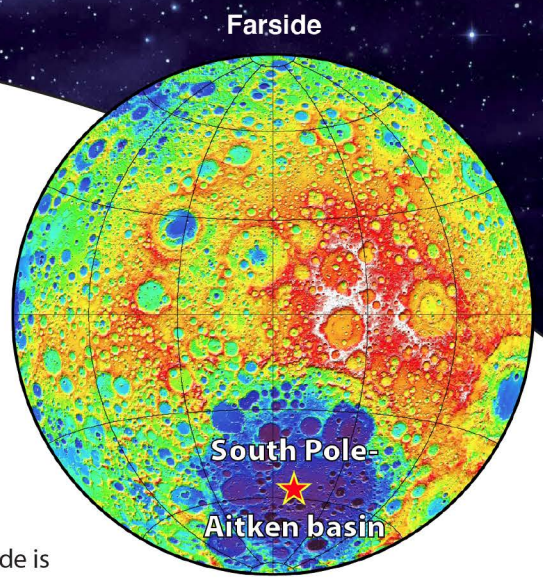
Radon monitor - Monitoring of outgassing events and ground truth for orbital measurements.

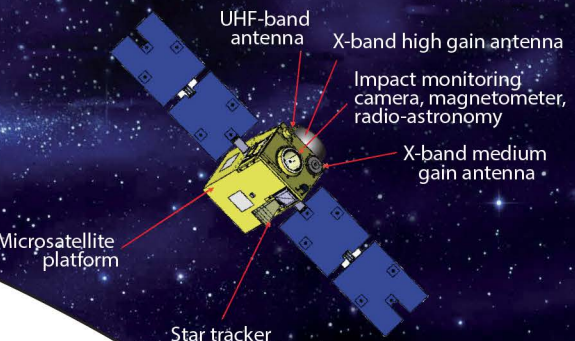
Satellite payload

Impact flash monitoring camera - Earth-Moon impact flux from visible and near-infrared measurements.

Radio astronomy receiver - Interferometric measurements when combined with surface observations.

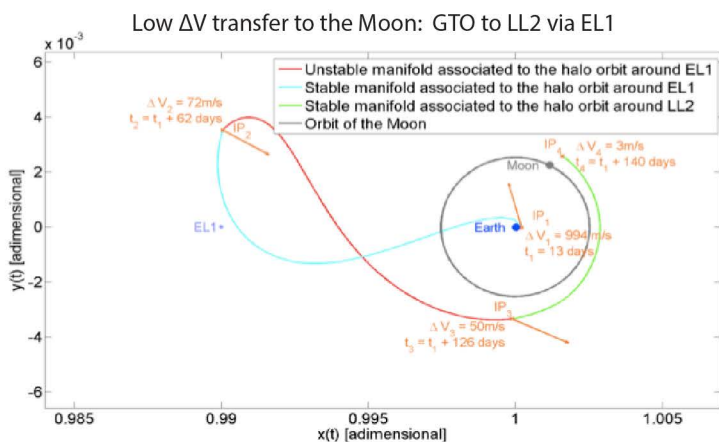
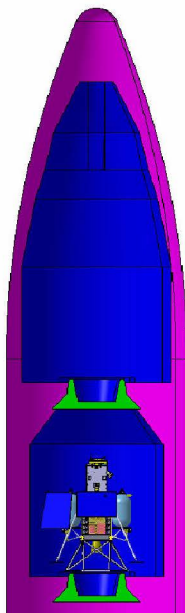
Magnetometer - Internal structure and thermal state of the Moon from electromagnetic induction.





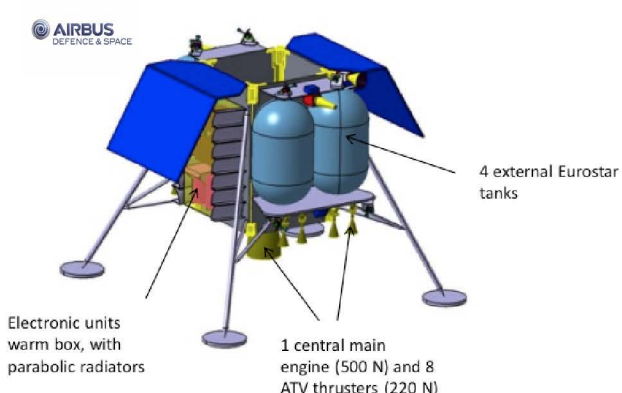
MISSION OVERVIEW

FAR SIDE will use a mass-efficient weak-stability boundary trajectory to reach the Moon. Following launch into a geosynchronous transfer orbit, the spacecraft will be inserted into a four-month ballistic trajectory that goes to the Earth-Moon L2 Lagrange point by way of the Earth-Sun L1 Lagrange point. Using a waiting GTO, the mission is compatible with launch by either a Soyuz-Fregat or a shared commercial Ariane 5.



At lunar arrival, the lander and relay satellite will both be placed into a 2:1 resonant 14-day halo orbit about the LL2 Lagrange point. This orbit enables the detection of farside impact flashes, and makes possible synergistic radio astronomy and magnetic field measurements with the lander. The lander will descend to the lunar surface at dawn, providing two weeks to deploy instruments on the surface.

FLIGHT SYSTEM



The dry mass of the lander is 700 kg, which allows for a 44 kg scientific payload. 50 Watts of power are generated by solar panels during the day, allowing full operation of all instruments. During the 14 day night, 5 W are provided by batteries, allowing core instruments to be operate in a reduced power mode.

With a dry mass of 350 kg, a Myriade Evolution-class satellite will accomodate a 20-kg scientific payload. From the LL2 halo orbit, it will provide continuous visibility of both the lander and Earth.

FAR SIDE STRENGTHS

Estimated cost of 429 M€ • Addresses directly all four Cosmic Vision science objectives • Targets jointly astronomy and planetary science questions • Innovative science with a leading European role • High TRL for all potential instruments • Low risk mission • Compatible with a launch in 2025

CONTENTS

EXECUTIVE SUMMARY.....	2
1 INTRODUCTION	5
2 SCIENCE OBJECTIVES	7
2.1 RADIO ASTRONOMY.....	9
2.2 LUNAR SCIENCE.....	12
2.3 EARTH-MOON IMPACT HAZARDS	16
2.4 SYNERGIES WITH OTHER MISSIONS	20
3 SCIENCE REQUIREMENTS.....	21
3.1 RADIO ASTRONOMY SCIENCE REQUIREMENTS	21
3.2 SEISMOLOGY SCIENCE REQUIREMENTS.....	21
3.3 HEAT FLOW SCIENCE REQUIREMENTS	22
3.4 ELECTROMAGNETIC SOUNDING SCIENCE REQUIREMENTS	22
3.5 SURFACE CHEMISTRY SCIENCE REQUIREMENTS	23
3.6 RADON SCIENCE REQUIREMENTS.....	23
3.7 IMPACT MONITORING SCIENCE REQUIREMENTS.....	23
4 MODEL PAYLOAD	24
4.1 RADIO ASTRONOMY RECEIVER (RAR)	25
4.2 SEISMOMETER (SEIS)	26
4.3 HEAT FLOW AND PHYSICAL PROPERTIES PACKAGE (HF ³)	28
4.4 SURFACE AND ORBITAL MAGNETOMETERS (MAG).....	30
4.5 SURFACE ELECTROMAGNETIC SOUNDER (EMS)	31
4.6 CONTEXT CAMERA (COCAM)	32
4.7 GAMMA-RAY SPECTROMETER (GRS).....	33
4.8 RADON AND POLONIUM DETECTOR (DORN).....	34
4.9 IMPACT MONITORING CAMERA (SPOSH)	35
4.10 FAR SIDE ACQUISITION AND CONTROL ELECTRONICS (FACE)	36
5 MISSION CONFIGURATION AND PROFILE.....	37
5.1 MISSION PHASES	38
5.2 OPERATIONAL HALO ORBIT	39
5.3 DESCENT AND LANDING	40
5.4 COMMUNICATIONS	40
5.5 MISSION OPERATIONS	41
6 SPACECRAFT DESIGN	42
6.1 LANDER SPACECRAFT	42
6.2 RELAY SATELLITE	45
6.3 LAUNCH COMPOSITE CONFIGURATION	48
7 MANAGEMENT	49
7.1 OVERALL MISSION MANAGEMENT STRUCTURE.....	49
7.2 PROPOSED PROCUREMENT APPROACH	49
7.3 GROUND SEGMENT AND OPERATIONS	49
7.4 DATA ARCHIVING	50
7.5 RELATION TO ESA'S DIRECTORATE OF HUMAN SPACEFLIGHT AND OPERATIONS	50
8 MISSION COST AND PROGRAMMATICS	50
8.1 MISSION COST ANALYSIS	50
8.2 TECHNOLOGY DEVELOPMENT REQUIREMENTS	50
8.3 MISSION SCHEDULE AND RISK ANALYSIS.....	51
A REFERENCES	52
B SCIENCE MEMBERS BY COUNTRY	56
C LETTERS OF COMMITMENT.....	59



Figure 1. The farside of the Moon with Earth in the background. This image was taken by the Chinese Chang'e-5 T1 spacecraft on October 28, 2014. The dark region at the center of the illuminated lunar hemisphere is Mare Moscovense.

1. INTRODUCTION

The farside hemisphere of the Moon (Figure 1) is a unique platform in the Solar System for a large range of scientific investigations, from cosmic to planetary evolution. Being shielded from terrestrial radio-frequency interference, the farside of the Moon is the most radio-quiet environment in near-Earth space. The farside hemisphere faithfully records the primary differentiation of the Moon and hosts the largest recognized impact basin in the Solar System. Uncontaminated by Earthshine, the farside hemisphere of the Moon is ideal for the continuous monitoring of meteoroid impacts with the lunar surface from the Earth–Moon L2 Lagrange point.

The mission FARSIDE aims to place a robotic lander on the farside hemisphere of the Moon and to put an instrumented relay satellite into a halo orbit about the Earth–Moon L2 Lagrange point. The landing will take place in the center of the oldest and largest unequivocal impact basin in the Solar System, the 2000-km diameter South Pole-Aitken basin. During the course of its 4-year nominal mission, FARSIDE will conduct three broad scientific investigations.

First, from the vantage point of the lunar surface, FARSIDE will make the first extensive radio astronomy measurements in the most radio-quiet region of near-Earth space. Combining radio measurements from the lander and the relay satellite, it will perform the first sky mapping at low frequencies and make pathfinder measurements of the red-shifted neutral hydrogen line that originates from before the formation of the first stars in our Universe. A number of other low-frequency radio phenomena will be studied, such as low-frequency radio bursts from our Sun, auroral emissions from the giant planets, pulsars, and the interaction of ultra-high energy cosmic rays and neutrinos with the Moon. The FARSIDE radio astronomy experiment will be a pathfinder technology demonstration for a future radio array on the farside of the Moon.

Second, from the same lander, FARSIDE will make geophysical measurements of the Moon's interior and measure the composition of its surface, while focusing these investigations on the

structure of a giant impact basin. From seismological, heat flow, and electromagnetic sounding measurements, these data will determine the bulk composition of the Moon, the thickness of its crust, the size and composition of its core, and the temperature profile of its interior. The surface geochemical data will provide critical ground-truth measurements for the interpretation of orbital remote-sensing data sets, and will clarify the formation and evolution of the giant South Pole-Aitken impact basin. Measurements of radon and polonium would detect lunar outgassing events and constrain the dynamics of the lunar exosphere.

Third, from the vantage point of the relay satellite, FARSIDE will quantify near-Earth impact hazards by continuously monitoring the farside of the Moon for meteoroid impacts. Unspoiled by Earthshine and an intervening atmosphere, this experiment would measure by the detection of impact flashes during the lunar night the lunar impact flux, the size-frequency distribution of impactors in near-Earth space, and spatial and temporal variations in the lunar impact rate. The measured impact times and locations will be used as known seismic sources for the seismology experiment, allowing for interior modeling of the Moon from just a single seismic station.

FARSIDE is an innovative mission that involves the development of European soft-landing capabilities on airless bodies that benefits from existing state-of-the-art, mature, geophysical and astronomical instrumentation in Europe. The scientific objectives of FARSIDE are supported jointly by the radio astronomy and lunar science communities, address directly all four of the top-level themes of ESA's Cosmic Vision program (Figure 2, Bigami et al. 2005), and are identified as top priorities in the United States planetary science decadal survey (Committee on the planetary science decadal survey, 2010). No other space agency is considering a mission to the farside of the Moon, and FARSIDE would show European leadership in the renewed international exploration of Earth's nearest celestial neighbor.

Theme	FARSIDE Relevance to CV theme	Measurement Objective	Instrument
<i>What are the conditions for planet formation and the emergence of life?</i>	1.1 From gas and dust to stars and planets FARSIDE will investigate the late stages of planetary formation, including the event that formed the Earth-Moon system and the impact that formed the South Pole-Aitken basin.	Bulk composition of the Moon, crustal thickness, core size, internal structure	Seismometer, heat flow probe, electromagnetic sounder, orbiting magnetometer, surface camera
	1.3 Life and habitability in the Solar System FARSIDE will quantify impact hazards in near-Earth space, elucidate the consequences of giant impact events that could have frustrated the development of life, and constrain the manner by which single-plate planets lose their heat.	Size-frequency distribution and flux of near-Earth objects, crustal thickness within the South Pole-Aitken basin, heat flow	Impact flash camera, seismometer, heat flow probe, radon detector, electromagnetic sounder
<i>How does the Solar System work?</i>	2.1 From the Sun to the edge of the Solar System FARSIDE will measure low-frequency radio emissions from the Sun, uncontaminated by terrestrial radio-frequency interference.	Low-frequency radio monitoring of the Sun	Radio astronomy receiver
	FARSIDE will quantify how the solar wind interacts with atmosphereless bodies.	Electromagnetic measurements from the surface and orbit	Electromagnetic sounder, orbiting magnetometer
	FARSIDE will investigate how planets differentiate into a crust, mantle and core, and how tectonic processes work on single-plate planets.	Internal structure of the Moon, surface heat flow	Seismometer, heat flow probe, electromagnetic sounder, orbiting magnetometer
	2.2 The giant planets and their environments FARSIDE will measure the magnetospheric emissions of the giant planets, their time variations, and the coupling with their satellites.	Low-frequency radio monitoring of the outer planets, uncontaminated by solar and terrestrial emissions	Radio astronomy receiver
	2.3 Asteroids and other small bodies FARSIDE will constrain the flux, size-frequency distribution and physical properties of small near-Earth objects.	Monitoring of visual and infrared impact flashes	Impact flash camera, seismometer
<i>What are the fundamental laws of the Universe?</i>	3.3 Matter under extreme conditions FARSIDE will detect interactions between ultra high energy cosmic rays and the lunar surface.	Low-frequency radio measurements	Radio astronomy receiver
<i>How did the Universe originate and what is it made of?</i>	4.1 The early Universe FARSIDE will investigate the cosmological dark ages through the red-shifted neutral hydrogen 21-cm line.	Low-frequency radio measurements uncontaminated by solar and terrestrial emissions	Radio astronomy receiver

Figure 2. Scientific relevance of the FARSIDE mission to Cosmic Vision science objectives.

2. SCIENCE OBJECTIVES

The science objectives of the FARSIDE mission are conceived to exploit the unique environment offered by the farside hemisphere of the Moon and to address directly all four of the top-level themes of ESA's Cosmic Vision program. The farside of the Moon is the most radio-quiet region in near-Earth space, it has kept a record of the original differentiation of the Moon, it hosts the oldest and largest unequivocal impact basin in the Solar System, and it is not contaminated by sunlight reflected off the Earth.

The farside of the Moon is a unique environment for low-frequency radio measurements. On Earth, several sources of radio-frequency interference exist, such as aurorae, radio broadcasts and lightning. Furthermore, extra-terrestrial signals with frequencies below 10-20 MHz cannot be studied since they are reflected off, or are severely distorted by, the Earth's ionosphere. The farside of the Moon does not suffer from either of these problems and is the ideal place to investigate one of the last unexplored regions of the electromagnetic spectrum (Figure 3, Jester and Falcke 2009, Klein-Wolt et al. 2012).

From the vantage point of the lunar farside, a single dual-polarized antenna would make extraordinary measurements: the red-shifted neutral hydrogen (HI) line that originates from before the formation of the first stars would be investigated, low-frequency radio bursts from the giant planets of our Solar System would be monitored, and the interaction of the Moon's surface with ultra-high energy cosmic rays and neutrinos that exceed the energies of modern particle accelerators would be detected. Finally, given the broad interest in the creation of a low-frequency aperture synthesis radio array on the Moon's surface, pioneering low-frequency interferometric radio measurements between the lander and the relay satellite would demonstrate the feasibility of such a future large-scale project.

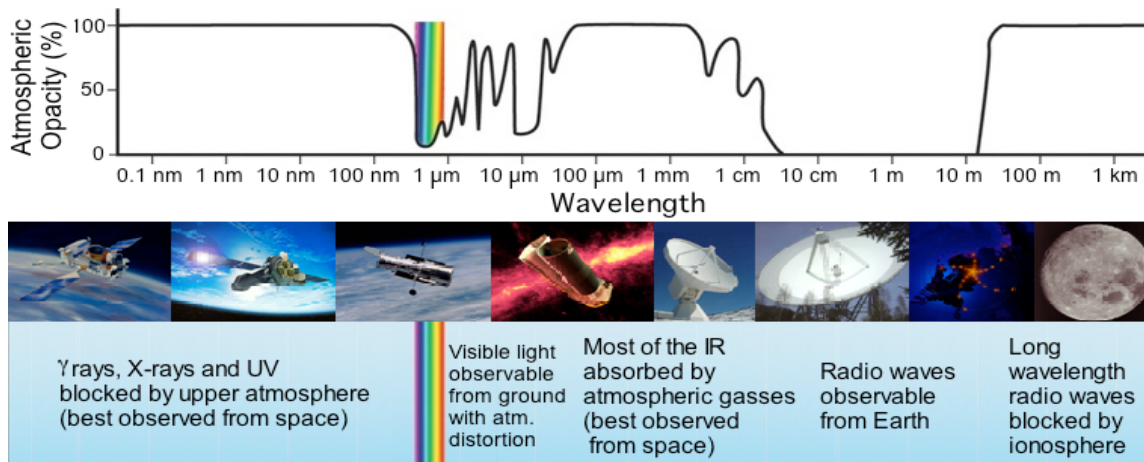


Figure 3. Atmospheric and ionospheric effects allow only a small portion of the electromagnetic spectrum to be investigated from the surface of the Earth.

The farside of the Moon is a unique laboratory for investigating planetary formation and evolution. The Earth-Moon system is thought to have formed by a giant impact between the nascent Earth and a Mars-sized object. This event led to the formation of globe-encircling magma oceans on both bodies and contributed to their primary differentiation and core formation. In contrast to Earth, the interior structure and composition of the Moon have evolved little since this time. Both Earth and the Moon suffered subsequently the consequences of large impact events, but this important period of time has been almost totally erased from the Earth's surface, whereas it is ideally preserved on the Moon. The Moon is an end-member of terrestrial planetary evolution and is the nearest celestial object to have preserved the record of early planetary processes.

Though the geophysical investigations of the Apollo era provided tantalizing clues to lunar formation, differentiation, and evolution, in retrospect, the Apollo nearside landing sites were not ideal for this purpose. As shown in Figure 4, it is now recognized that these measurements are biased by their proximity to an atypical geological province called the Procellarum KREEP Terrane (Jolliff

et al. 2000). The most prominent terrane that records the formation of the primordial crust is located largely on the farside hemisphere, as is the largest and oldest recognized impact basin in our Solar System, the South Pole-Aitken basin. FARSIDE will investigate the relics of planetary differentiation that are recorded beneath its surface by making the first geophysical measurements on the farside hemisphere of the Moon.

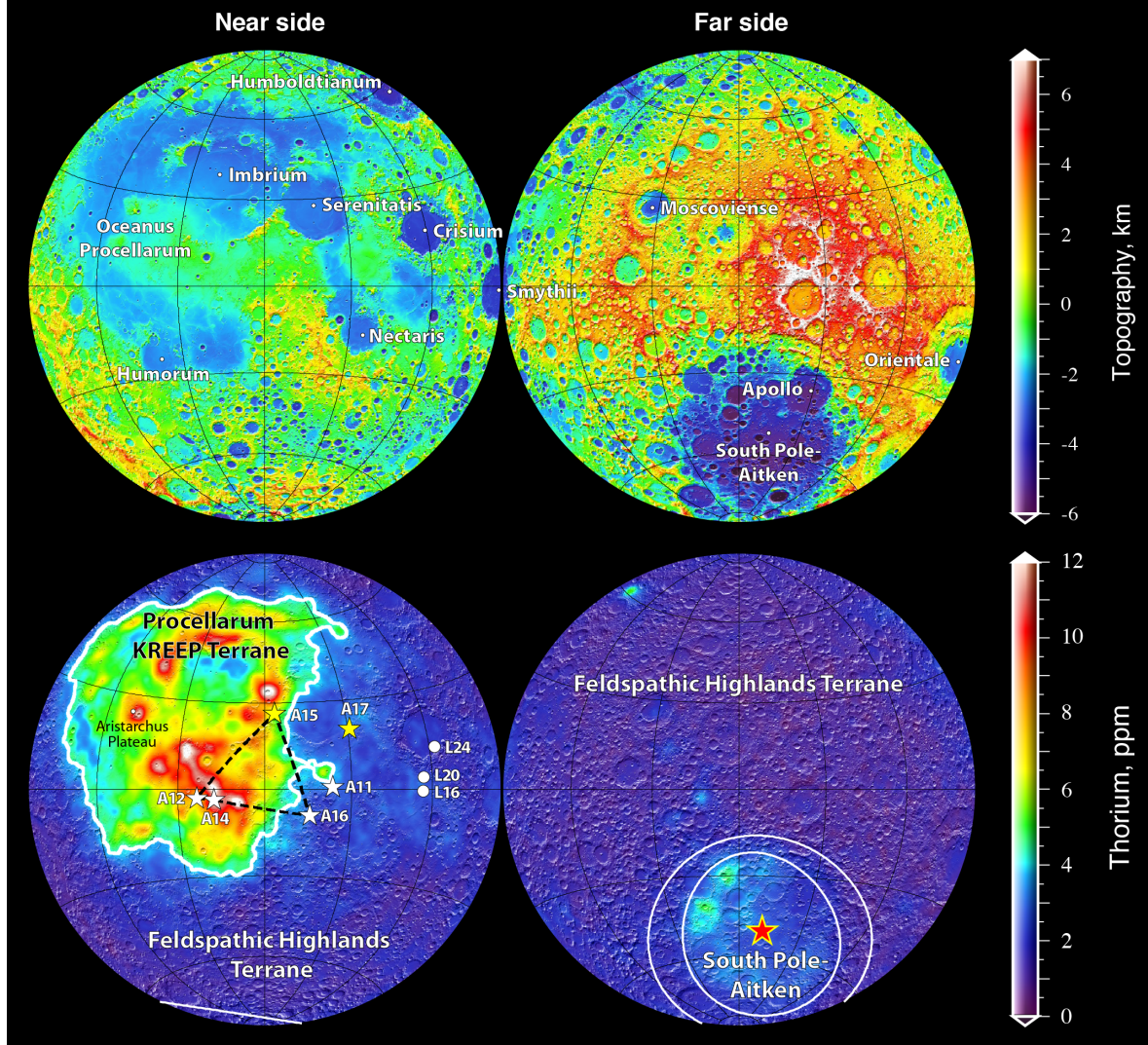


Figure 4. (top) Topography of the Moon from the Lunar Reconnaissance Orbiter altimeter (Smith et al. 2010) and (bottom) surface abundance of thorium from the Lunar Prospector gamma-ray spectrometer (Lawrence et al. 2004). The thick white line delineates the confines of the nearside Procellarum KREEP Terrane, and the thin white ellipses on the farside outline the floor and structural rim of the South Pole-Aitken basin. Stars and circles on the nearside represent the Apollo and Luna sample return stations, respectively. Yellow stars correspond to the locations where two heat-flow measurements were made, and the black dashed lines connect the four Apollo stations containing seismometers that operated in a network manner. The ALSEP geophysical network covered only a small portion of the nearside hemisphere that is highly atypical. The red star on the farside hemisphere marks the proposed FARSIDE landing site in the center of the South Pole-Aitken basin.

Impacts between near-Earth objects and the Moon are monitored ideally from the Earth-Moon L2 Lagrange point. From the vantage of the L2 Lagrange point, about 60,000 km above the lunar surface, a camera could make measurements of the visible and thermal flashes generated by meteoroid impacts during the lunar night that would be superior to those made on the nearside hemisphere from Earth (Ortiz et al. 2006, Suggs et al. 2008). These observations would not be affected by local weather conditions like on Earth, and given the lack of an intervening atmosphere, critical near-infrared observations would be possible. Since there is no Earthshine on the farside of the

Moon (sunlight that is reflected off of Earth), and since the L2 point is significantly closer to the Moon than is Earth, impact flashes would be detectable for objects considerably smaller than could be seen from a comparable optical system on Earth's surface.

In combination with simultaneous seismic measurements on the surface, these impact flash measurements will make it possible to constrain both the present day impact flux and size-frequency distribution of centimeter to meter sized near-Earth objects. Through long-term monitoring, both temporal and spatial variations in the impact flux on the Moon would be quantified (Le Feuvre and Wieczorek 2011), allowing for a better understanding of near-Earth objects.

FARSIDE will exploit these three unique properties of the Moon's farside hemisphere and will make synergistic measurements from both orbit and the surface. The lander will contain a suite of state-of-the-art astronomical, geophysical, and geochemical instruments, including: a *radio astronomy experiment*, a *broad-band seismometer* for lunar internal structure and impact investigations, a *heat flow probe* for thermal evolution and bulk composition studies, an *electromagnetic sounder* for electrical conductivity and temperature profile estimation, a *gamma-ray spectrometer* to provide compositional measurements of the South Pole-Aitken basin interior, a *radon and polonium detector* for monitoring of degassing events and exosphere dynamics, and a *surface camera* for landing site characterization and monitoring. The relay satellite will contain an *impact flash camera* for the monitoring of impact hazards, a *magnetometer* for electromagnetic sounding of the lunar interior, and a second *radio-astronomy receiver* for interferometric measurements.

The surface payload of FARSIDE contains all instruments that the International Lunar Network (Morgan and the ILN WG1, 2009) identified as core instruments for any future geophysical network. The following three sections describe the radio astronomy, lunar science, and impact monitoring objectives of the FARSIDE mission (Mimoun et al. 2010). Following these sections, synergies between FARSIDE measurements and other spacecraft and Earth-based observations are discussed.

2.1. Radio Astronomy

The Moon, in contrast to Earth, has an extremely thin ionosphere that allows radio-frequency measurements from its surface down to 500 kHz during the day, and even lower during the night. Its farside hemisphere is shielded from terrestrial radio interference, lightning, and auroral radio emissions, and during the lunar night the farside is also shielded from strong solar emissions (Figure 5). For these reasons, the farside of the Moon has been considered to be an excellent site for low-frequency radio astronomy since the 1960s (Bely et al. 1997, Takahashi 2003, Jester and Falcke 2009, Woan 2011).

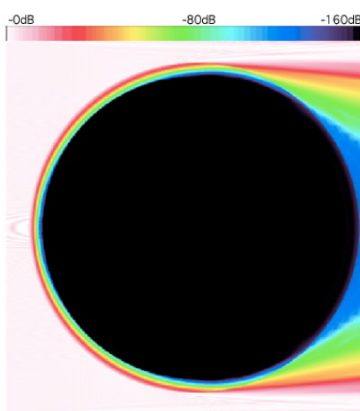


Figure 5. Attenuation of a 60 kHz continuous plane radio wave (incident from the left), as it propagates through and around the Moon. On the farside, at latitudes equatorward of $\sim 45^\circ$, strong radio signals originating from the Earth, Sun, or Jupiter, would be attenuated in strength by more than a factor of 10^{10} (Takahashi 2003).

The two Radio Astronomy Explorer satellites, RAE-1 and RAE-2, launched respectively in 1968 and 1973 (Alexander et al. 1975), are the only dedicated radio-astronomy missions to have made observations in the low-frequency range from 0.02 to 13.1 MHz. The RAE-1, in orbit around Earth, encountered severe terrestrial radio-frequency interference (RFI), which made the data practically useless for radio astronomy. Though solar and planetary studies can be performed from spacecraft above Earth's ionosphere, such observations are made in permanent view of strong contaminating

sources from the Sun, Earth and Jupiter. The RAE-2 spacecraft was therefore sent to an orbit around the Moon to take advantage of the effective radio shielding on the farside. The radio receivers were limited to total flux and no polarization measurements were made. As a result, since no new low-frequency astronomy missions have become implemented, astrophysics at frequencies below 10-20 MHz is today almost entirely unexplored.

From the unique radio-quiet location on the lunar farside, the only sensitivity limitation would come from the galactic radio background, and even those signals could be lowered by broad frequency and long time integrations. Being an unexplored portion of the electromagnetic spectrum, low-frequency radio measurements from the farside of the Moon will elucidate many processes (Figure 6). As described in the following sections, a wide range of investigations are enabled by the unique platform offered to us by the farside of the Moon.

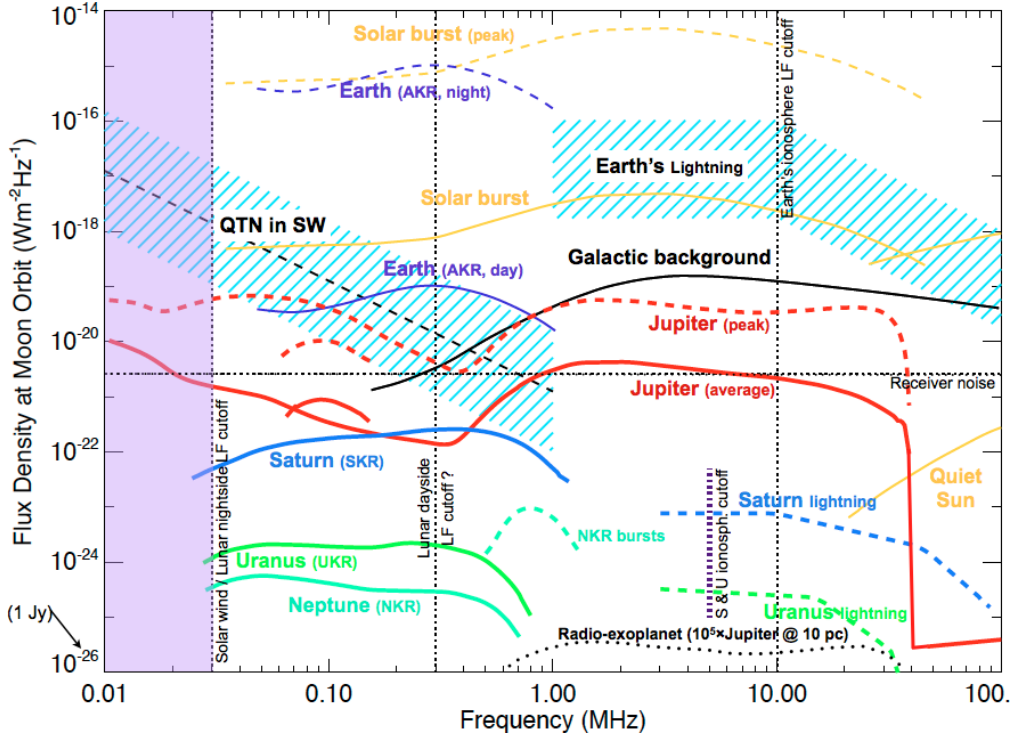


Figure 6. Planetary, solar and predicted exoplanetary radio emission levels on the surface of the Moon, compared to the galactic background detected with a single dipole (Zarka et al. 2012). From the farside, no terrestrial signal (violet/light blue) pollutes the observations above 0.2–0.5 MHz. Below \sim 1 MHz, the main limitation comes from the electrostatic quasi-thermal noise (QTN), whose equivalent density in the solar wind (SW) at lunar orbit is indicated (the upper and lower limits correspond to 2 and 20 m long antennas). During the lunar night, no solar emissions (orange) are present and observations can be extended down to the solar wind cutoff of \sim 30 kHz. For half of the lunar month, strong contaminating signals of Jupiter (red) will be absent. SKR, UKR and NKR are Saturn, Uranus and Neptune auroral kilometric radiation, respectively.

Cosmology. The frequency range below 40 MHz corresponds to the red-shifted neutral hydrogen (HI) 21-cm line at redshifts $z \geq 35$, and thus to the so-called “dark ages” that preceded the epoch of reionization in our Universe. Theoretical modeling of the global HI signature predicts a specific spectral variation with amplitudes about 10^6 times the sky background around 20 MHz (Figure 7, Pritchard and Loeb 2012). Such sensitivity should be reachable with a few months time integration in 1 MHz bands. Single-dipole detection of this weak global signal is made difficult by the variations with time, space and frequency of the foreground sources, but an experiment on the farside of the Moon will be much more sensitive than any of its ground-based counterparts (Voytek et al. 2014) because of the absence of Earth-reflected RFI (Vedantham et al. 2015) and ionospheric perturbations.

Sky mapping. Combining the time-variable occultation of one-half of the sky by the Moon, goniopolarimetric measurements by the lander and relay satellite, and inversion of series of

interferometric measurements (complex visibilities obtained by correlation of time-shifted signals from the lander and relay satellite), radio sky maps will be built at several frequencies together with an accurate spectrum of the sky background intensity and polarization. This mapping, with expected resolution of degrees to tens of degrees, will provide information on distant radio galaxies and large-scale structures such as clusters with radio halos and cosmological filaments (Dulk et al. 2010).

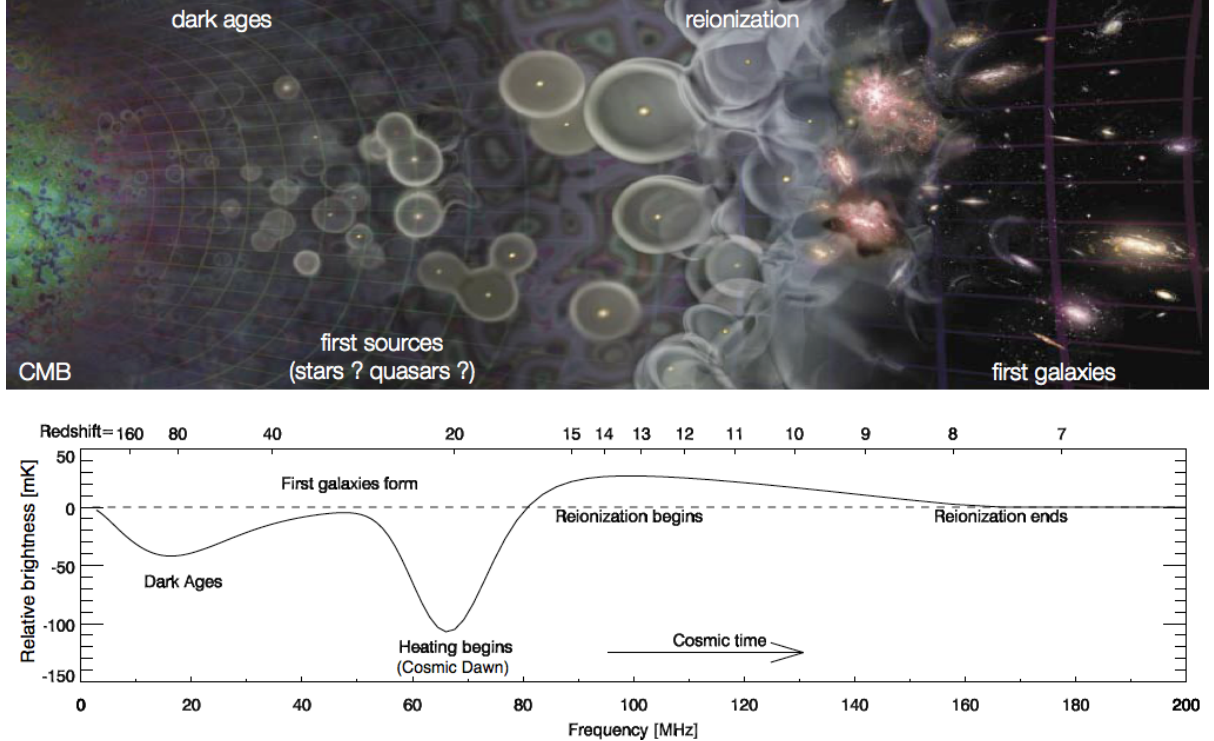


Figure 7. (top) A schematic outline of cosmic history with (bottom) modeled fluctuations of the red-shifted 21-cm global signal (from Pritchard and Loeb 2012). The detailed spectral fluctuations depend on, and constrain, models of the early Universe.

Solar physics. The frequency range of 0.1–40 MHz corresponds to plasma frequencies in the solar corona between about two and several tens of solar radii from the center of the Sun. As solar type II and III radio bursts are emitted at 1–2 times the plasma frequency (such as on shock fronts at stream interfaces in the solar wind, coronal mass ejections, and by energetic electron beams), occurrence and evolution of these structures will be monitored throughout the solar corona. Goniopolarimetry will provide directional information on the emitting structures (Mann et al. 1999), and FARSIDE observations will be used synergistically with spacecraft observations at similar frequencies as well as with ground-based observations at higher frequencies (Morosan et al. 2014).

(Exo-)planetary magnetospheres. With two crossed dipoles, detection of magnetospheric radio emissions from all giant planets will be possible on a regular basis. Such long-term observations will permit fundamental studies such as the accurate determination of planetary rotation periods and their variations (Hess and Zarka 2011, Zarka et al. 2014). They will also address, by the modulations of radio emissions by natural satellites and solar wind strength, magnetospheric dynamics and electrodynamic coupling with satellites. FARSIDE will provide the first radio measurements of Uranus and Neptune since the Voyager 2 flybys in 1986 and 1989. For Jupiter, these measurements will allow investigation of the plasma torus of Io, and possibly to monitor Io's volcanism and detect secular magnetic field variations. For Saturn, FARSIDE will extend the long series of Cassini measurements, permitting seasonal and secular studies (Lamy 2011). Though exoplanetary radio emissions will not likely be detectable with only a few dipoles, FARSIDE measurements will set the context for future exoplanet low-frequency radio searches.

Pulsars and radio propagation. Due to their periodic nature, radio emissions from a few known intense pulsars should be detectable by an adequate processing of waveform measurements followed

by long integrations. These challenging observations would provide us with the first measurements of a few pulsar spectra down to very low frequencies, allowing the quantification of propagation effects (such as dispersion and temporal broadening) down to increasingly lower frequencies. Temporal broadening of pulses, if found to depart from Kolmogorov-induced $\lambda^{4.4}$ variations, could reveal a cutoff in the distribution of turbulence in the interstellar medium, and open the possibility of low-frequency radio observations of variable sources at lower frequencies than expected (Bruck et al. 1976, Popov et al. 2006).

Transient events. Using data obtained from the surface experiment, radio transient events produced by the interaction of Ultra High Energy Cosmic Rays (UHECR) hitting the Moon will be investigated. These events should produce a cascade of particles propagating in the regolith, leading to Cerenkov emission. Particle shower lengths of a few meters imply a coherent radio pulse of 10–1000 nanoseconds and a spectral increase between \sim 1–100 MHz. FARSIDE surface measurements should allow to detect UHECRs within 5 km of the lander at a rate of \sim 1 event/year above 10^{20} eV.

High-energy neutrinos behave like UHECRs, but with a much deeper penetration depth and detector volume. Not being deviated by interstellar fields, their direction of arrival points towards their original source, and the FARSIDE interferometric measurements will allow determination of a plane containing the direction of arrival. These studies could eventually be competitive with the largest existing cosmic-ray detectors of neutrino experiments in Antarctica (Jester and Falcke 2009).

Local environment studies. By observing the Sun, the radio-emitting planets, and strong compact sources such as Cassiopeia A, FARSIDE will monitor the peak plasma frequency and total electron content above the landing site as a function of lunar local time, solar activity, and traversal of the Earth’s magnetotail. Charging of lunar dust due to ultra-violet illumination, charged particles, or micrometeoritic impacts could result in detectable electrostatic noise and discharges. Radio signals from moonquakes and impacts could potentially be detected (Zito 1989, St-Laurent et al. 2006).

Pathfinder measurements for an eventual lunar array. A longer-term goal in radio astronomy is the construction of a large, low-frequency radio array on the Moon’s farside (e.g., Jester and Falcke 2009). FARSIDE will provide invaluable pioneering measurements that will influence the design of such an array, fulfilling many goals of the radio and plasma experiment that were planned for the ESA Lunar Lander project (Klein Wolt et al. 2012).

2.2. Lunar Science

The Moon is the only terrestrial object for which we have samples from known locations, geophysical data from dedicated stations on the surface, and observations from trained field geologists. From these data, the origin of the Moon from a giant Mars-sized impact with the proto-Earth, the existence of a globe-encircling magma ocean that formed an ancient primary flotation crust, the existence of distinct geologic terranes, a chronology of the impact flux in the inner Solar System, and a 3 billion year record of volcanic activity have been elucidated (Jolliff et al. 2006).

Despite pathfinder observations from the Apollo Lunar Surface Experiment Package (ALSEP) that included a passive seismic experiment, heat flow probes, magnetometers, and laser retroreflectors, the interior structure and geologic evolution of the Moon remain poorly understood (Neal 2012). The Moon represents an end-member of how terrestrial planets form and evolve, and it is only by deciphering the processes involved in lunar formation and differentiation that similar processes on the larger terrestrial planets will be fully understood.

FARSIDE has two primary lunar science goals: (1) to determine the internal structure of the Moon from crust to core, including lateral variations of the upper mantle and crust of the South Pole-Aitken basin, and (2) to elucidate the thermal evolution and internal temperature profile of the Moon. Two secondary science goals are to determine the composition of the surface within the South Pole-Aitken basin, and to monitor the degassing of radon that will constrain exosphere dynamics.

Interior structure. Much of our knowledge of the Moon’s internal structure comes from analyses of the Apollo seismic data that were collected from a rudimentary four-station network between 1971 and 1977. Other measurements that bear on internal structure are electromagnetic sounding acquired simultaneously from surface and orbiting magnetometers, and Lunar Laser Ranging that enabled precise measurement of lunar librations. Unfortunately, the limitations of late-60s digital technology, the narrow frequency range of the seismometers, cross-calibration problems with the magnetometers,

and the small footprint of the network near the sub-Earth point placed severe limitations on data interpretation.

Following more than 40 years of analysis of the ALSEP data, it has been possible to place some constraints on the properties of the lunar crust, mantle, and core. Nevertheless, as the summary in Figure 8 demonstrates, fundamental first-order questions remain concerning lunar internal structure. It is not even known if the apparent lack of deep farside moonquakes represents a bias related to the nearside emplacement of the Apollo seismometers, or if the farside of the Moon is seismically inactive (perhaps as a result of the limited volcanic activity that took place on this hemisphere).

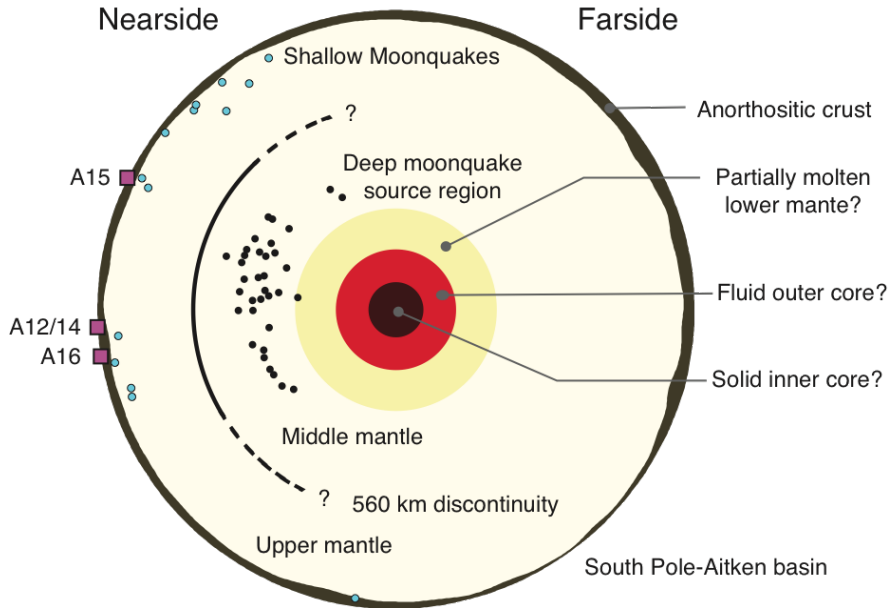


Figure 8. Schematic diagram (to scale) of the Moon's interior structure. Shown are the Apollo seismic stations (squares), all shallow moonquakes (blue circles), the deep moonquake source regions that are periodically activated by Earth-raised tides (black circles), inferred variations in crustal thickness, and a possible discontinuity ~ 560 km below the surface. The structure below the deep moonquake source region is only weakly constrained, and little is known about the farside hemisphere. Image from Wieczorek et al. (2006).

Concerning the crust, a variety of thickness estimates have been proposed beneath the Apollo seismic network that differ by a factor of two, from 30 to 60 km (Lognonné and Johnson 2007). Furthermore, as shown in Figure 4, the Apollo network straddled the boundary of two distinct geologic provinces, and the crustal properties of these two terranes were not observed unambiguously. Though it is possible to infer variations in crustal thickness using gravitational and topographic data obtained from orbit (Wieczorek et al. 2013), these models require an anchoring to a ground-truth value.

The lunar mantle is related to several fundamental questions in lunar science. The relic depth of melting of the lunar magma ocean is unknown and could be present as a seismic discontinuity. There are some indications from Lunar Laser Ranging and seismic data that the deepest portions of the mantle might be partially molten today (Khan et al. 2014). If true, this would have profound consequences for our understanding of the thermal evolution and volcanic history of the Moon.

Deeper still, the size and structure of the lunar core play a critical role in constraining the giant Moon-forming impact event and the generation of an ancient magnetic field (e.g., Canup 2012, Cuk and Stewart 2012, Weiss and Tikoo 2014). Studies using multiple lines of evidence generally conclude that the Moon possesses a liquid metallic core (Fe with some Ni, S, and C) that is less than 400 km in radius. Due to the non-detection of seismic phases propagating through the lowermost lunar mantle, the lower mantle and core are only weakly constrained. Reflected phases from a possible molten layer above the core and from the core-mantle boundary (Weber et al. 2011, Garcia et al. 2011) have been detected. However, considerable differences remain in the core radius estimations, and the existence of a solid inner core and molten zone above the core is debatable.

FARSIDE proposes to resolve these issues by placing a modern, state-of-the-art, broad-band seismometer and electromagnetic sounder on the farside of the Moon, and a magnetometer on the relay satellite to monitor the ambient magnetic field. A novel aspect of these experiments will be to use observed impact events as seismic sources. Impactors as small as 100 g generate light flashes that have been detected by Earth-based telescopes on the nearside hemisphere (Ortiz et al. 2006, Suggs et al. 2008) and which will be detectable on the farside by the FARSIDE dedicated impact flash camera. With knowledge of the locations and occurrence times of these seismic sources, it is possible to invert for internal structure *using only a single seismic station*. (Three stations would be required to locate the event if the event location were not already known). Impact flashes were not used during the analysis of the Apollo data, and simulations show that the FARSIDE seismology experiment will detect about 1000 of these events per year. This active seismic experiment using geographically controlled sources will allow for very precise studies of the crust and upper mantle.

A key science objective is to determine the size of the Moon's liquid core and solid inner core. The FARSIDE strategy is based on the refraction and reflection of seismic waves by the core from the known deep moonquake nests that are periodically activated by Earth tides (Figure 9). This is accomplished by observations of the PKP phase, a P-wave that travels through the core, and the ScS phase, an S-wave reflected from the core-mantle boundary. These phases were not detected by Apollo, but are above the detection threshold of modern planetary seismometers. The deep moonquake nests on the near side are well localized, and the ideal location of a seismic station on the farside hemisphere will allow for the detection of a solid inner core, if one is present. Inversions of electromagnetic sounding data will provide additional constraints on the size of the highly electrical conductivity core (Grimm and Delory 2012).

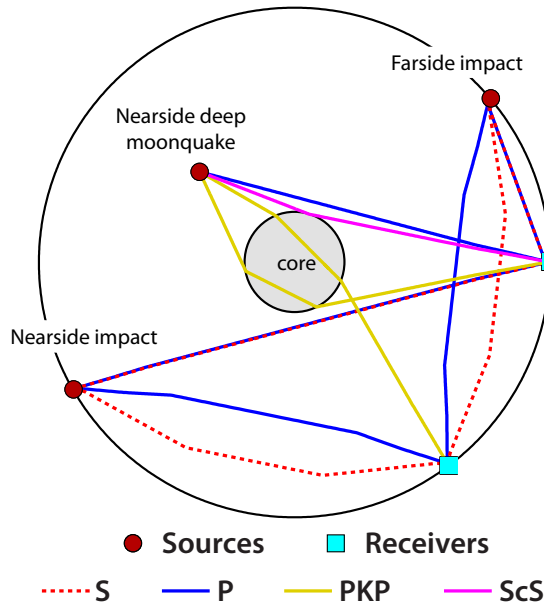


Figure 9. Example P and S seismic ray paths associated with meteoroid impacts and deep moonquakes. Seismic waves from the nearside deep moonquakes that are refracted (PKP) and reflected (ScS) from the core are ideally observed on the farside of the Moon. Farside impacts detected from the relay satellite, and nearside impacts detected from Earth observatories will constrain the lunar mantle and crust. Ray paths are shown for a receiver at two different latitudes on the farside hemisphere.

Thermal evolution. To decipher the thermal evolution of the Moon, it is necessary to know the amount of heat that is currently escaping its surface. The surface heat flow is a critical ground truth measurement that any thermal evolution model must satisfy, and provides important constraints on both the Moon's internal temperature profile and bulk composition.

Two heat flow measurements were made during the Apollo missions. At the Apollo 15 and 17 landing sites, hollow fiberglass borestems were drilled to depths of approximately 1.5 and 2.5 meters, and thermal probes inserted into these measured the thermal conductivity and temperature at fixed depths. By measuring the temperature gradient and thermal conductivity, the heat flow (which is the product of the two) was estimated (Langseth et al. 1976). Heat flows of 21 and 14 mW m^{-2} , with uncertainties of about $\pm 15\%$, were reported ultimately for the Apollo 15 and 17 sites, respectively.

The analysis of these data revealed several problems. First, the thermal conductivity that was estimated from an active heating experiment was found to be unreliable: The drilling of the borestems into the surface compacted the surrounding regolith, enhancing the thermal conductivity by about

50% (Grott et al. 2010). The thermal conductivity instead was estimated by measuring the attenuation with depth of the surface annual thermal wave. A second, and still unresolved, problem is that the subsurface temperatures were found to increase slowly with time. This was attributed to astronaut disturbance of the surface boundary layer, but other possibilities exist.

Subsequent observations by the Clementine (1994) and Lunar Prospector (1998) spacecraft (Jolliff et al. 2000) demonstrated that the Moon is divided into distinct geologic terranes, with the Procellarum KREEP Terrane having much higher concentrations of radioactive elements than the adjacent Feldspathic Highlands Terrane (Figure 4). Because both Apollo heat flow measurements were made close to the boundary of these terranes, they are unlikely to be representative of either (Laneuville et al. 2013). Representative heat flow measurements far from terrane boundaries are required to constrain the abundances of radioactive elements in the lunar interior. Given the ambiguities in the Apollo heat flow results, estimates of the Moon's bulk uranium content vary by more than a factor or two, from an Earth-like 20 ppb to 46 ppb. This range of uncertainty is too large to serve as a useful test of lunar origin models.

Until recently, it was thought that lunar volcanism was most active from 4 to 3.1 billion years ago, eventually terminating about 1.2 billion years ago (Hiesinger et al. 2010). Lunar Reconnaissance Orbiter Camera images have shown evidence for the eruption of small irregular mare patches up until geologically recent times, about 20–60 million years ago (Figure 10, Braden et al. 2014). This observation is difficult to reconcile with our current understanding of the Moon's thermal evolution (though, see Laneuville et al. 2013). Furthermore, some interpretations of Apollo seismic data and Lunar Laser Ranging data suggest that the deepest portion of the lunar mantle might be partially molten today (Weber et al. 2011, Khan et al. 2014). To understand recent volcanism (Grove and Krawczynski 2009), better estimates of the Moon's internal temperature profile are required.

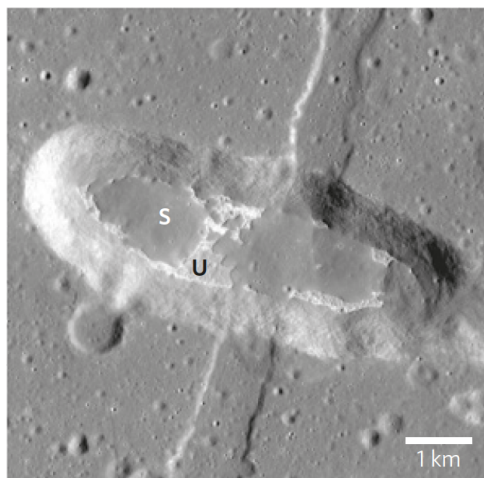


Figure 10. Lunar Reconnaissance Orbiter Camera images show that lunar volcanism extends up until geologically recent times (20–60 million years ago). Understanding how young lavas could be generated on a small body such as the Moon requires better estimates of the amount of heat that is currently escaping the surface and the interior temperature profile. Image from Braden et al. (2014).

These questions will be resolved by joint analyses of data obtained from the FARSIDE heat flow and electromagnetic sounding experiments. Two heat flow probes will be deployed at the landing site, reaching depths of 3 meters using a self-penetrating percussive mole device (Spohn et al. 2012). This experiment will measure temperature every 20 cm depth to ± 0.05 K and measure the thermal conductivity and dielectric permittivity to $\pm 5\%$ every 30 cm. Electromagnetic sounding will use electromagnetic impedance measurements over a range of frequencies to determine electrical conductivity as a function of depth below the surface. A full electromagnetic sounding will be acquired at the lander, and magnetic induction studies will be performed using simultaneous magnetic field measurements from the surface and relay satellite. From these measurements, the electrical conductivity profile of the Moon will be determined, as will be the size of a high-conductivity core. By using laboratory measurements of the temperature dependence of electrical conductivity, the temperature of the mantle will be constrained (Hood 1982, 1986).

Surface composition. The samples collected during the Apollo and Luna missions are well documented and have provided a wealth of data from a few known locations on the surface of the Moon. Global chemistry of the lunar surface has also been assessed from orbiters using UV-VIS

spectroscopy for iron and titanium, and gamma-ray spectroscopy for a few major and radioactive elements. Importantly, these global datasets reveal the existence of rock types that are unlike any known rock in the Apollo and Luna sample collections.

One prominent region mapped from orbit that is unaccounted for in the lunar sample collection is the floor of the giant South Pole-Aitken basin. The floor is more mafic than typical highland rocks and also has a slight enhancement in rare-earth and radioactive elements (see Figure 4). As a result of the small number of elements that have been mapped from orbit and their associated low precisions (Prettyman et al. 2006), it is unclear if the floor of this basin represents pristine lower crustal materials, a differentiated impact melt sheet, or a mixture of crustal and mantle materials.

It is a challenging task to obtain absolute elemental abundances from remotely sensed data, and such measurement techniques are often calibrated by ground truth measurement. FeO abundances derived by spectral reflectance and orbital gamma-ray spectroscopy differ by several wt% (Lawrence et al. 2002). The South Pole-Aitken basin is sufficiently different from the Apollo samples as to call into question the validity of remote compositional estimates for these regions (Lucey et al. 2006). Furthermore, one of the most important elements for distinguishing lunar rock types is magnesium, but this element has not been obtained at the precision required to distinguish different types of crustal rocks (Prettyman et al. 2006, Peplowski and Lawrence 2013).

The FARSIDE mission proposes to obtain high-precision elemental abundances at the South Pole-Aitken landing site, enabling a determination of the origin of the materials that make up the basin floor. The long integration times obtained by a static instrument on the surface would eclipse the typical hour-long integrations per location obtainable for an orbital instrument by several orders of magnitude. With such long integration times, not only will all of the major elements be determined to high accuracy, but also will a handful of minor and trace elements.

Degassing and exospheric dynamics. The lunar exosphere is extremely tenuous and fragile, and very sensitive to both human and robotic activities. Therefore, before the lunar exosphere becomes contaminated by exploration activities, it is imperative to first characterize this unique environment. This includes determining the time variability of the atmosphere, as well as identifying the primary atmospheric sources and sinks. To this end, radon has long been recognized as a valuable tracer of lunar regolith-exosphere exchanges.

^{222}Rn and ^{210}Po , which originate from the radioactive decay of uranium, are popular tracers of gases, fluids and aerosol transport in the lithosphere and atmosphere of both Mars and Earth (Tanner 1980, Nazaroff 1992, Papastefanou 2006, Meslin 2008). Since ^{222}Rn is a gas with a half-life of 3.82 days, any radon that is detected in the exosphere must have a recent origin. The 22.3-year effective half-life of ^{210}Po allows investigating the consequences of radon degassing over decade timescales. Previous measurements of the concentrations of these two elements from orbit have revealed both temporal and spatial variability, and this has been attributed, in part, to the presence of active degassing at geologically active regions. As on Earth, it has been suggested that radon outgassing might be correlated with moonquake occurrences.

Despite the number of experiments that measured these radioisotopes, a consistent and comprehensive picture of radon outgassing on the Moon is lacking, in part due to the limited spatial and time coverage of these experiments, or due to problems of contamination of the detectors with ^{210}Po or ^{241}Am radionuclides during their calibration on Earth. Long-term monitoring of the radon cycle on the surface of the Moon would provide valuable ground truth for orbital measurements, acquired most recently by the Lunar Prospector and Kaguya missions. FARSIDE proposes to detect ^{222}Rn and ^{210}Po on the lunar surface over the course of its four-year mission. Long time-series of these measurements would provide the first direct measurements of the regolith exhalation rate and would address several key issues related to the transport of volatiles and dust in the lunar regolith and exosphere. Understanding the time variability of ^{222}Rn would constitute a reference to study the transport of other gases.

2.3. Earth-Moon Impact Hazards

Asteroidal and cometary materials are derived from beyond the orbit of Mars, and by the dynamic interaction of celestial bodies they occasionally encounter the terrestrial planets of the inner Solar System. The vast majority of these meteoroids are small, and burn up during their interactions with

planetary atmospheres, but a smaller number of larger objects occasionally pass through the atmosphere to make an impact crater on the surface or disrupt in the atmosphere causing blast wave damage. Crater forming impacts are rare on Earth, but can be catastrophic to life, either locally or globally. Airbursts caused by the disruption of decameter-scale meteoroids in the atmosphere occur more frequently and could be extremely hazardous if one occurred in a populated area, such as in the case of the unpredicted Chelyabinsk event (Popova et al. 2013).

A vital component of impact hazard assessment is an accurate estimate of the rate at which objects of different sizes collide with Earth. Due to its proximity to Earth, the Moon is an ideal “witness plate” for constraining the flux of impactors in near-Earth space. On Earth, impact structures are rapidly eroded and small bodies are destroyed in the atmosphere before hitting the ground. In contrast, the inactive, unprotected lunar surface is an excellent recorder of collisions with objects at all sizes. Meter-sized objects create craters 10s of meters in size that are occasionally detected in orbital images. The more numerous smaller collisions give rise to flashes of light that are detectable by simple cameras (Bouley et al. 2012, Suggs et al. 2014, Figure 11).



Figure 11. A 0.1 second impact flash (circled in red) detected by an impact-flash monitoring telescope in Morocco (Baratoux et al. 2012). Today, more than 400 impact flashes have been observed on the nearside hemisphere of the Moon (Suggs et al. 2014). In this image, taken during the lunar night, the Moon is illuminated by Earthshine.

The primary objectives of investigating meteoroids in near-Earth space are (1) to determine the size-frequency distribution and the nature of these objects (cometary fragments associated with meteoritic showers versus sporadic asteroid fragments), (2) to determine their collision probabilities with both Earth and the Moon, (3) to determine the spatial and temporal variations in the lunar impact flux, (4) to determine the partitioning of energy during crater formation, and (5) to set new absolute constraints on ages of geological units derived by crater counts. FARSHIDE will achieve these objectives by combining data obtained from a dedicated impact-flash camera in orbit with simultaneous data acquired from a seismometer on the surface.

Present-day impact flux. Estimates of the terrestrial impact flux have combined infrasound records of detonations of meteors in Earth’s atmosphere with asteroid observations from telescopic surveys of larger near-Earth objects. However, a recent synthesis of these techniques indicates a large discrepancy in the estimated impact rate for objects 10 to 50 m in diameter (impact energy 0.1-10 Mt), which can generate hazardous airbursts (Brown et al. 2013). For this size range, the impact rate based on infrasound measurements is an order of magnitude higher than estimates based on telescopic surveys.

An alternative approach is to use the record of impacts with the Moon as it is subjected to the same types of objects that collide with Earth. The present impact flux on the Moon gives rise to new decameter-sized impact craters that have been observed from orbiting spacecraft (Daubar et al. 2011). A direct record of the near-Earth meteoroid flux is also available from the Apollo seismic network that detected about 1700 impacts with masses ranging from 0.1 to 100 kg during eight years of operations. Video observations have confirmed that these lunar meteoroid impacts are observable via the light they emit during impact, and impact-monitoring programs (Suggs et al. 2008) have since detected more than 400 such light flashes.

Satellites in orbit about the Earth have recorded the frequency of light bursts that occur during the atmospheric entry of meteoroids that are less than 10 meters in diameter, and these can be converted

into masses using an empirically derived luminous efficiency parameter (Brown et al. 2002). Camera surveys have extended these estimates down to 10 cm (Grisevitch et al. 2011) and radar techniques down to millimeters. If the orbits of the smaller meteoroids mimic those of their larger parent bodies, estimates of the terrestrial impact rates can be converted to that expected on the Moon. These estimates, however, appear to be three times smaller than those derived from lunar impact flash data (Ortiz et al. 2006). Seismic modeling of Apollo meteoroid impacts (Lognonné et al. 2009) favor the high impact rates derived from lunar impact flashes. Recent impact rates deduced from crater counts on the youngest units sampled by Apollo (Ivanov 2006), in contrast, are consistent with atmospheric detonation estimates, but this modeling procedure involves several parameters that are imperfectly known, such as the optical burst efficiency and impact-crater scaling-law exponents (Figure 12).

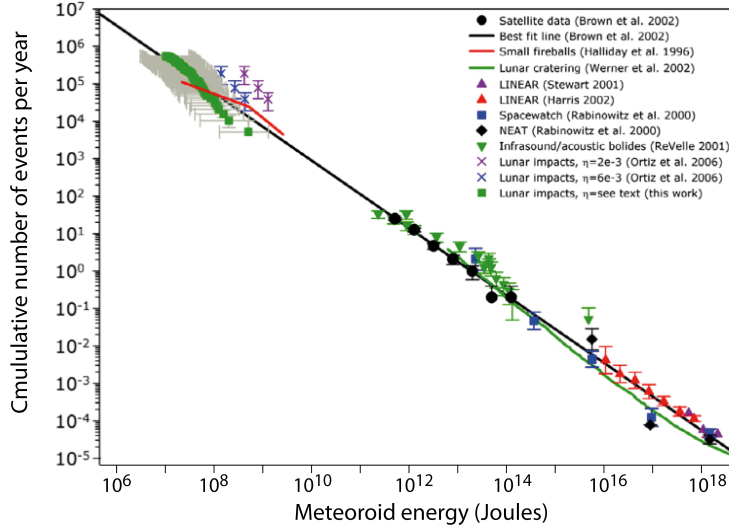


Figure 12. Cumulative histogram of collisional events with Earth as a function of energy using several different constraints: bolide detonation in the atmosphere observed by satellites, fireballs, crater counts on the Moon, monitoring of near-Earth objects, meteors detected by infrasound and lunar impact flashes detected from Earth. Lunar data have been corrected for gravitational focusing for comparison to the terrestrial observations. Figure after Suggs et al. (2014).

FARSIDE will determine the present-day impact rate on the Moon by the continuous monitoring of impact flashes from the vantage point of the Earth-Moon L2 Lagrange point. These observations will benefit from a complete lack of Earthshine illuminating the unlit portions of the Moon's farside hemisphere, and the lack of an intervening atmosphere will enable near-infrared measurements that are difficult to obtain from Earth. Combined with the proximity of the L2 Lagrange point to the lunar surface (which is about 6 times closer than Earth), these observations will enable detection of much smaller impacts than could be accomplished from a comparable terrestrial observatory. Masses of the colliding objects will be obtained by joint analyses of the seismic data and evolution of the thermal and visible light emissions. The lunar impact rate determined by FARSIDE will be complemented using the more limited ground-based observations made from Earth.

Impact mechanics. The collision of Solar System objects at hyper-velocities has traditionally been investigated by a combination of laboratory experiments that form cm-sized craters, numerical simulation, and investigation of ancient terrestrial impact craters. The detection of impact flashes from orbit, combined with data obtained from a surface seismometer, will provide a natural experiment for investigating impact processes at scales that are unattainable in the laboratory.

FARSIDE will explore the partitioning of an impactor's kinetic energy into seismic, thermal, and visible energy for craters that are 10s to 100s of meters in diameter. Simultaneously acquired seismic data and repeated monitoring of the thermal evolution of impact flashes will quantify the relationships between emitted light, impactor mass, impact velocity, and luminous efficiency. If images of the newly formed crater could be provided from orbital imagery, scaling relations between the seismic signal, luminous intensity, and final crater diameter would be obtained.

Dating of planetary surfaces. If the flux of objects colliding with the Moon were known, it would be possible to estimate the rate at which craters form on its surface. Conversely, by counting the number of craters superposed on a given geologic unit, it would be possible to estimate the age of the unit. This technique has been calibrated and applied successfully to the Moon by counting the number of craters with diameters greater than 100 m accumulated on the geologic units that were

dated by isotopic chemistry. The lunar impact-crater chronology method is the basis for the dating of other objects in the inner Solar System.

Though this technique is well calibrated for ages between 3 and 4 Gyrs (the most frequent ages of Apollo samples), application of the crater chronology technique to younger surfaces (less than hundreds of millions of years old) is considerably more complicated. Even if the flux of objects colliding with the Moon and Earth were assumed constant, this flux is uncertain by a factor of three. Furthermore, counts of smaller craters (<100 m) are contaminated by an unknown contribution of secondary craters produced by ejecta from distant large impacts.

Impact rates obtained from the observation of impact flashes can be compared to the size-frequency distribution of small lunar craters using impact crater scaling laws. If the two were found to be comparable, this would indicate that secondary cratering is a relatively unimportant process. If differences between the recent (1–100 My, from crater counts) and present impact rates were found to exist, this could reflect long- or short-term temporal variations in the lunar impact flux (such as might result from collisions in the asteroid belt). Such tests will become possible as crater-scaling laws are improved by joint analyses of impact flash data and their associated seismic signals (Suggs et al. 2014).

Temporal and spatial variations in lunar impact flux. Telescopic surveying of near-Earth objects is now almost complete for objects with diameters greater than about 1 km (Bottke et al. 2002). These observations constrain the impact rates on the Moon and Earth, and predict significant temporal variations in impact flux (by a factor of several), either as a time-of-day phenomenon for Earth or solar phase for the Moon (Campbell-Brown 2008). Furthermore, the synchronous rotation of the Moon predicts a time-averaged impact flux that is greater on its leading western hemisphere than its trailing eastern hemisphere (Le Feuvre and Wieczorek 2011). Predicted by theory, the magnitudes of these temporal and spatial variations are difficult to measure solely from the number of craters on the lunar surface (Werner and Medvedev 2010). Impact flash monitoring from Earth has detected east-west variations in the impact flash rate, but these observations cover only a fraction of the nearside hemisphere and are biased by variations in observation time (Figure 13).

FARSIDE will provide unbiased measurements of temporal variations in the lunar impact rate by the continuous monitoring of the farside impact flux. Temporal variations of the impact flux over the span of a lunar month will provide constraints on the meteoroid sources as these variations are directly related to the radiant distribution of impactors entering the Earth-Moon system. Comparison with estimates based on orbital-element models and encounter probability calculations will improve our understanding of the fate of meteoroids once they separate and evolve from their parent bodies. Monitoring of the impact flux over the course of a year will quantify the relative importance of cometary materials that give rise to meteor showers and streams, and the more continuous sporadic bombardment of materials derived from the asteroid belt.

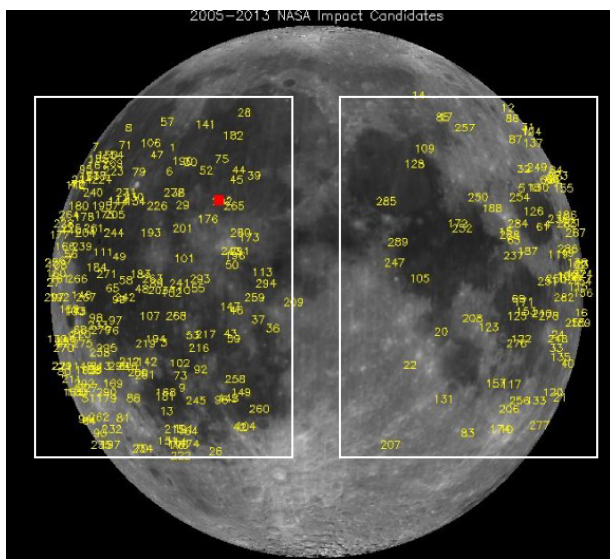


Figure 13. Spatial distribution of the ~400 impact flashes detected by the NASA impact-flash monitoring program (Suggs et al. 2008). Rectangles denote the approximate extent of the camera field of view during the waxing and waning observation phases. Observation times are limited by the time of day and local weather conditions.

2.4. Synergies with other missions

The FARSIDE mission will make use of data from a wide range of previous, current, and forthcoming mission. In addition to providing critical ground truth for lunar orbital missions, low frequency radio data collected by FARSIDE will allow for synergistic studies with higher frequency data collected by terrestrial astronomical observatories.

LOFAR. The overlapping frequency range between FARSIDE and the large European ground-based array LOFAR, the Ukrainian low-frequency array UTR2, and the Nançay decameter array will allow extensive comparisons, cross-calibrations of intensity and polarization, evaluation of the Earth's ionospheric absorption, and VLBI interferometric measurements (Zarka et al. 2012). LOFAR observations will extend the FARSIDE measurements to higher frequencies (up to 250 MHz).

Lunar Reconnaissance Orbiter. The FARSIDE mission reduces landing risk by using the numerous narrow-angle camera images that have been taken of the South Pole-Aitken basin by the Lunar Reconnaissance Orbiter Camera. Roughness maps based on laser altimetry data and rock abundance maps from radiometer data will be used to find sites with the least risk to the lander. The interpretation of Diviner radiometer data will benefit from the FARSIDE-derived subsurface temperature profile and surface rock abundances.

Impact monitoring. A complete view of the lunar impact rate will be obtained by combining FARSIDE impact monitoring results of the lunar farside hemisphere with terrestrial nearside impact-flash detections. The observations of the nearside hemisphere will be conducted by the Marshall Space Flight Center (NASA), the European led International Lunar Impact Astronomical Detection network (ILIAD), and amateur groups such as the Association of Lunar and Planetary Observers (ALPO) and the Geologic Lunar Research Group (GRL). Given the renewed international interest in lunar exploration, it is probable that a camera would be in lunar orbit during the FARSIDE mission that could image these newly formed craters, providing the crater diameter for the impact mechanics investigation.

Lunar Atmosphere and Dust Environment Explorer (LADEE). FARSIDE will perform the first direct measurements of the electric field in the lunar photoelectron sheath, whose structure and variability may contribute to the levitation and transport of lunar dust. FARSIDE will also monitor radon emissions that will constrain exospheric dynamics. These two measurements will provide important ground truth for the LADEE orbital mission that is investigating the lunar exosphere.

MoonRise. MoonRise is one of five potential missions being considered for NASA's New Frontiers 4 program. The sole objective of this mission is to return to Earth 1 kg of material from the South Pole-Aitken basin on the farside of the Moon. Analyses of these samples will determine the age of the basin and the nature of its geochemical anomaly. Seismic data obtained from FARSIDE will provide a critical crustal thickness determination that will constrain the origin of these samples.

Gravity Recovery And Interior Laboratory (GRAIL). NASA's lunar gravity mapping mission GRAIL has acquired high-resolution gravity data over both the near and farside hemispheres of the Moon. Global crustal thickness models have been generated by these data, but these models require anchoring by a seismically determined crustal thicknesses, of which the Apollo estimates vary by a factor of two. An unambiguous crustal thickness determination by FARSIDE will permit the construction of a reliable global crustal thickness model.

Lunar Geophysical Network. The Lunar Geophysical Network is a mission that is being considered by NASA in the New Frontiers 5 program. Four identical landers would carry a payload of seismometers, heat flow probes, electromagnetic sounders, and laser retroreflectors. All stations would be on the nearside of the Moon, and would operate concurrently for 6 years. FARSIDE, if operational at the same time, would complement the network and provide invaluable data from the opposite hemisphere of the Moon.

Luna 25, 26 and 27. As a continuation of the previously successful Luna program, Russia is considering three missions to the lunar surface: Luna 25, 26, and 27. (Luna 24, launched in 1976, was the last of the Luna series). The last of these landers may contain a seismometer that could allow for the construction of a lunar network if operational at the same time as FARSIDE or NASA's Lunar Geophysical Network. These three missions would all land on the nearside hemisphere of the Moon.

3. SCIENCE REQUIREMENTS

3.1. Radio astronomy science requirements

A sensitive radio receiver on the lander performing spectrometry, goniopolarimetry and waveform capture, connected to electrical monopole or dipole antennas, and a simpler radio receiver connected to short dipoles on the relay satellite dedicated to interferometric measurements above ~ 1 MHz, will fulfill the requirements of all radio astronomy science goals. The radio-spectrometer mode will be used as a baseline for monitoring the lunar environment from 16 kHz to approximately 40 MHz. Its goniopolarimetric mode will be the basis for separating solar, planetary and other emissions detectable with limited integration over sky background fluctuations. Waveform capture, with an instantaneous bandwidth of several MHz, will be the basis of interferometric measurements for constraining the extent of sources intense enough to be localized by goniopolarimetry. Synchronized waveform snapshots from the lander and relay satellite will be correlated on the relay satellite, and complex visibilities will be stored to perform imaging of the static radio sky. Individual waveform snapshots will also enable studies requiring high time resolution (like burst detection) or high sensitivity (such as pulsar detection and study of propagation effects), for which they can be processed on the relay satellite, or onboard the lander, in order to increase the duty cycle. Time coincidence between radio pulses detected at the lander and relay satellite will also be used.

The unique character of lunar farside radio measurements is their extreme sensitivity due to the extreme radio quietness of the site. Special care must thus be taken to achieve high electromagnetic cleanliness of the lander's payload and communication links, and to measure the effective pollution brought by the mission itself to the pristine lunar environment. Electrical properties of the lunar regolith and uppermost crust, measured in situ and in the lab on returned samples, indicate that radio signals can penetrate to km-depths without strong scattering. The low conductivity and moderate dielectric constant should cause only small distortion of the skyward beam pattern of the radio astronomy experiment. Echoes of strong natural radio signals may be used for lunar subsurface sounding in complement to EMS measurements.

3.2. Seismology science requirements

The FARSIDE seismometer will investigate the crust, mantle and core of the Moon. For the mapping of the crust and the upper mantle structure beneath the South Pole-Aitken basin, the science objectives can be achieved by the joint detection of ~ 50 impacts by the seismometer and impact flash camera. Yamada et al. (2011) estimated that the number of impacts detected jointly by a nearside seismic station and Earth-based telescope monitoring (with a detection efficiency of 12%) would be 20–30 per year. Over the course of four years, this would provide relative errors of only 2–3 % for the velocity model beneath the landing site. With the farside impact camera, more than 100 impacts should be detected jointly per year.

No seismic waves penetrating the deep mantle and core were detected by Apollo. The detection of mantle and core phases from the known deep moonquake sources will enable the measurement of the core radius with a resolution better than 20 km. This will be performed using P, S, and ScS phases for epicentral distances less than 120° . With P, S, Pcp, and PKP phases (for epicentral distances between 120 – 140°), additional constraints on core structure will be provided by the core P-wave velocity structure. The seismic activity of the Moon during the FARSIDE mission can be constrained with confidence using the known periodicity of deep moonquake activity. 2800 deep moonquakes events are expected that will exceed the Apollo detection threshold during a 4-year mission. For a conservative detection level 5 times more sensitive than Apollo, about 10,000 deep moonquakes are expected. Location errors of the deep moonquakes will generate a maximum error of only 2–5% in the deep mantle seismic velocities.

Seismic waves reflected and refracted by a small lunar core are below the detection threshold of the Apollo seismometers (Figure 14) and were identified only after stacking of data from repeating deep moonquakes (Weber et al. 2011, Garcia et al. 2011). Detection of these phases from a single record requires an instrument sensitivity ten times better than the Apollo seismometers (Yamada et al. 2013). The FARSIDE seismology instrument is based on the seismometer that will fly on NASA's

InSight mission to Mars in 2016. The large dynamic range of the instrument allows precise sampling of waveforms below the instrument noise floor, allowing the coherent stacking of deep moonquake signals. It realizes an $\sim 10\text{--}20$ factor increase in sensitivity in the body-wave band 0.1–10 Hz and explores for the first time the 10–40 Hz and <0.1 Hz bands. As shown in Figure 14, nearside deep moonquakes, their core reflected and refracted phases, and their differential P-S arrival times will be detectable from the observation point of a farside station.

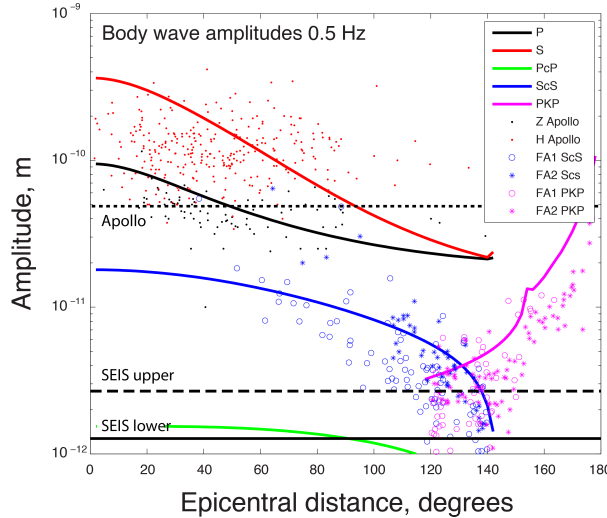


Figure 14. Detection of seismic core phases by the FARSIDE seismometer. (red and black) Mean P and S amplitudes of the Apollo deep moonquakes as a function of epicentral distance, (blue and magenta) expected amplitudes at two possible FARSIDE stations for reflected (ScS) and refracted (PKP) core arrivals from the known near-side deep moonquake nests. Solid colored lines represent average expected amplitudes. The horizontal dotted, dashed, and solid lines are the instrument noise levels for the Apollo and FARSIDE upper and lower estimates. A large fraction of the core arrivals will be detectable by the FARSIDE seismometer.

3.3. Heat flow science requirements

Heat flow probes will be deployed at the landing site using a self-penetrating percussive mole device (Spohn et al. 2012). To achieve the science objectives, the probes should reach a depth of 3 meters, measure temperature every 20 cm depth to ± 0.05 K and measure the thermal conductivity every 30 cm. The heat flow must be determined with an accuracy of better than 15%, and to achieve this, both the thermal gradient and thermal conductivity must be determined to better than 10% (Grott et al. 2007). Thermal conductivity can also be estimated from the thermal diffusivity, and this will be measured in both the active heating mode and from the propagation of the annual thermal wave. This method will be used to perform a consistency check for the active-heating thermal conductivity experiment.

A major difference between modern mole-based systems and the Apollo heat flow experiment is that moles do not involve the drilling of a high-conductivity borestem into the lunar regolith. This will minimize the amount of compaction and disturbance the surrounding regolith will experience, and will also remove a substantial thermal shunting effect that was visible in the Apollo data. The FARSIDE landing site must be chosen to ensure that the regolith is more than 3 meters thick.

3.4. Electromagnetic sounding science requirements

Electromagnetic sounding uses electromagnetic impedance measurements over a range of frequencies to determine electrical conductivity as a function of depth below the surface. For FARSIDE, two approaches are possible. First, the magnetic transfer function will be constructed using the FARSIDE relay satellite, and the sum of the source and lunar induced fields on the surface. This technique, which only requires vector magnetic field measurements, was used previously during the Apollo-era, though cross-calibration problems of the two magnetometers limited the accuracy of the approach. A second technique, the method of magnetotellurics, provides a complete sounding at a single surface station using orthogonal horizontal components of the electric and magnetic fields (Simpson and Bahr 2005). This method provides measurements with horizontal resolution comparable to the electromagnetic skin depth.

The electromagnetic sounding experiment requires to deploy four electrodes to distances of ~ 10 m by spring launchers. This allows the reconstruction of two horizontal components of the electric field. A fifth electrode on a mast (not required) would provide the vertical field. Three-axis fluxgate

magnetometers deployed on a simple boom on the lander are required to enable to the electromagnetic sounding experiment, and a second set of three-axis fluxgate magnetometers on the relay satellite is required for the magnetic induction experiment. To fulfill the science objectives, the magnetic transfer function requires a resolution of $250 \text{ pT}/\sqrt{\text{Hz}}$ at 1 mHz. The magnetotellurics method requires a resolution of $10 \text{ pT}/\sqrt{\text{Hz}}$ at 1 Hz, $10 \text{ mV/m}/\sqrt{\text{Hz}}$ at 1 mHz, and $100 \text{ }\mu\text{V/m}/\sqrt{\text{Hz}}$ at 1 Hz.

3.5. Surface chemistry science requirements

The geochemistry package must be able to measure with a precision better than 1 wt% the major elements Fe, Mg, Ca, Al, Si, O, Ti and K. In addition to major elements, the composition and/or limits on several minor and trace elements such as Th, U, Ni and H, (Peplowski et al. 2015) and the rare-Earth elements Gd and Sm should be characterized, which are critical for deciphering the origin of lunar rocks. Given the long integration times that will be made possible over the course of 4-years, a gamma-ray spectrometer is the most suited instrument for this mission. The primary constraint of a surface gamma-ray spectrometer is that the instrument have a clear view to the surface given its 2π viewing geometry. The sensor can either be body mounted to the lander or placed on the surface by a robotic arm.

In addition, the Context Camera accommodated on the robotic arm will provide high-resolution images of the lunar surface analyzed by the gamma-ray spectrometer. This instrument will also acquire images to characterize the lunar rocks and regolith around the lander at various distances and viewing angles. The combination of geological imagery and geochemical data will provide valuable information to better understand the lunar regolith of the South Pole-Aitken basin.

3.6. Radon science requirements

The radon outgassing experiment must be able to measure with a precision of 10% the concentrations of both ^{222}Rn and ^{210}Po over the course of an entire lunation. Orbital measurements suggest an average surface activity of about 1 Bq m^{-2} for ^{222}Rn and 15 Bq m^{-2} for ^{210}Po . With proper rejection of the galactic cosmic-ray background (achieved by anticoincidence), modeling of the detector detection efficiency has shown that measuring 1 Bq m^{-2} can be achieved after 40 hours of integration with a detector surface area of 30 cm^2 . 120 hours of operation/lunation (80 hours of operation during daytime/lunation and 40 hours of operation during nighttime/lunation) starting at different times of the day would allow capturing the full diurnal cycle of ^{222}Rn at the landing site and allow the detection of anomalous emissions associated with a venting events (an increase of the local surface activity by a 40 Bq m^{-2} venting event would be measurable within about 1 hour). Detection of a seismic event by the seismometer could be used as a trigger to wake the instrument out of its sleep state if the event occurred outside the nominal integration time window.

The measurement of radon originating from about 800 km around the landing site requires the detectors to be placed near the rim of the lander. The presence of two detection units on opposite sides of the lander, with one in the lander shadow, would allow to better characterize the effect of surface temperature on radon adsorption. The measurement of the local radon flux requires trapping radon atoms as soon as they escape from the ground. This can be achieved by deploying a small accumulation volume containing two small detectors facing a 95 K “cold finger” provided by a Stirling micro-cooler. A flux as low as $1 \text{ atom m}^{-2} \text{ s}^{-1}$ (the terrestrial flux is about $7000 \text{ atom m}^{-2} \text{ s}^{-1}$) would be measured after about 10 hours of integration. Measuring the flux at dawn and dusk is of special interest.

3.7. Impact monitoring science requirements

Impact flashes are very short events, and present ground-based observations are limited by the frame rate of the sensors. For shorter events than the frame rate, light emitted by Earthshine during the exposure time exceeds the light emitted by the flash precluding their detection. The absence of Earthshine on the farside allows for the detection of fainter and shorter events. The detection limit is constrained exclusively by the sensitivity of the detector, and the 10 times closer distance between the detector and the lunar surface (in comparison to Earth-based detections) represents another improvement of the observation conditions.

The instrument field of view should allow for monitoring of the entire farside. For the complementary seismic investigations, the spatial resolution and absolute time recording should be better than 1 km and 0.5 s, respectively. Observations in at least two spectral bands are essential for monitoring the thermal evolution of the impact site and ejecta cloud.

The main technical specifications of the instrument dedicated to impact-flash monitoring include a frame rate better than 0.5 fps, a field of view covering the entire disk of the Moon, the possibility to observe in at least two spectral bands, and a real-time processing of images for downloading only images with positive detections (Oberst et al. 2011). Ideally, one spectral band should be in the visible ($\sim 0.4\text{--}0.8\text{ }\mu\text{m}$), corresponding to peak emissions from the vapor/plasma phase, and a second band should focus on the near infrared ($\sim 1\text{--}2.5\text{ }\mu\text{m}$), corresponding to peak emissions for silicate melts and cooling solid fragments present in the ejecta.

4. MODEL PAYLOAD

The FARSIDE mission consists of two components: an instrumented relay satellite to be inserted into a halo orbit about the Earth-Moon L2 Lagrange point, and a spacecraft that will make a soft landing on the lunar surface. The lander will contain a suite of state-of-the-art instrumentation: a radio astronomy receiver, a broad-band seismometer, a heat flow probe, an electromagnetic sounder, a gamma-ray spectrometer, a radon and polonium detector, and context cameras on the deck and deployment arm. The seismometer and heat flow probe are to be deployed on the surface, and though this could be accomplished by use of a robotic arm, lighter alternatives with fewer degrees of freedom are also available. A separate data acquisition and control electronics system will be shared among the instruments. The relay satellite will contain an impact-flash camera, a second radio astronomy receiver, and a magnetometer. The surface and orbital experiments are synergistic (Figure 15).

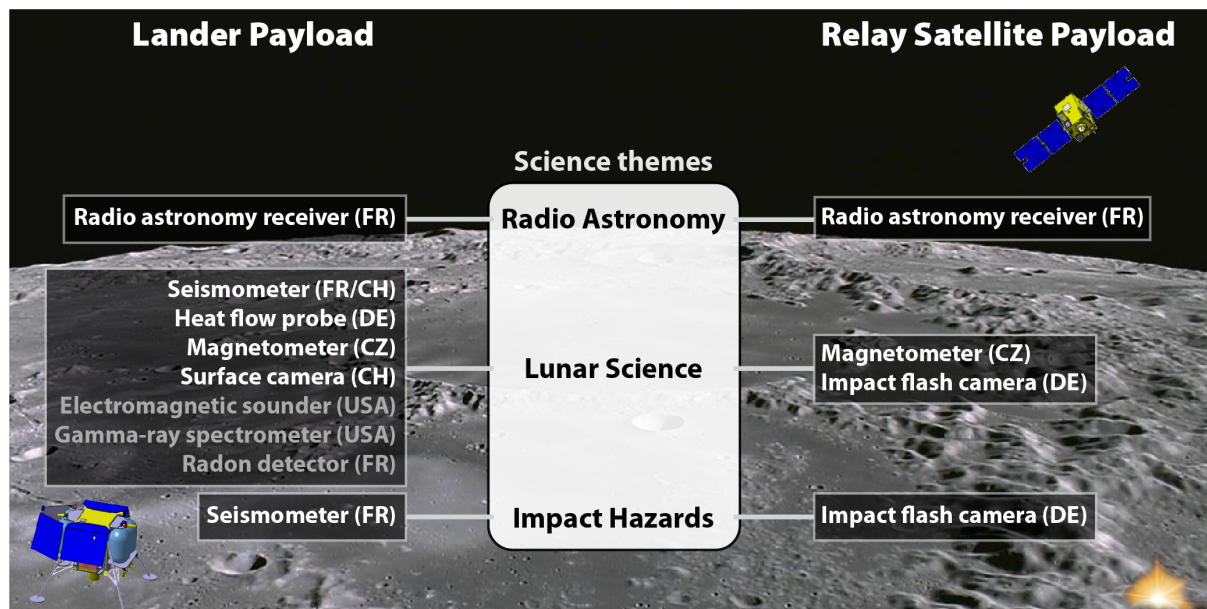


Figure 15. Relationship of FARSIDE science themes to the lander and relay-satellite payload. Instruments in grey are part of the full-science payload. Instruments not depicted are the acquisition and control electronics (CH) and the instrument deployment system. Background image is of the northern portion of the South Pole-Aitken basin.

The amount of mass and power available for the payload of a small lander powered by solar panels and batteries is limited. Preliminary spacecraft mass budgets and margins indicate that all proposed instruments can be accommodated (Section 6). To offer potential descope options, two versions of the lander payload are considered: a **core version** and a **full-science version** (Table 1). The resources of the relay satellite are less critical and pose no constraints on the orbiter payload.

The core version of the lander payload consists of a radio-astronomy receiver, a seismometer, a heat flow probe, and a magnetometer. The full science version contains a second heat flow probe for redundancy, a gamma-ray spectrometer, electrodes for electromagnetic sounding, and a radon and polonium detector. If it is necessary to reduce the mass of the payload, the possibility exists that the radio astronomy and electromagnetic sounding experiments could share common antennas. To reduce the amount of data transmitted to Earth, radio astronomy interferometric correlations could be performed on the orbiter.

Table 1. Lander and satellite payload with mass, power and data budgets. (The acquisition and control electronics have here been accommodated in the SEIS power and mass budgets.)

LANDER					
Payload / Bus	Remark	Power budget		Mass budget	
		Average power / day (W) with 20% margin	Average power / night (W) with 20% margin	Current best estimate (kg)	Mass with 20% margin (kg)
Seismometer (SEIS)	3-axis long period	2.6	2.6	12.5	15
Radio astronomy receiver (RAR)	3 monopoles (5-7 m)	8	1.2	5.6	6.7
Heat flow probe (HP ³)	1 mole	2.2	0.5	3.4	4.0
Surface cameras (CoCam)		1.5	0	1	1.2
Magnetometer (MAG)	3-axis fluxgate	2.5	0	1.2	1.4
Deployment mechanism	2 degrees of freedom	/	/	4	4.8
Core payload		17	4	28	33
Heat flow probe (HP ³)	1 additional mole	2.2	0.5	1	1.2
Electromagnetic sounder (EMS)	4 electrodes	4	0	5.6	6.7
Radon/Polonium detector (DORN)	DORN-1 and 2	1.1	0.3	1.8	2.2
Gamma-ray spectrometer (GRS)		2.5	0	1.4	1.7
Bus communication / Timer		10	Negligible	/	/
Full Payload		37	5	37	45

RELAY SATELLITE					
Payload / Bus	Remark	Power budget		Mass budget	
		Average power (W) with 20% margin		Current best estimate (kg)	Mass with 20% margin (kg)
Impact flash camera (SPOSH)	Infrared and visible cameras	33.6		10	12
Magnetometer (MAG)	2 x 3-axis fluxgate	4.2		1.5	1.8
Radio astronomy receiver (RAR)	3 monopoles (5-7 m)	5.5		2.4	2.9
Total Payload		43		14	17

4.1. Radio Astronomy Receiver (RAR)

The lander and relay satellite radio astronomy experiments consist of a suite of receivers connected to electrical antennas. Full description of the signal from a compact radio source requires 7 parameters (total flux, linear and circular polarizations, source direction, and angular source size). A system of 2 dipoles connected to a receiver allows the measurement of 4 instantaneous quantities (signal auto- and cross-correlations), whereas with 3 dipoles, 9 quasi-instantaneous quantities can be measured (3 auto- and 3 complex cross-correlations) allowing full description of the wave.

Waveform snapshots recorded simultaneously at two locations (the lander and relay satellite) can be cross-correlated to compute the complex visibility corresponding to the instantaneous baseline, or its projection perpendicular to the source direction. Measured time shifts between the two waveforms allow selecting source directions along circles on the celestial sphere prior to correlation. Interferometric measurements will constrain the instantaneous angular extent of strong radio sources along the baseline direction, and will be used to build average low-frequency radio sky maps by global inversion of time series of visibilities.

Antenna design. As shown in Figure 16, the measurement sensitivity is limited primarily by the galactic radio background for frequencies above 1 MHz and is nearly independent of antenna length. In contrast, the sensitivity increases greatly with antenna length for frequencies below 1 MHz. Goniopolarimetric and interferometric measurements require short dipoles compared to the observed wavelength. Thus the radio experiment on the relay satellite, which will focus on interferometry in the range 1–40 MHz, must be connected to 3 orthogonal short dipoles (2–2.5 m). The radio experiment on the lander will perform the sensitive quasi-continuous spectral analysis, goniopolarimetry and waveform capture from 16 kHz to 40 MHz using 2 to 3 long electric monopoles (≥ 5 m); 3 additional short monopoles or dipoles on the lander are required for the interferometric measurements. One possible lander configuration consists of 2 long and 3 short monopoles. The possibility to have only 3 antennas with variable electrical length (through switches) on the lander will be investigated.

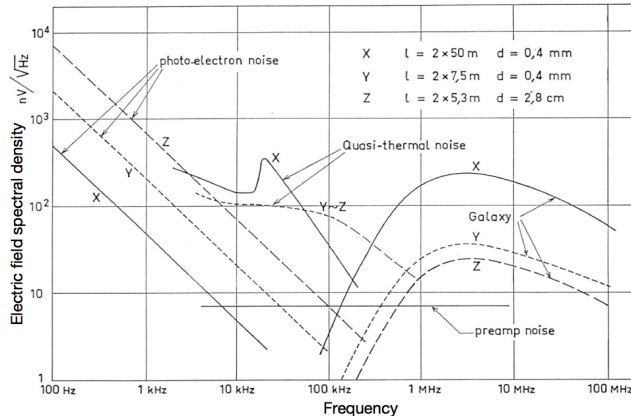


Figure 16. Typical electrical noise densities for three antenna configurations (length, diameter) in the near-Earth solar wind compared to the RAR preamplifier noise threshold.

Instrument characteristics. The radio astronomy scientific objectives require a few kHz spectral resolution at the lowest frequencies and 100-200 kHz at higher frequencies. The radio spectrometer will consist of a low-frequency spectrometer (LFS) analyzing the band 16-1024 kHz in baseband (without frequency shift) and a superheterodyne high-frequency spectrometer (HFS) sweeping through the band 1-40 MHz. In the LFS and HFS, wavelet-like transform and channel auto- and cross-correlations provide flux and polarization spectra that are compressed and sent to the digital processing unit (DPU). Waveform capture will be performed by a time domain sampler (TDS) digitizing voltages from the dipoles at ~ 50 Msamples/sec ($\times 12$ bits). It is possible to combine the TDS with the HFS in order to digitize a limited spectral band at a reduced sampling rate. The digitized waveform can be processed locally for event detection, synchronous and de-dispersion, or sent to the relay satellite for computing interferometric visibilities by cross-correlation. Waveform processing can be done in the TDS or alternatively the TDS can be restricted to A/D conversion and the processing done in the DPU. The radio astronomy experiment on the lander will include the LFS+HFS+TDS connected to the above long and short antennas, whereas the radio astronomy experiment on the relay satellite will include only the TDS connected to 3 short dipoles.

Performance assessment. With a typical receiver noise of $7 \text{ nV Hz}^{1/2}$, the sky-limited sensitivity regime is reached above 1 MHz for monopole lengths of 1–2 m, while lengths ≥ 5 m significantly increases the sensitivity below 0.5–1 MHz (Figure 16). Goniopolarimetric measurements will have a directional accuracy of $\sim 2^\circ$. For interferometric measurements, a separation of $\sim 30,000$ km between the lander and orbiter allows a maximum interferometric angular resolution of about $3''$ at 1 MHz for discrete sources, but interplanetary and interstellar scattering of radio waves limit the effective angular resolution to $\sim 1''/f^2$ (with f in MHz). Sky images synthesized via the inversion of long series of measurements will thus have a coarser resolution.

Instrument resources. Triads of short dipoles will have a mass of 1–1.5 kg (including deployment system). Long monopoles (5–7 m) such as the ones used on the STEREO spacecraft have a mass of ~ 1.3 kg per monopole. These masses are upper limits compared to the tubular antennas from SRC-PAS that we plan to use for FARSIDE. Three colocated preamplifiers at antennas base have a total mass of 500 g and a peak power consumption of 1.5 W. LFS and HFS based on the receivers developed in LESIA have a total mass of 750 g (for 3 input channels) for a volume $< 2000 \text{ cm}^3$ and a power consumption of ~ 2.5 W. The TDS will have a mass ~ 400 g and a power consumption ~ 4 W. The total mass and power for the lander is ~ 5.6 kg and 8 W, and for the relay ~ 2.4 kg and 5.5 W. The power consumption of the DPU (1-3 W) must be added, as well as the mass of the DPU and Power Supply Unit (~ 400 g each) and of the mechanical boxes and harness (~ 2 kg), but parts of these will not be necessary if there is a FARSIDE acquisition and central electronics system (FACE).

The LFS and HFS data rate can be adjusted between ~ 100 bps and ~ 1000 bps, and onboard lossless compression allows a reduction by a factor of about 1.3. Further reduction can be obtained by a $< 100\%$ duty cycle. Waveform capture produces a raw data rate $\sim 6 \times 10^8$ bps during brief snapshots timed to be compatible with the transfer rate to the relay satellite and/or storage capability.

Specific interface requirements. Electromagnetic cleanliness is an important requirement for sensitive and accurate radio measurements, and the orientation of the antennas should be known a posteriori with an accuracy ≤ 1 m and 1° . During interferometric measurements, accurate

synchronization between the lander and orbiter is required. A central processor on the relay satellite is desirable to correlate the lander and orbiter data streams in order to obtain the complex visibility function of an observed celestial source.

Preliminary management plan, heritage and TRL. Antennas will be provided by SRC-PAS (Poland), where short dipoles have a TRL 8-9 (heritage from RELEC, JUICE) whereas longer and variable-length antennas have a TRL of ~ 4 . Alternative solutions include triads of short dipoles developed by Radboud University Nijmegen with TRL 3-4, and long monopole antennas used on STEREO (from SSL/Berkeley, with TRL 9; Bougeret et al. 2008). Preamplifiers would be provided by LESIA. Present models (used on Cassini, STEREO, and BepiColombo) have a TRL of 9 but are limited to 20 MHz. Adapting preamps to the range 16 kHz-40 MHz implies a present TRL 5-6. Alternatives include TARANIS HF preamps developed by the LPC2E (TRL 8-9) or JUICE/RPWI preamps provided by ISAS/Japan (TRL ~ 8). The LESIA LFS and HFS have numerous predecessors (WIND, Ulysses, and Cassini; Gurnett et al. 2004), STEREO (Bougeret et al. 2008), and BepiColombo, and dedicated signal processing algorithms and software have been developed. Their concept is very mature with a TRL about 8. The TDS is also a mature concept with a TRL of 4-5 at LESIA, but procurement would rather rely on Radboud University Nijmegen or other participating laboratories (ASTRON, IRFU, LPC2E, IAP/Prague).

A new receiver concept of “stacked” ADC receiver (100 MHz \times 20 bits, ~ 100 dB dynamic range) is being developed by LESIA and Sup’Telecom Paris with CNES support, that would allow to save $>20\%$ of the receiver (LFS+HFS+TDS) resources while allowing us to implement advanced onboard processing (including RFI mitigation and smart averaging). The TRL will be 3-4 in 2015 (end of development), and 7 in 2018 (flying onboard the Circus nanosatellite), and may thus be an interesting alternative to the present design.

LESIA has a long experience in spectrometry and goniopolarimetry. Bandpass calibration and processing of interferometry data is expected to benefit from the ground-based expertise from Dutch laboratories (Radboud, JIVE, Groningen, ASTRON).

4.2. Seismometer (SEIS)

The FARSIDE seismometer is based on the instrument that is scheduled to fly on NASA’s InSight mission to Mars in 2016 (Figure 17). It is composed of a sensor assembly that encloses three very broad-band (VBB) oblique sensors, secondary sensors (temperature, tilt meters), a leveling device, and acquisition and control electronics. The VBB sensor itself (Lognonné et al. 2000), designed at IPGP (France), is an inverted leaf-spring pendulum with a highly sensitive displacement transducer and feedback, and the electronics are provided by ETH Zurich (Switzerland).



Figure 17. The SEIS flight model that is being developed for NASA’s geophysical discovery mission to Mars, InSight (launch in March 2016).

Deployment and shielding. The deployment system is locked during launch, cruise and landing. The seismometer, along with its thermal shield extending 0.5 m from the SEIS outer diameter, is deployed on the surface at a distance exceeding 1 m from the lander. Once deployed, the sensor assembly is decoupled from its thermal shield. Leveling is performed by the seismometer itself, so the only specification is to deploy the instrument within $\pm 23^\circ$ with respect to local gravity. An alternative,

simpler deployment system could be a simple arm rotating around a vertical axis equipped with a hoist (this would allow a 1 m deployment from the lander, but would increase the mass by 1.7 kg). A robotic arm similar to InSight Instrument Deployment System (IDS), weighting about 7 kg, could also be envisioned.

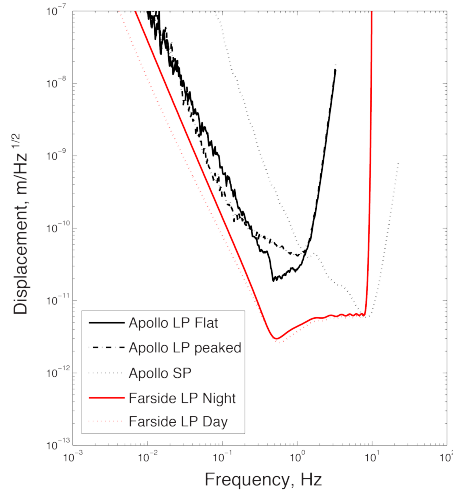


Figure 18. Comparison of the Apollo and SEIS frequency responses. Apollo curves (black) were estimated during non-seismic periods, and SEIS (red and green) are from hardware tests. SEIS is considerably more sensitive and possess a wider frequency response than the Apollo seismometers.

Thermal control strategy. With a significant temperature excursion and a long night duration, SEIS thermal control is a key element. SEIS is already qualified to withstand -120°C non-op during the lunar night, allowing a safe mode for the instrument with a very low power consumption. During the night, heaters will be used to allow the instrument to stay within its operational temperature window boundary (over -80°C).

Data production and performance. The measurement objectives dictate continuous data collection in order to detect as many seismic events as possible over the 4-yr nominal mission. The instrument records 24-bit data continuously at 20 samples/sec, stored in a mass memory. To save power during the night, the displacement transducers are operated at a lower voltage with reduced performances (Figure 14). Even in this case, SEIS resolution and noise represent major improvements over Apollo. In the Apollo bandwidth (0.1–10 Hz) the VBB sensor is 10–20 times better in resolution than the best Apollo output, and digitization noise is below sensor noise. Frequencies outside the Apollo bandwidth are explored for the first time below 20 mHz (Figure 18). Impact events will be an important source of seismic signals, which will be localized by the relay satellite impact flash camera.

Mass, power, and data budgets. The current best estimate for the mass of SEIS is 12.5 kg (15 kg with 20% margin). During daylight, the seismometer power is 2.6 W and 4.9 Gbits of raw data are generated over 14 Earth days. The night mode allows a reduction of power consumption. The seismometer records continuously during both lunar day and night, generating 22.4 Gb of raw data per lunation. Limitations in downlink volume make it impossible to return all SEIS data at the highest instrument rates. A “quick-look” selection strategy (where only low frequency data plus ground selected windows of high frequency data are uploaded) leads to about 6.3 Gbits of data downloaded per lunation; on board compression would reduce this by a factor of about 2.

SEIS instrument heritage. SEIS relies on the design and development experience of several missions and projects. The VBB is derived from the OPTIMISM experiment developed for the Russian Mars '96 mission and SEIS for the European NetLander and ExoMars missions. The current version of SEIS is slated to launch as part of the NASA InSight mission in 2016. Vibration tests have been performed during previous projects at levels expected for a Soyuz launch. No new technology developments are required.

4.3. Heat Flow and Physical Properties Package (HP³)

The Heat Flow and Physical Properties Package (HP³) is an experiment that places a probe into the lunar regolith to a depth of 3 m by means of self-hammering mechanism. This experiment description is based on the HP³ as designed for NASA's InSight mission to Mars, to be launched in 2016. The

HP³ is being developed by DLR, Germany (Figure 19) in cooperation with the Space Research Center of the Polish Academy of Sciences (CBK), Poland.

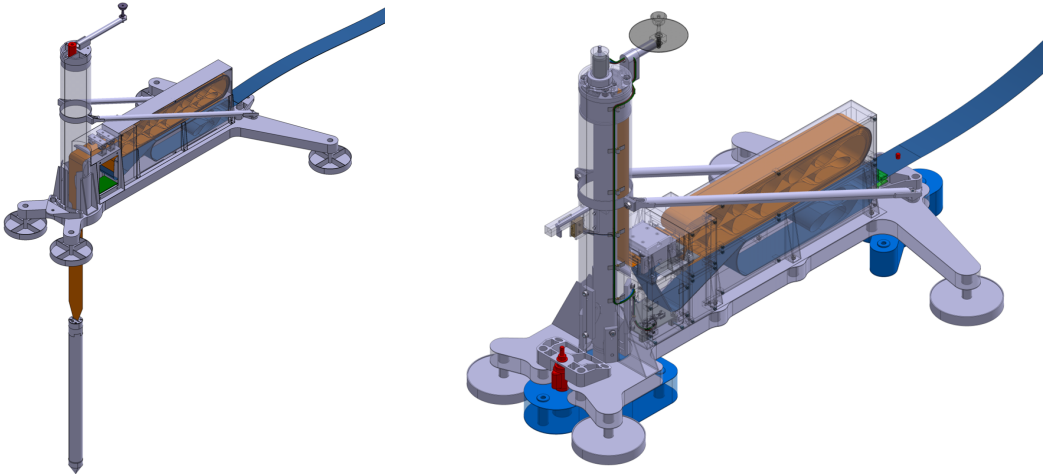


Figure 19. (left) HP³ system showing the deployed mole (towards the bottom), science tether (brown), support structure (gray), and engineering tether (blue). (right) Same, but undeployed.

HP³ sensors include temperature sensors and heaters that measure the thermal gradient and thermal conductivity using a line-heat source approach, as well as motion and tilt sensors that determine the instrument position in the ground. The instrument consists of four subsystems: the mole that houses the internal hammering mechanism to provide penetration into the regolith, the tilt sensors that determine instrument orientation, and heaters for thermal conductivity determination; an instrumented tether that provides power and data link between the mole and surface and that acts as a carrier for the temperature sensors for the thermal gradient measurement; the support system that provides secure in flight storage of all subsystems and houses the tether length monitor; and the back end electronics that are located in the lander warm electronics box.

Deployment and performance. After verification and release of launch locks, the HP³ is placed on the ground by the robotic arm >1 meter away from the lander. If a robotic arm is not provided, a dedicated unfoldable boom could also accomplish deployment. Such a system weighs approximately 2 kg, has a single degree of freedom, and is capable of a 3 m deployment distance.

During penetration, which can take up to 6 lunations because of intermittent thermal conductivity measurements, the HP³ displaces any subsurface rocks that are less than 2 times the mole diameter or deflects from larger rocks. If penetration is stopped before reaching the target depth of 3 m, heat flow measurements can still be achieved, but with reduced accuracy. The minimum penetration depth to achieve the science goal is 1.5 m. In this case, the heat flow uncertainty would increase from 10 to 15%.

There are two phases to instrument operations: (1) Penetration: soil intrusion is achieved by mole hammering. The net hammering time is expected to be ~24 hr to reach the final depth of 3 m, but hammering can be interrupted every 50 cm to conduct thermal conductivity measurements. A period of up to 10 Earth days after each hammering episode is needed to reach a sufficiently equilibrated thermal state before each measurement starts, and heating then takes up to 168 h. (2) Monitoring: this begins when terminal depth is reached, and consists of column temperature readings every hour through end of mission.

Thermal control. Electrical heaters in the mole are required to thermally condition the instrument prior to operations. The back-end electronics are accommodated in the lander's warm electronics box and need no survival heaters. Depending on the operation scenario, the tether length monitor may need survival heaters during the lunar night. Alternatively, the penetration phase can be compressed such that the length monitor is operated during the first lunar day only.

Mass, power, and data budgets. The weight is estimated at 3.35 kg for a complete mole system and 5.9 kg for a dual-mole system. Maximum power consumption occurs during hammering and is 17

W, with a minimum during monitoring at 2.2 W. Data rates are extremely low: penetration phase 0.1 Mb/hr; monitoring phase 20 kb/hr.

Instrument heritage. The HP³ instrument has been developed for flight on NASA's InSight mission to Mars, and the instrument has passed CDR in April 2014. The instrument therefore has reached TRL 6, and modifications necessary for a lunar application are expected to be small. Pre-InSight prototypes have demonstrated that penetration into lunar regolith simulant is feasible, and future instrument optimization will focus on further improving the mole's penetration performance and tunable power settings.

Future Development. Further development of the mole concept is focused on implementing an electromagnetic direct drive system termed EMOLE, which is currently under development in the framework of the ESA-PECS project. The project is executed at CBK-PAN and scheduled to be finished by mid-2015. The EMOLE mechanism has been designed to fit into the HP³ mole hull, and the drive system is thus fully compatible with the present TRL design. The major novelty of the EMOLE concept is twofold: (1) Due to the simpler mechanical design, the penetrator will have much higher reliability, and (2) the new drive system can operate at different power settings, which can be realized through the electrical power supply. EMOLE has significant heritage from the MUPUS penetrator, flown onboard the PHILAE lander on ESA's Rosetta mission, the CHOMIK sampling device flown on the ill-fated Russian Phobos-Grunt mission, as well as the HEEP prototype (High Energy and Efficiency Penetrator). As compared to the HP³ mole, the EMOLE will increase the total hammering energy from 0.8 to 2.25 J. The EMOLE will reach TRL 6 at the end of the ESA-PECS project.

4.4. Surface and orbital magnetometers (MAG)

The magnetometer experiment comprises two components: a 3-axis fluxgate magnetometer on the surface, and two 3-axis fluxgate magnetometers on the relay satellite. The magnetometers are based on those developed by the Czech Technical University in Prague and consist of two sensor heads and an electronics box connected to the sensors by twisted-pair cables (Figure 20). One of the key parameters of the magnetometer is the accuracy of the measured vector field. For the ring cores, the fluxgate transducers use a stable and low-noise, field-annealed amorphous magnetic material.

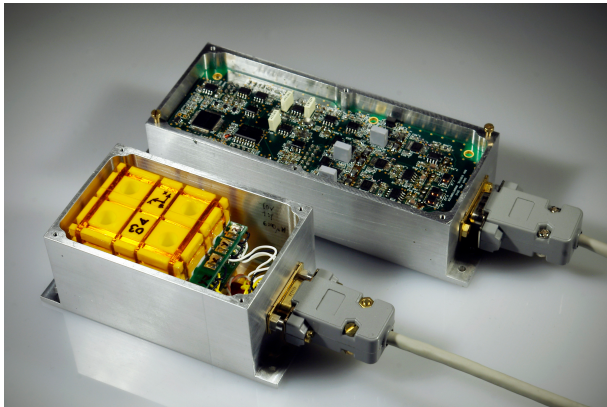


Figure 20. The magnetometer developed by the Technical University and Czech Space Research Centre s.r.o. for the Technology Agency of the Czech Republic.

Deployment and thermal control. For the relay satellite, the sensor heads must be mounted on a 3-4 m long boom in order to minimize magnetic noise from the spacecraft. By placing one sensor head at the end of the boom and the other closer to the spacecraft, any remaining magnetic signature and noise of the satellite will be estimated and corrected. The two instruments are redundant as the electronics are concerned. For the lander, the magnetometer will be placed on a 1.5-meter long boom. Magnetic cleanliness procedures will be performed for both the relay satellite and lander in order to minimize their magnetic signatures. This will include optimized layout of solar panels to limit current loops that could create interfering magnetic fields.

The unregulated voltage is supplied to the magnetometer by a dedicated input connector, and the telemetry/telecommanding with the communication bus is carried out by standard protocol (i.e., RS422 or LDVS) via another dedicated connector. To timestamp the measurements with sufficient

accuracy, a synchronization signal will be provided to the instrument. Alternatively, the analogue parts of the magnetometer could be plugged into a central electronics box. The instrument electronics operate in the temperature range $\pm 50^\circ \text{ C}$ and can survive in the range $\pm 60^\circ \text{ C}$.

Performance. The magnetometer total dynamic range is $\pm 65536 \text{ nT}$ to 0.0625 nT (21 bits), and its linearity is 0.001% of the full scale. The instrument range will be switchable, as the expected magnetic field is below 1000 nT. The intrinsic sensor noise is as low as 15 pT RMS in the band 0.05–10 Hz, and the intrinsic electronics noise is 63 pT RMS at the highest range in the same band. At the lowest range the electronics noise becomes negligible. The thermal and long-term zero stability is less than $\pm 1 \text{ nT}$. The thermal offset drift is below 0.1 nT/K for the sensor and $\sim 0.05 \text{ nT/K}$ for the electronics.

Mass, power, and data budgets. The total mass of the relay satellite system is 1.5 kg, and the estimated power is 3.5 W. For the lander, the total mass is 1.2 kg with a total power consumption of 2.5 W. The sampling frequency is nominally 50 Hz and the data rate corresponds to ~ 200 bytes/second. The sampling frequency can be adjusted during operation to fit the scientific needs up to 200 Hz.

Instrument heritage. The magnetometer is derived from the instrument flown on the Mimosa satellite (Cerman et al. 2003) and from the instrument developed in collaboration with the Czech Space Research Centre s.r.o. company. A similar magnetometer design was used on Oersted, Astrid-2, CHAMP and other satellites. Members of the team have participated in the development of magnetometers and calibration systems for the Oersted and Swarm satellites (Nielsen et al. 1995, Petruha et al. 2009).

4.5. Surface electromagnetic sounder (EMS)

The surface electromagnetic sounding experiment requires the measurement of horizontal electric (E) and magnetic (B) fields. The proposed instrument uses high-heritage E-field sensors based on the instrument in development at the Southwest Research Institute (US) and the University of California, Berkeley (US), and the magnetic sensors will be provided separately as described in section 4.4. Spring launchers (Figure 21) deploy electrodes on the surface to measure the horizontal E-fields (four electrodes on the surface yield two orthogonal components). The addition of a fifth vertical electrode is being investigated, but is not required to meet the science goals.

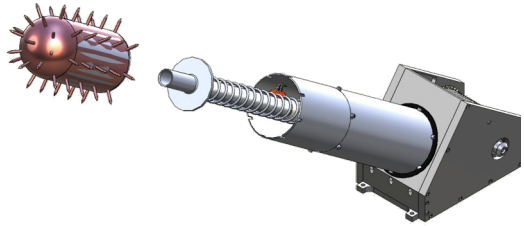


Figure 21. Electrode deployment system. Four electrodes will be launched off the four sides of the spacecraft to a distance of 10 meters using spring launchers.

Data production and performance. The EMS operates in two modes: low- and high-rate. Low-rate acquisition from the electrometers at 20 samples/sec (sps) is the norm and covers the mantle and core objectives. The high-rate acquisition at 256 sps allows for intracrustal sounding and occurs only for 10 min/day during daylight and 1 min/day during the night. The EMS has a 50% duty cycle during the lunar day and a 1% duty cycle during the night. This short duration during the night samples frequencies $>10^{-3} \text{ Hz}$ that form the basis of the deep mantle investigations. The instrument performance is 0.1 mV at 1 mHz and 1 μV at 1 Hz, which is 100 times better than required by the science objectives.

Data from the EMS sensors must be acquired at relatively high rates to investigate the crust and upper mantle, and must be acquired over long baselines (days) to delineate deep mantle and core structure. EMS satisfies these two requirements within downlink data volume limits by adjusting the duty cycle and taking high-rate data during discrete time periods when the external EM signal is

expected to be strongest. The exact time can be changed from the ground to sample different parts of the lunation if desired.

Mass, power, and data budgets. The sensors are designed to survive the full lunar temperature range and are heated by their own power dissipation. With two times onboard lossless compression, the data rates are 1.1 Gb/lunation. The EMS has 16 Gb of NVRAM and can store several months of data, although data are automatically downloaded to the lander at the beginning of each lunar day and downloaded at 24 hr intervals during the lunar day. The full payload has a mass of 4.4 kg (5.3 kg with 20% margin) and uses 2.7 W.

EMS instrument heritage. The E-field sensors are based on those designed by UC Berkeley who have decades of experience with these sensors. UC Berkeley has developed the deployment mechanisms and central sensor electronics, whereas SwRI has developed the digital processing, power supply, and system integrations. SwRI is an established supplier of spacecraft avionics and power supplies and is the payload integrator for IMAGE, STS-ATLAS, and MMS.

Specific requirements. The electrometers and magnetometers are deployed away from the spacecraft at distances that minimize interference and contamination from other spacecraft components. An electromagnetic interference/compatibility (EMI/EMC) control plan will be implemented that follows GSFC-STD-7000 (“GEVS”) at a minimum. Recovery of the horizontal E-field depends only on knowing the sensor locations, and this will be accomplished by imaging the deployed electrometers with the surface cameras. If the sensor locations are known to within ~ 0.1 m, the E-field error will be negligible (<0.5%).

Development track to TRL 6. The EMS has not flown as a system, but its components have high heritage. The only new component is the E-launcher, and a prototype with flight-like parts was tested under ambient conditions and deployed to 180% of the required distance. The El-launcher does not have heritage in the prolonged cold of the lunar night, but the E-launcher deploys during daylight and all electronics are in the spacecraft warm electronics box.

4.6. Context Camera (CoCam)

Context cameras on the lander are required to establish the geological context of the geophysical measurements at the deployment site, investigate the lunar regolith from large rocks to grains down to the order of 10 μ m in size, and monitor the lunar surface. In addition to these scientific questions, surface cameras are required to enable and support instrument deployment by providing 360° panoramas and 3D stereo images of the lander’s surrounding, select instrument deployment sites and eventually deploy the instruments, and allow refining the exact position and orientation of the lander by comparison with high-resolution imagery from orbit.

The CoCam (Context Cameras) instrument is composed of 2 cameras, LRAC (Lunar Robotic Arm Camera) and LOC (Lunar Overview Camera), accommodated such that imaging from the lander base up to the lunar horizon is possible. The LRAC is a color close-up camera accommodated on the robotic arm of the lander and the LOC is a wide-angle camera accommodated on the deck of the lander.

Instrument design. The LRAC (Figure 22) is a powerful miniaturized, low-power, efficient and highly adaptive imaging system. It is composed of optics with a focus mechanism (FOV of $14^\circ \pm 2^\circ$ diagonal), a direct high-resolution color image sensor ($2652 \times 1768 \times 3$ pixels), and controlling/processing electronics. The LRAC color detector keeps the spatial resolution so that no Bayer filter is needed, and the instrument will perform autofocus and auto-exposure before taking images. Thanks to the focus mechanism (mobile lenses), the instrument can take images of an object located at distances from 10 cm to infinity. The angular image resolution at the centre is <80 μ rad/pix, with spatial resolutions of 7 μ m/pixel at 10 cm (viewed area 1.9×1.3 cm), 39 μ m/pixel at 50 cm (viewed area 10×7 cm), and 79 μ m/pixel at 100 cm (viewed area 21×14 cm). Depending on the depth of field, a target can be sharp on different areas of the images; using an embedded z-stacking algorithm, it is possible to combine all those images to produce an image sharp on every part of the object. With this process, a z-stacking map is generated, containing the object distance information and enabling the creation of a numerical model of the local micro-topography. The LRAC is designed to operate from -120°C to $+30^\circ\text{C}$, and to survive temperatures from -120°C to $+50^\circ\text{C}$ without an active thermal system.

The LOC is composed of fixed 100° FOV optics, a Star1000 1024×1024 pixel detector, and controlling/processing electronics. The angular image resolution is 1.8 arc-minutes/pixel, with spatial a resolution of ~0.5 mm/pixel at 1 meter. The LOC is designed to operate from -120°C to +30°C, and to survive temperatures from -135°C to +50°C without an active thermal system.

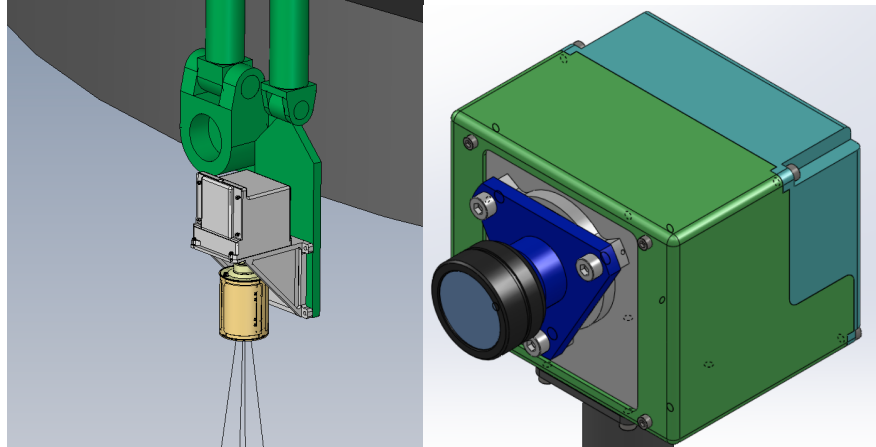


Figure 22. CAD view of the LRAC (left) and LOC systems (right).

Mass, volume, interfaces and data rates. The LRAC is 170×100×80 mm in size, with a mass of 760 g (950 g including 20% margin). The camera will be operational only for a small duration each day, during which time the maximum mean power consumption is <15 W including 20% margin. The electrical interface is SpaceWire on LVDS. The instrument can store 4 Gb of data. Quantization can be 8 bit or 14 bit, and binning/windowing can be performed in order to decrease the data volume. Z-stacking also induces a reduction of the data produced by the instrument by downloading more information-rich images. The LOC is 80×120×80 mm in size, with a mass of 250 g (300 g including 20% margin). The maximum mean power consumption is 6 W (including margin). The electrical interface is RS422. The instrument can store 4 Gb of data. Quantization can be 8 bit or 12 bit.

Design and flight heritage. The LRAC has direct heritage from the CLUPI instrument, currently part of the science payload on the ESA ExoMars 2018 mission. The LOC 100° optics has direct heritage from the PROBA-2 mission, and the Star1000 detector has extensive space heritage.

4.7. Gamma-ray spectrometer (GRS)

The surface gamma-ray spectrometer (GRS) is based on the instrument that is being developed at the Johns Hopkins University Applied Physics Laboratory (USA). The GRS is a compact instrument consisting of three CsI scintillators read out with low-resource photodiodes (Figure 23). The GRS is sensitive to gamma rays with energies in the range 300 keV to 10 MeV, which includes signatures for elements of interest (Fe, Mg, Ca, Al, Si, O, Ti, K, Th, and U). The sensors provide omnidirectional measurements from the surface of the Moon; the large mean free path of gamma rays allows the GRS to sample the regolith to tens of centimeters depth. Advantages of CsI include its good energy resolution (superior to NaI and BGO), ability to operate at room temperature (eliminating the need for cryogenic cooling), and spaceflight heritage. Statistically significant measurements will be obtained within the span of tens of hours to a few days.

Mass, volume, and data rates. The instrument is composed of three sensors, a digital processing unit, and harnesses. The total estimated mass is 1.4 kg (1.7 kg for 20% margin). The science objectives can be obtained with daytime measurements only, and power consumption during the day is estimated at 2.5 W. Data rates during the day are low, 10-100 bps. The sensor size is 8×8×8 cm³, and the size of the DPU is 10×15×5 cm³. The duty cycle is simple where the instrument is turned on and spectra are collected with a commandable and flexible data rate.

Major system constraints. The primary constraint on the gamma-ray spectrometer is that the sensors have a clear view to the surface, given its 2π viewing geometry. The sensor can be body mounted to the lander, or placed on the surface by a robotic arm.

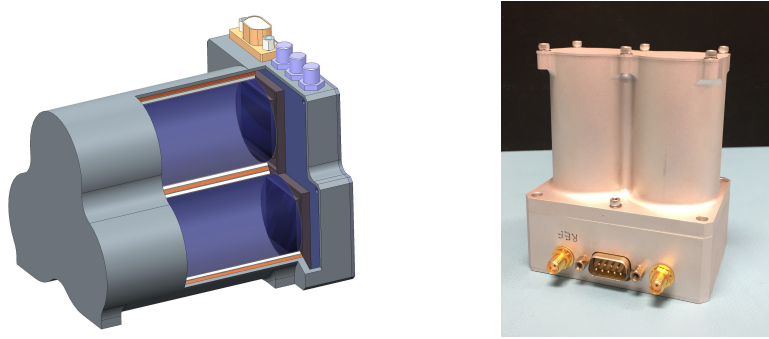


Figure 23. (left) CAD rendering of the GRS, including a cutaway of the housing to expose the CsI scintillator (purple) and photodiodes (brown). (right) GRS prototype, which flew on the BOPPS high-altitude balloon on Sept. 14, 2014.

Instrument heritage and TRL. CsI gamma-ray scintillators have flown on multiple spaceflight missions, including U.S. national security missions, the NASA Mars Science Laboratory (MSL), and the Chinese Chang'e-1 mission that orbited the Moon. A photodiode readout is currently implemented on the MSL Radiation Assessment Detector (RAD). The GRS electronics are based on similar electronics that operated the Gamma-Ray and Neutron Spectrometer (GRNS) on NASA's MESSENGER mission. A prototype of the GRS was flown to the edge of space on a Balloon Observation Platform for Planetary Science (BOPPS) in September 2014, validating its sensor and electronics performance in a space-like thermal and radiation environment. The proposed GRS instrument is thus considered TRL6.

4.8. Radon and polonium detector (DORN)

The radon detector DORN (for “Detection of Outgassing Radon”, after the name of the physicist Friedrich Dorn, who discovered radon) is a light, simple and long-heritage sensor aimed at measuring ^{222}Rn , ^{210}Po , ^{220}Rn and their short- and long-lived decay products (^{218}Po , ^{214}Po , ^{210}Po , ^{216}Po , ^{212}Pb , ^{212}Bi , and ^{212}Po) by alpha spectroscopy in the 5–10 MeV energy range with sets of Planar Implanted Passivated Silicon detectors (PIPS® Areva/Canberra). Each detection unit is made of a series of 6 cm^2 detectors that are paired to provide efficient background rejection of cosmic rays by anticoincidence. Energy calibration is achieved using appropriate radionuclides deposited on the surface of the detectors.

Accommodation. The instrument suite is split into two modular and independent subsystems: DORN-1 and 2. DORN-1 is a subset of alpha detectors (1 or 2 detection units made of 5 pairs of detectors) aimed at measuring radon and polonium atoms around the lander. This is an “exospheric” instrument: located near the rim of the lander platform, it points toward the ground, either in the close vicinity of the lander or toward remote targets, to measure atoms adsorbed on the surface.

DORN-2 is made of two pairs of small alpha detectors aimed at measuring the subsurface flux of radon at the landing site. This is a contact instrument, which must be laid on the ground and be able to trap atoms released from the ground before they escape using an accumulation volume. These atoms are trapped by a “cold finger” (facing the detectors), whose temperature of ~95 K is reached by means of a small 185 g Stirling micro-cooler (Ricor K562S). The accumulation volume ($20 \times 20 \times 5 \text{ cm}^3$) could be deployed together with the HP³ mole system.

Mass, volume, and data rates. The masses of DORN-1 and 2 are 1.2 and 0.9 kg, respectively (including 20% margin). The size of DORN-1 is only $200 \times 150 \times 25 \text{ mm}^3$. The instruments are low power, requiring only 1.1 W for operation of both during the day, and only 0.3 W for minimum operations during the night. Data rates are only 0.2 Gb/lunation.

Instrument heritage. The silicon detectors of DORN and their acquisition chain benefits from the long heritage of APS (Alpha Particle Spectrometers) and APXS (alpha particle X-ray spectrometers) that have flown on numerous spacecraft. Novel developments pertain to the mechanical mounting of the silicon detectors, which are grouped by pairs for background rejection. A

breadboard of DORN-1 was built in 2014 with CNES funding that reached TRL 4, and functional tests are currently being performed (Figure 24).

Development track to TRL 6. In 2015, efforts will focus on the reduction of the size, mass and power of the detection unit, and on the design of the accumulation volume and mini-cooler/detectors assembly for DORN-2. Environmental (thermal and mechanical) tests of DORN subsystems and tests of the anticoincidence unit in a proton irradiation facility will be conducted in 2016.



Figure 24. Front and rear view of the DORN-1 breadboard, with silicon detectors, connectors and mounts exposed on the right.

4.9. Impact monitoring camera (SPOSH)

The impact-monitoring camera is based on a modified version of the Smart Panoramic Sensor Head (SPOSH) that is being developed by DLR, Germany. SPOSH is an assembly of detectors to observe meteoroid impacts on the farside of Moon from meteoroids with masses larger than a few grams (Oberst et al. 2011).

The camera comprises two main parts: SPOSH-VIS for observations in the visible (400–800 nm), and SPOSH-IR for observations in the near infrared (1000–2500 nm). Each of these contains separate camera heads (CH) that consist of an optical telescope with an approximately 0.5 m focal length and a detector unit. Both SPOSH units are enclosed in a common housing, and a common digital processing unit (DPU) on flexible printed circuit boards is folded around the camera heads (Figure 25). The cameras both take three images per second and use CCDs with a pixel size of 1024×1024 and 14 bit intensity resolution.

Deployment and performance. SPOSH-VIS and -IR will start operations after the positioning of the relay satellite in the L2 halo orbit. Images of star fields will be used for geometric and radiometric calibration of the two camera heads. The SPOSH DPU uses powerful event-detection software, and in typical operations the DPU will reduce the data stream dramatically by transmitting only those portions of images that contain events. During the commissioning phase, full image frames will be stored and transmitted to Earth for evaluation and setting of the detection thresholds.

Thermal control. The operating temperature of the VIS and IR detectors is between -20° and -80° C, respectively. The preferred cooling mechanism is radiative cooling by radiators to free space, though cooling by Peltier elements is an alternative. The operating temperatures of other parts of the instrument are about 10° C and the non-operating temperature shall be not lower than -10° C.

Mass, power, and data budgets. The mass of the instrument is estimated to be 10 kg, and the required power is estimated to be lower than 8 W. An additional 10 W for each sensor would be required in the case of an active cooling system. The overall instrument dimensions are estimated to be 13×30×25 cm³. For an estimated 1000 observed events per year 10-20 Mb of event data are expected, or about 25-50 Kb per day. However, the data rate may be variable, and during meteoroid showers, data rates may increase 20-fold.

Specific requirements. To assure high data quality, low detector temperatures have to be maintained. To ensure event localization with pixel precision, the pointing stabilization of the relay satellite is required to be better than ~8 arcsec/sec, and the pointing knowledge better than ~4 arcsec (supposing optical focal lengths of ~0.5 m for detectors with 13 μm pixel pitch as used in the classical SPOSH breadboard). Impact events will be localized in time to better than 0.3 seconds, and the spatial

resolution will be determined by the chosen focal length. SPOSH-VIS and SPOSH-IR will operate continuously after commissioning, and twice a year, calibration of the instrument using imaging of star fields will be performed. The instrument must be pointed so that the Sun does not enter the instrument's narrow field of view.

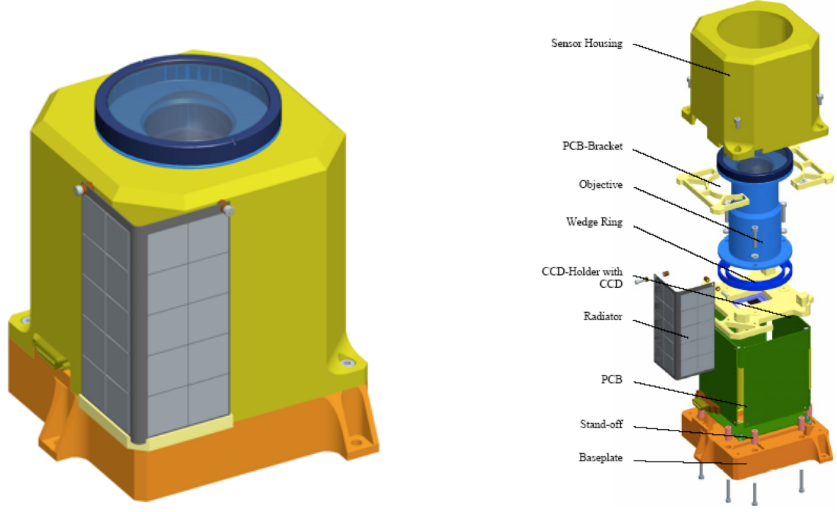


Figure 25. Integrated (left) and exploded (right) view of a single wide-angle SPOSH designed for visual meteor observations.

Instrument heritage and TRL. Jena Optronik and DLR developed and built a SPOSH breadboard in 2003/2004. The camera was developed under contract for ESA/ESTEC explicitly for monitoring of planetary night hemispheres from an orbiting spacecraft in the visual spectral range. The breadboard is prepared to interface with a spacecraft bus, and all 4 breadboards have undergone thorough outdoor testing. In 2008/2009, an infrared version of the SPOSH breadboard was developed and built for ESA/ESTEC.

SPOSH-VIS is estimated to have reached TRL 6. For FARSIDE, the fish-eye-like optics in the SPOSH breadboards will have to be replaced by narrow-angle optics with larger focal lengths, similar to that of the established optics of the super resolution channel of the HRSC on Mars Express. The implementation of a special fast photometer will be investigated, as well as gray filters and/or high dynamic range techniques to enable SPOSH to observe sunlit surfaces.

4.10. FARSIDE Acquisition and Control Electronics (FACE)

The FARSIDE Acquisition and Control Electronics (FACE) are responsible for acquisition and control of the seismometer and all other instruments requiring continuous night and day operation. This instrument is based on the acquisition electronics of the InSight seismometer, provided by ETH Zurich (Switzerland). Use of a common acquisition system on the lander is expected to reduce the mass and power constraints of the combined payload in comparison to the numbers quoted in this proposal. As FACE is central to the mission and essential to operate the core sensors, it is built redundant with cross-strapped sensor interfaces. FACE consists of three main blocks:

DC/DC converter module. This module receives the primary voltage from the lander's power distribution unit. The input power filter serves to limit surge currents and voltage ripple on the input power line and attenuates the electromagnetic interference (EMI) coupled to the input power. It provides the required secondary power lines to the different sensors and sub units. The secondary power lines are regulated and are protected against over-current, under- and over-voltage.

Control electronics module. This module controls all instruments, even when the lander is in sleep mode. It contains a FLASH mass memory (8 Gbit) as an intermediate data storage. This module also controls the digital interfaces to the lander (serial command and telemetry interfaces) and controls the instruments and sensor assemblies via dedicated interfaces. Instrument control, data processing and data packaging is provided by resident software running on a low-power

microprocessor. The implementation is on low-power FLASH based FPGAs. Due to the power constraints the data processing is limited.

Acquisition electronics module. This module acquires the pre-amplified scientific temperature signals with ultra-low-noise/high-resolution 24-bit Analog-to-Digital converters. It acquires housekeeping channels with a scanning low-power ADC and incorporates environmental and housekeeping data in the data stream.

Interfaces. FACE contains interfaces to the lander, an analog interface to those instruments requiring acquisition electronics, and a scientific temperature sensor. The lander interface includes a power interface to the lander's Power Conditioning and Distribution Unit (PCDU, 28 V DC unregulated), a serial asynchronous interface to the lander's transmitter for Command and Telemetry, and discrete control/status lines.

5. MISSION CONFIGURATION AND PROFILE

The FARSIDE mission uses a launch by a Soyuz-Fregat, but an Ariane 5 launch together with a telecommunication satellite is also compatible (Table 2). A direct injection into a ballistic trajectory to LL2 or a trans-lunar injection is not favored since previous studies using Soyuz launchers have proven to be marginal in mass (such as the Airbus Defense and Space “MoonTwins” study). We propose instead a longer, but more mass-efficient, mission profile where the spacecraft are first injected into a geosynchronous transfer orbit (GTO) and then wait for the proper configuration to fly along a weak-stability boundary (WSB) trajectory that goes to the Earth-Moon L2 Lagrange point (LL2) by way of the Earth-Sun L1 Lagrange point (EL1). This scenario is similar to that used by NASA's gravity mapping mission GRAIL. Both lander and relay satellite then wait in LL2 orbit for the proper timing to initiate the landing sequence. Once triggered, the landing strategy is to follow the unstable WSB down to the surface and to set to zero the relative speed with respect to the landing site. Ground control would constantly monitor the spacecraft landing through the relay satellite.

FARSIDE uses a low risk and optimized mission analysis: The use of a GTO allows safe waiting for the proper ephemeris configuration with a minimal orbit control; the use of a GTO intermediate orbit allows for a backup option with a dual launch together with a commercial mission; the WSB trajectory provides a significant spacecraft mass increase with respect to other transfer options; and the LL2 orbit injection cost is very low.

Table 2. Mission analysis synthesis.

	Soyuz launch GTO then composite transfer to LL2	Shared Ariane V GTO then composite transfer to LL2	Shared Ariane V GTO then independent transfer to LL2
Staging approach	Upper composite	Upper composite	Separate
ΔV GTO to LL2 halo orbit (m/s)	1119	1119	1119
ΔV LL2 to lunar surface (m/s)	2500	2500	2500
TCM and Station keeping allocation (m/s)	100	100	100
Lander dry mass allocation (kg)	704	704	704
Landing propellant mass (kg)	942	942	942
Lander wet mass LL2 (kg)	1646	1646	1646
Relay satellite LL2 mass (kg)	363	363	483
Relay satellite GTO mass (kg)	363	363	706
Lander transfer propellant mass (kg)	930	930	762
Total mass mission spacecraft (kg)	2939	2939	3114
Launcher adaptor (kg)	60	200	200
Total mass mission spacecraft at launch (kg)	2999	3139	3314
GTO Launch vehicle performance (kg)	3250	4000	4000
Launcher margin	8%	22%	17%
Remark	Best baseline	Backup	Backup Higher reliability

5.1. Mission phases

The primary phases of the FAR SIDE mission include launch and early orbit phase (LEOP), transfer, lunar arrival, and descent.

LEOP. This phase starts with a Soyuz-Fregat launch from Kourou to GTO of the spacecraft and relay satellite, mounted one on top of the other. A shared Ariane 5 GTO launch (together with a commercial spacecraft) is considered as a backup: it allows a significant mass increase for the spacecraft composite, yet does not affect the total cost adversely (Table 2). Communications are achieved through spacecraft omni-directional X-band low gain antennas to 15-m terrestrial ground stations.

A GTO waiting orbit offers several advantages over a direct trajectory: it allows several launch windows per month with a similar ΔV , it requires less post-launch ΔV , and it provides a longer cruise time for calibrations, readiness tests, and flight system performance. Following insertion into GTO, two staging options are possible. In one scenario, the lander and relay satellite include separately the propellant for the rest of the mission (transfer to LL2 and landing, or transfer to LL2 for the relay satellite). In the second (baseline) scenario, the lander and relay satellite act as a composite, carrying propellant to LL2 orbit. The relay satellite is then separated from the composite after LL2 halo orbit injection. The second strategy allows for a very simple bus for the relay satellite.

Transfer. From GTO, the lunar probes are injected (along the L1 gravity manifold) into a 150-day ballistic orbit to the Moon through two or three perigee burns. The ballistic trajectory is directed towards the Earth-Sun L1 Lagrange point, and uses the instability of the manifold next to EL1 to return to the vicinity of the Moon (Figure 26). Many opportunities exist per month for the transfer from GTO to the ballistic trajectory towards L1 (Figure 27).

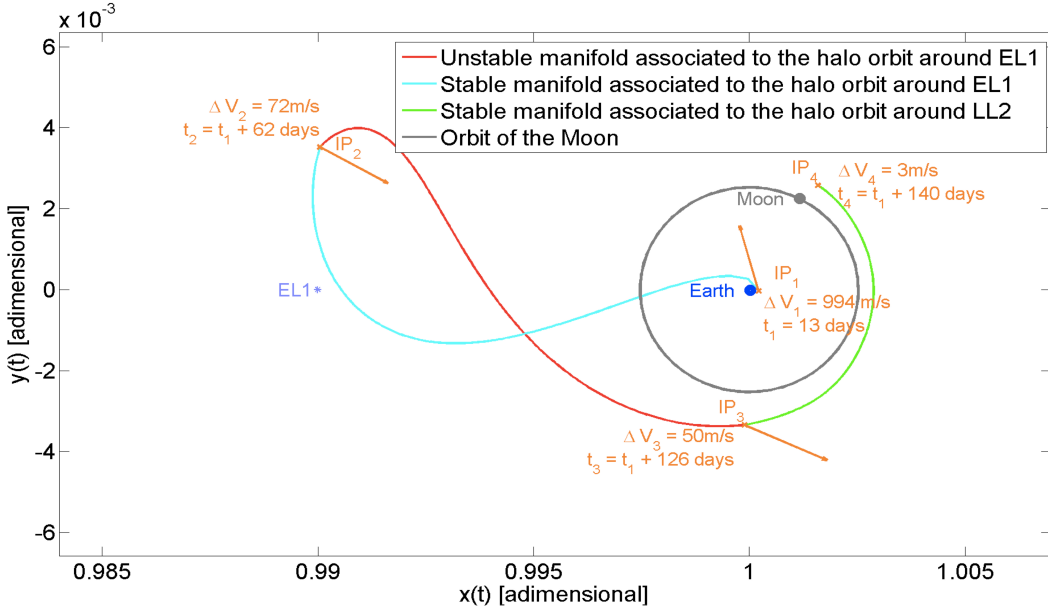


Figure 26. Transfer to the Moon: GTO to LL2 via EL1.

Lunar arrival. At lunar arrival, the intersection of the manifolds of the Earth-Sun and Earth-Moon system allows for the insertion, at a very low ΔV , into an Earth-Moon LL2 halo orbit. This orbit will be the quasi-final orbit for the relay satellite, but only a waiting orbit for the lander (Figure 28). The spacecraft composite is injected into a 14-day quasi-periodic halo orbit and the relay satellite is then separated from the lander. The first in-orbit tests are performed on the relay satellite, as it is required to be operational for landing of the lunar probe. The LL2 halo orbit allows access to any location on the lunar surface for the lander with a single large maneuver (the braking burn).

Landing phase. After 15 days to 1 month, the lander is inserted into a ballistic trajectory down to the lunar surface. At about 20 km altitude, the main braking maneuver is initiated. After braking, a small correction is performed to enable a fine state vector alignment and a zero local horizontal speed. The attitude of the spacecraft is slewed into its landing attitude and landing is autonomously

performed using a Doppler radar altimeter. The whole process is performed under ground control in real-time. No specific hazard avoidance capabilities are required.

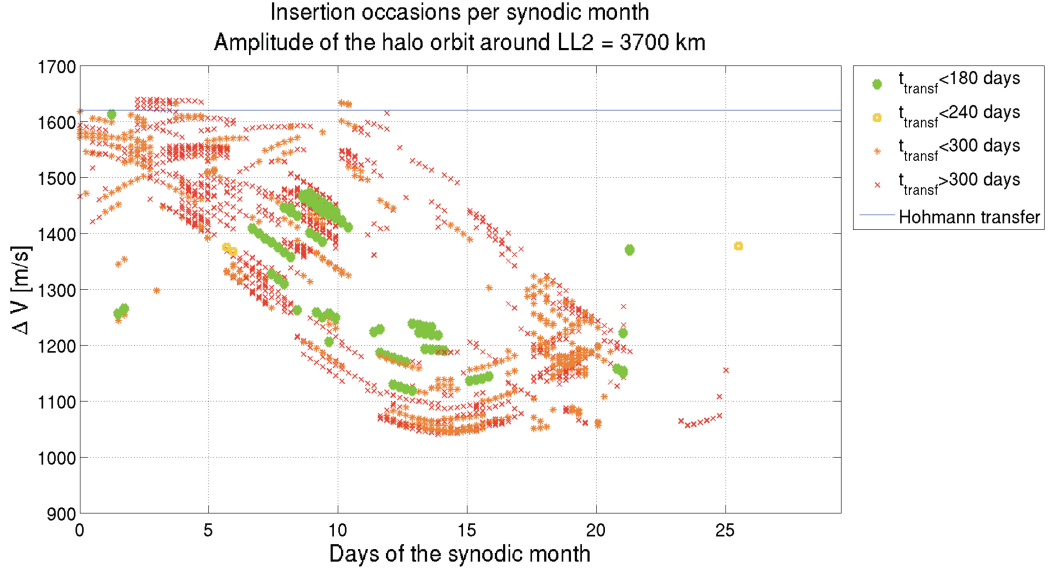


Figure 27. From the GTO waiting orbit, there are many WSB lunar transfer insertion possibilities per synodic month. The ΔV of a Hohmann transfer is shown for reference.

The operational lifetime of the lander and relay satellite will be four years. The initial localization of the lander on the surface will rely on differential Doppler measurements (Cebreros station) and lander star-tracker attitude and inertial measurements. Comparing images from the surface with Lunar Reconnaissance Orbiter images and topography will enable a more precise localization.

5.2. Operational halo orbit

The operational halo orbit chosen results from a compromise among several mission requirements: use for a relay satellite to allow an almost constant visibility of the farside landing site from Earth; implementation of the lunar impact flash, radio-astronomy, and magnetic field payloads; minimization of maintenance requirements for long time durations; and low cost injection from the transfer orbit. Several LL2 halo orbits are possible, and for operational reasons, a 2:1 resonant orbit (14 days period) is preferred, which provides constant visibility of both Earth and the lander in the South Pole-Aitken basin. This pseudo-orbit has lunar altitudes that vary between about 30,000 and 60,000 km. A slightly higher altitude orbit is also possible.

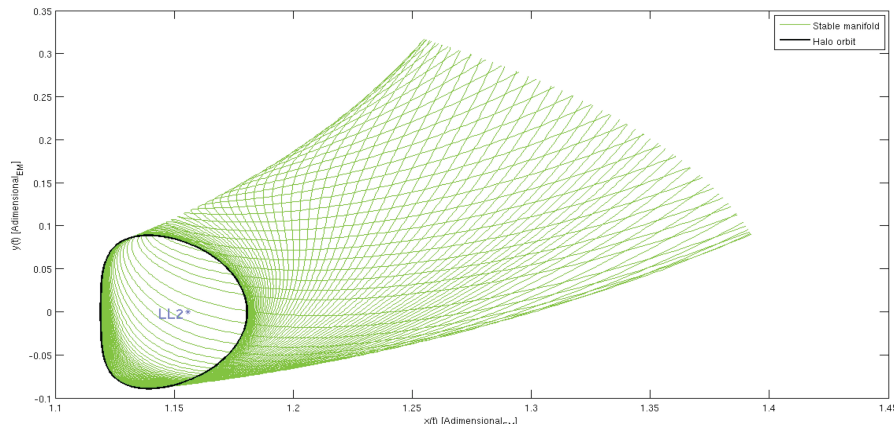


Figure 28. With a ballistic trajectory, the insertion into the lunar halo orbit does not require a significant ΔV . The halo orbit allows constant visibility of both the farside lander and Earth.

5.3. Descent and landing

The landing phase starts from a de-orbit boost to the final stationing of the probe on the lunar surface. Two strategies can be considered: a simple strategy similar to a Hohmann transfer, or a weak boundary transfer to a low altitude. In both cases, a final boost is required to align the state vector of the probe to the landing dynamic state (Figure 29). As there are no precise landing requirements, hazard avoidance can be made on the basis of a passive approach (target within safe zone) with a classical attitude acquisition by Doppler radar. Other options, such as precise landing, could be envisioned as a technology demonstration. The baseline strategy is a ballistic (inertial) transfer, followed by a radar-guided landing for altitude determination. The landing is foreseen at dawn of the landing site, which would allow two weeks to deploy the scientific instruments before lunar night.

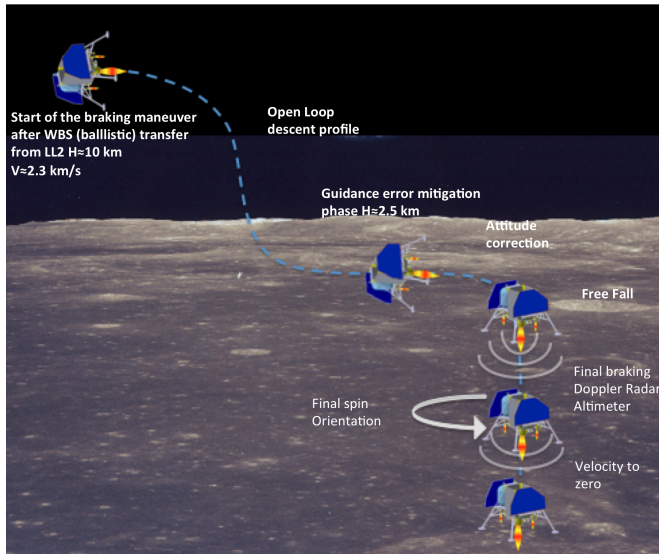


Figure 29. A possible landing phase outline.

In the unlikely case where the relay satellite fails before landing, the landing site could be repositioned to the nearside, allowing for direct communication with Earth. Nearside landing sites would not be protected from terrestrial radio-frequency interference, but would allow for measurements at frequencies lower than attainable on Earth. The geophysical investigations would be able to achieve many of the international lunar network science goals (Morgan and the ILN WGI 2009).

In order to simplify the probe guidance, navigation and control (GNC), no precision landing is foreseen, with the exception of altitude and descent speed being monitored by Doppler radar. The American and Soviet space programs have demonstrated that it is not necessary to have precision landing or hazard avoidance capabilities to safely land a spacecraft on the Moon. Seven landings were attempted as part of the Surveyor program, of which 5 were a success, and 2 failed for reasons unrelated to the landing. For the Luna program, 16 landings were attempted, of which 8 were successful, 7 failed for reasons unrelated to the landing, and one failed during landing. In total, a maximum of only one out of 14 mission failed as a result of possibly landing on hazardous terrain. All previous robotic landings were attempted with little detailed information about the lunar surface. Site selection for FARSIDE will mitigate against surface hazards by using high-resolution images, slope maps from high-precision laser altimetry and stereo images, and rock abundances from orbital radar and radiometer data.

5.4. Communications

The proposed communications and ground segment baseline (Figure 30) is to use ESA's network of ground stations (Redu, Vilspa, Kourou, Perth) during LEOP, transfer, and landing, and NASA's stations in case of contingency. Due to the duration of the transfer phase, a reduced number of stations is required to allow monitoring during the ballistic transfer, while for critical phases, the full network might be reserved. Due to the high data rates, X band is preferred for the telecommunication link

between the relay satellite and ground. Communications between the relay satellite and lander are foreseen in both UHF (low rate) and X band (high rate). The lander will be visible from the relay satellite 100% of the time, and communication with the relay satellite is foreseen only during daylight. Preliminary estimates of the UHF return link allows 256 kbps.

5.5. Mission operations

Ground system functions will be performed by ESA through the launch, cruise, landing and instrument deployment phases of the mission. Routine surface science operations will be performed by ESA for at least the first two years after landing. These operations could be transitioned to another center, such as CNES in Toulouse, France, for the remainder of operations, using the SISMOC ground segment developed for InSight.

The FARSIDE ground segment (Figure 30) will consist of a command and data acquisition element composed of ground stations from the ESOC network, and a mission operation and control element located at ESOC facilities in Darmstadt. The science facilities will be located at the instrument PI's institution. FARSIDE will use primarily telecommunication services from the ESA network. In case of dire need, a request would be made to use the DSN for telecommunications with the spacecraft, using the 34-m beam wave-guide sub-network. The FARSIDE spacecraft will use standard CCSDS formats and protocols to ensure international interoperability. The mission is designed such that except for initial acquisition after launch, simultaneous multiple ESA antennas for mission critical events will not be required for the orbiter and relay satellite at the same time.

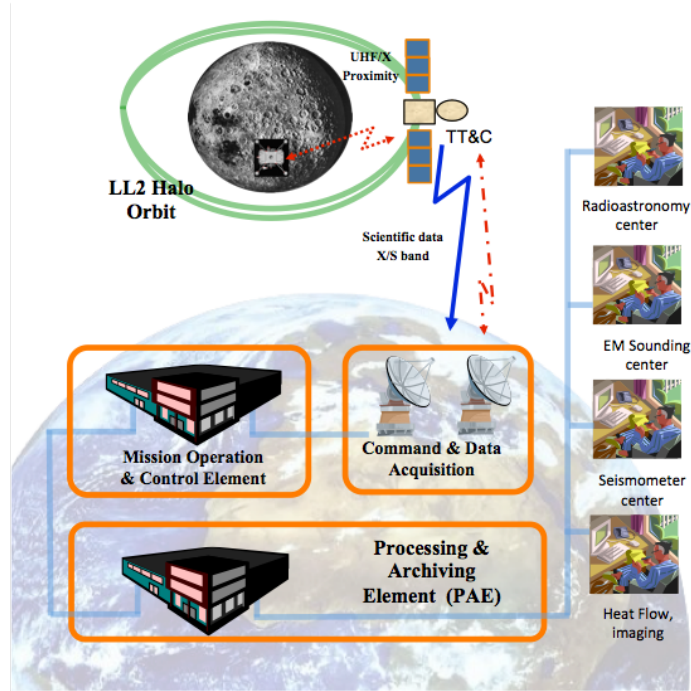


Figure 30. Ground segment outline. The Mission operation control and data archiving centers will remain at ESA facilities, but science centers, and possibly instrument operations, could be located at the PI institute's facilities. As an example, SEIS operations could be remotely done from CNES.

After launch and early operations, the tracking of the composite spacecraft is dominated by the needs of cruise navigation. This is especially important for the three weeks before landing. Surface deployment is scheduled to be as long as two weeks, corresponding to the maximum length of daylight after landing.

Shortly after launch, the composite satellite (lander and relay satellite) separate from the launch vehicle. Command sequences for the spacecraft will be designed, written, and uplinked on a non-interfering basis so that a sole navigation event (such as a trajectory correction maneuver) will occur at a given time. The landing operational sequence will be run autonomously onboard the spacecraft, and monitored in near real-time by the operations team. Telecommunications during this phase of operations will be based on the amount of tracking needed for navigation.

In order to minimize power consumption, there will be limited telecom sessions with the lander during the lunar night. Data is to be returned in several tracks scheduled for each of the two weeks during lunar daytime, depending on ground station availability.

The FARSIDE mission will collect continuously science data over the full lunar day/night cycle. During daylight operations, the lander will operate in its normal mode, collecting continuously engineering and science data from the instruments. These data will be stored onboard the lander and downlinked periodically to the orbiter. Data taken during the lunar night will be stored in the instrument memory for daytime transfer to the relay satellite. Short wake up sequences will occur on a daily basis to allow health checks and time synchronization.

6. SPACECRAFT DESIGN

The FARSIDE spacecraft consist of two elements: a surface lander, and a small, instrumented relay satellite that provides communication from Earth to the lander.

6.1. Lander spacecraft

6.1.1 Lander outline

Given the stringent mass constraints on the lander, a design relying on the heritage of previous lunar lander studies (Airbus Defense and Space “MoonTwins”) is chosen (Figure 31). The power system relies on solar power provided by fixed solar panels and enough batteries to enable a minimum set of instruments to operate during the night at reduced levels. An automated wake-up system is implemented in the power system to restore avionics to nominal operations at sunrise, or to allow minimal communication during night.

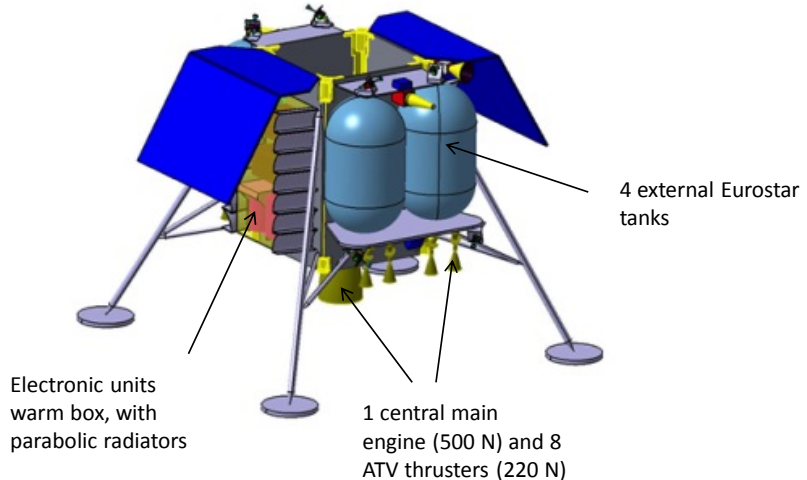


Figure 31. Lander preliminary accommodation. After landing, an arm (not shown) will deploy the seismometer and heat flow probe on the ground. Image courtesy of Airbus Defense and Space.

The avionics architecture is based on a dual structure: The Command and Data Management Unit (CDMU) that contains the processor module and memory, and the Electrical Interface Unit (EIU) that manages the interface and power lines with the attitude and orbit control system (AOCS), the propulsion units, and the heater lines. The architecture is based on an RS422 interface bus. A summary of the lander mass and power budgets is given in Table 3.

6.1.2 Propulsion

The propulsion system implemented on the lander serves two purposes. First, it realizes the required ΔV to bring the composite from GTO to the LL2 point where the relay satellite is separated.

This ΔV is 1119 m/s. Second, it realizes the braking ΔV for landing on the surface from LL2. This ΔV is 2500 m/s.

The propulsion system is constrained by three main drivers. First, it must provide a very high thrust to quickly brake the lander's velocity during the landing phase. Second, it must be very mass efficient (high ISP) in order to minimize propellant mass. Lastly, it should rely on proven, high TRL technologies. The proposed propulsion system consists of (1) a central 500 N main engine, and (2) 8 ATV-like 220 N thrusters. The system is used in a bi-propellant mode for high ISP efficiency (a 300 s ISP assumption is considered, as a mix between the 500 N main engine and the 220 N thrusters, to size the propellant budget).

6.1.3 Attitude and orbit control

The lander GNC system makes use of an efficient set of sensors that are able to handle all of the mission's phases, including a star tracker, an inertial measurement unit (gyrometers-accelerometers), a Doppler-radar altimeter, Sun acquisition sensors, and micro-machined (MEMS) gyroscopes (as spare sensors during safe mode). An alternate option would be to use a camera for the landing. The actuators are all propulsive, based on a high thrust system for landing and a low thrust reaction control system (RCS) for fine attitude and orbit control with eight thrusters. An alternate design, using solid-rocket motors such as ATK STAR 30BP, could also be considered for the final landing braking.

6.1.4 Spacecraft modes

There are a total of nine spacecraft modes for the entire mission: 6 modes for orbital and cruise operations, 1 landing mode, and 2 modes after landing on surface.

The six orbit and cruise modes are classical modes for interplanetary space missions, although their fine implementation might include specificities. The *launch mode* is the standby mode during all launch operations. The *rate reduction mode* is the first mode after launcher separation. The *Sun acquisition mode* is the next mode with acquisition of the Sun on the solar arrays using Sun sensors, and the stabilization around the Sun direction using the fine gyroscopes and the full RCS system. This mode ensures a safe power and thermal spacecraft state and robust Earth communications through the low gain antenna (LGA).

Follow Sun acquisition mode, it is possible to enter the *normal mode*, which can perform any type of 3-axis pointing (inertial, and Earth- or Moon-pointed) with the star tracker as the main attitude sensor. The *orbit correction mode* is in charge of all maneuvers, requiring to slew the satellite before and after the burn (in order to align the main engines with the direction of desired ΔV), and once aligned, to fire the main engine (and/or the ATV thrusters), while maintaining the spacecraft's attitude for an accurate realization of the ΔV . The spacecraft switches automatically to *safe hold mode* in case of detection of a malfunction. This mode plans to use spare microgyrometers together with the internal redundant branch of the Sun sensors.

The management of the final descent and landing is through the *descent and landing mode*. During the final phase of the descent, the alignment of the solar panels is performed using the degree of freedom around the axis of the main engines. Descent speed is managed by a Doppler radar or to a specially tailored landing camera, which provides speed output.

Once on the surface of the Moon, there will be two main modes, according to the time of day. The first is the *daylight surface mode*, where the spacecraft is safely laying on the surface with its solar arrays correctly pointing at the Sun. After deployment of the science package, scientific data are downloaded to Earth via the relay orbiter using the UHF antenna. The second is the *nighttime surface mode*, which is to be used during the 14-day lunar night. It is design to spare as much resources as possible, with all avionics in a hibernation-like state, except for the core scientific payload.

6.1.5 Power

The power subsystem is based on a classical design (PCDU, unregulated 28 V bus, 30 kg solar panels and 70 kg battery with new generation cells). The available payload power provided by the solar panel is about 50 W during the day, and the available payload power provided by the battery during the night is about 5 W. Increasing the payload power load at night would directly increase the battery mass. As the lander mass is very critical, the baseline design (70 kg battery for 5 W night payload power) is a workable compromise. A low energy consumption mode is used for payload

elements that remain on during the night, with all other equipment switched off. Only remaining on is a timer for the lander wakeup and the power conditioning and distribution unit (PCDU) for the payload power supply. Short periodic wake-ups (with a negligible impact on energy budget) are used to store all data in the CDMU and perform basic communication, such as time synchronization of the landers with the orbiter.

6.1.6 Data handling and telemetry

Telecommunications with Earth are handled differently depending on the mission phase. During LEOP and ballistic transfer, X-band communications are preferred. An omni-directional coverage is provided by means of two LGAs. For the science mission phase, a UHF antenna provides the low-rate satellite to lander link; this choice limits the data upload to about 256 kbps. Supposing an uplink during the lunar day only, it allows for between 150 and 300 Gbits of data transfer per lunation. The UHF link is also used to allow time synchronization of the two landers through the orbiter. Two UHF antennas are accommodated on the spacecraft to provide omni-directional coverage during the landing phase. The high data rate X-band link can also be used to allow for high-rate uploads.

6.1.7 Thermal concept

Surviving the lunar night, while keeping enough resources for minimum payload operations and keeping the avionics warm to operate during 14 terrestrial days, is one of the biggest technical challenges of the mission. The choice of the thermal concept has a considerable impact on the lander spacecraft sizing.

The design of the lander thermal system is driven by several factors, including: low overnight ambient temperatures; the need of keeping the heating power during the night low to minimize the energy consumption; the compatibility with thermal design without radio isotope heat sources (RHUs); the protection of the battery from extreme temperatures; the protection of operational electronics from temperatures outside their operational range; and the capability to dissipate enough heat in the environment hot case.

The majority of the lander equipment is assembled to a set of frames which are coupled to each other thermally, but isolated from the lander structure. Inside the lander, almost all the electronic units are accommodated in a warm box in order to guarantee them to operate within a more controlled thermal environment. The battery is also accommodated into the warm bay. The warm bay is connected, through a single thermal bus, to parabolic shaped radiators that reject the overheating during the day (Figure 32). The thermal bus connecting the warm box to the radiators is controlled by heat switches, which provide a very good insulation between the box and the radiators during the night while driving the heat to the radiators during the day. Only heating of equipment within the warm box is considered, and no external appendage heating is considered.

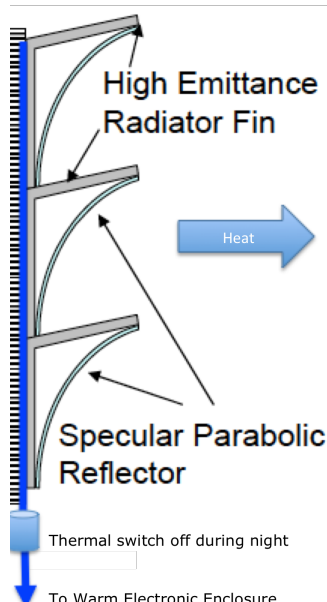


Figure 32. Thermal concept using thermal switches and radiators. This radiator configuration allows for very efficient heat rejection in the day. The solid angle under which the radiator sees the ground is reduced, as heat is rejected in a direction parallel to the ground. During the night, the thermal switch is closed to preserve heat in the electronics enclosure.

6.1.8 Lander mass budget

A preliminary mass budget estimate for the lander is given in Table 3. The nominal dry mass is 700 kg. An allocation of 45 kg for the full payload is considered, which is compatible with 70 kg of batteries and 5 W of nighttime power. The underlying lander design is based on the Moons Twins study, performed by Airbus Defense and Space, revisited for the needs of FARSIDE.

Table 3. Lander mass budget (courtesy of Airbus Defense and Space).

Lander	Mass budget		
	Current best estimate (kg)	Maturity / Margin (%)	Mass with margin (kg)
Core payload	27	20	32
Full payload	37	20	44
Structure (platform, thermal)	120	10	132
Propulsive subsystem	170	10	187
Power subsystem (battery+bus)	101	10	112
TTC (Antennas)	20	10	22
Harness	50	20	60
Landing gear	60	20	72
Command and Data Handling subsystem	15	10	17
AOCS / GNC	25	20	30
Thermal HW (heating)	25	15	29
Total Lander mass (kg)	Core Payload		692
	Full payload		704

6.1.9 Environmental constraints

Specific EMC cleanliness procedures are to be foreseen to avoid any perturbation of the radio astronomy and electromagnetic sounding payloads. An electromagnetic interference/compatibility (EMI/EMC) control plan will be implemented that follows GSFC-STD-7000 (“GEVS”) at a minimum.

6.1.10 Redundancy

As the science objectives require a long life on the lunar surface, the overall redundancy philosophy is linked to the choice of a good reliability during the mission. We have chosen to have redundancy for all units operational after the landed phase, but not for the transfer phase (CDMU, EIU, Trans-ponders, and PCDU). Thrusters are also not redundant (only 4 of the 8 in the “MoonTwins” design are required).

6.1.11 Current heritage and TRL

The lander will use primarily off-the-shelf equipment. The propulsion system has been built around ATV heritage in order to save technological development costs and associated risk, and the avionics require no specific developments. The overall TRL of all baseline subsystems is very high, ranging from 8 to 10. The only exception is the possible use of RHUs for the thermal design, which requires additional developments (an ESA TRP study is already in progress). Assuming RHUs will not be possible (baseline), the thermal design relies on a warm box enclosing the whole electronics, and on the use of thermal switches to handle the hot case. Thermal switches are currently under qualification in Europe.

6.2. Relay satellite

6.2.1 Satellite outline

The relay satellite must accommodate a small scientific payload (an impact flash camera, radio astronomy receiver and antennas, and magnetometer) while providing a telecommunications relay for the lander (Figure 33). We propose to use a Myriade Evolution-class bus (mini-satellite jointly developed by CNES, Airbus Defense and Space and Thales Alenia Space). The control of the satellite attitude allows satellite orientation on 3 axes. In the nominal mission, the relay satellite is oriented along a North-South line, with the relay antenna on its “East” side. The satellite remains pointed towards the night side of the Moon for impact-flash monitoring.

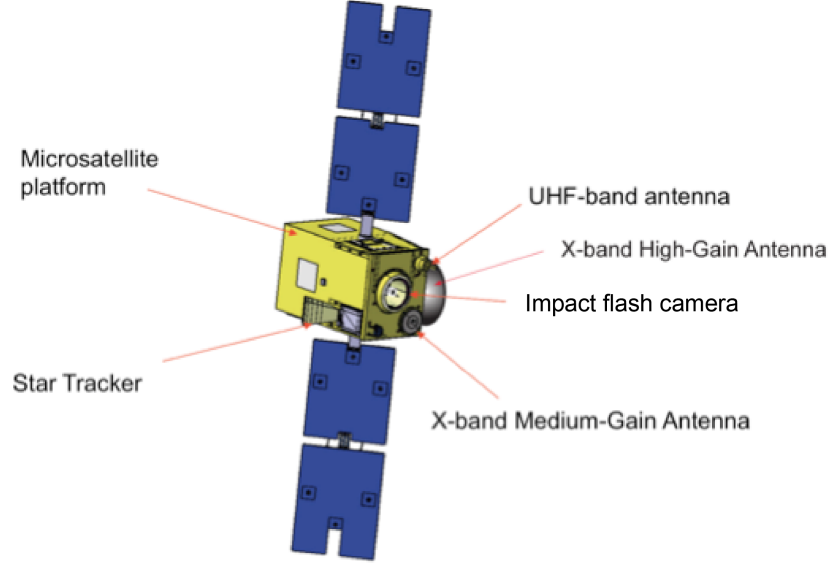


Figure 33. The relay satellite is based on a micro-satellite platform. The satellite includes the impact monitoring camera on the front side, and a deployable high gain antenna on the side. The magnetometer and radio astronomy antennas (not shown) are to be deployed on booms. Image courtesy of Airbus Defense and Space.

To allow minimal changes at on-board software level with respect to existing designs, the satellite follows a tabulated attitude function of the orbit (pseudo-)period, and the solar panels rotate with the Earth-Moon synodic rotation period. To enable the telecom relay capability, two options are considered (Figure 34): an X-band beam forming network (BFN) keeps a synthetic Earth tracking, or a simpler option imposes Earth pointing when flashes cannot be observed (such as when the farside disk is fully illuminated by the Sun). Satellite pointing precision is about 5×10^{-3} degrees, which is sufficient for the impact flash detection payload. In the nominal mode, the satellite uses a stellar sensor and four reaction wheels, with Sun sensors being provided for safe mode. Cold gas thrusters allow wheel desaturation.

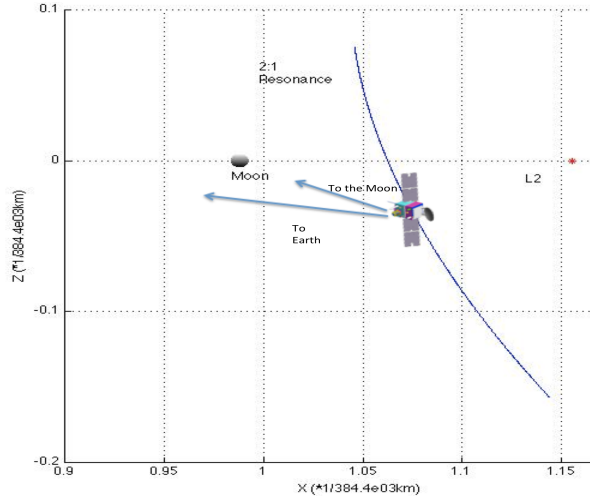


Figure 34. Relay satellite pointing geometry. The mission requires two different pointings: one to the Moon for the impact flash camera and to provide a relay-link to the lander, and another to communications with Earth. The baseline is to point continuously toward the Moon, with a synthetic aperture antenna that allows keeping a continuous Earth link. A backup option could be to share the time between Earth and Moon pointing.

6.2.2 Electrical power subsystem (EPS)

The EPS derives from the Myriade Evolution power generator, with a fixed, 4-panel (folded during launch) solar array. The overall surface area of the solar panels is approximately 2.3 m^2 , which allows for more than 600 W power as a result of the use of highly efficient triple junction As-Ga cells.

The system also includes a Li ion battery and an electronics box supplying a regulated power delivered to all spacecraft equipment.

6.2.3 Data handling

The overall architecture of the satellite is centralized. A serial data bus using a star architecture ensures communications with all equipment. The Myriade Evolution avionics is based on new generation equipment (having all passed PDR milestones) and commercial off-the-shelf units. The avionics decode and execute the commands from the ground, format housekeeping and science telemetry, manage the on-board data distribution, and do all real-time computations onboard. The flight software runs on the on-board computer (Airbus AS250 product line taken as a reference). A 512 Gbits solid-state mass memory is used to store housekeeping and science data telemetry until its transmission to the ground. Due to the severe environment, redundancy of critical systems could be considered.

6.2.4 Telemetry

The telemetry strategy used is similar to that of other interplanetary missions (Figure 35). We make use of a UHF local link between the lander and relay satellite (following the Proximity-1 Space Link Protocol) with an uplink capability of about 128 to 256 kbps. Furthermore, an X/S-band link (direct to Earth) is used for the relay satellite (X band is used during cruise phases), which allows for high-speed uplink from the lander.

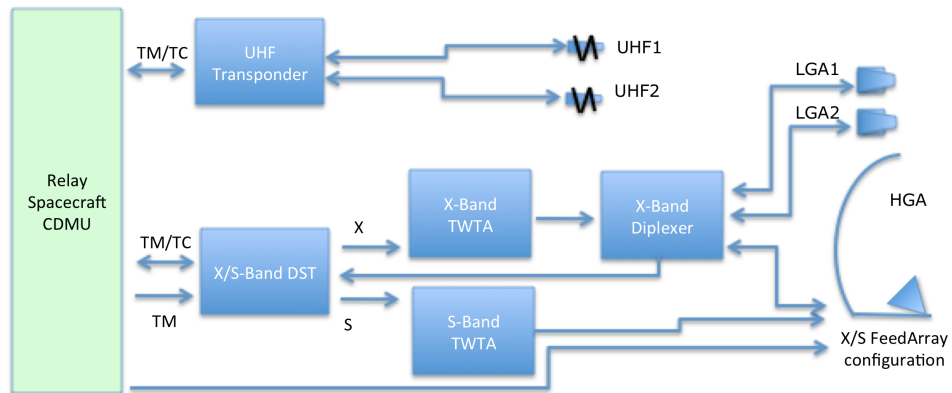


Figure 35. A possible telecommunications architecture for the relay satellite. Data can be uploaded through all possible links and is download to Earth via the X-band high-gain antenna. UHF1/2 and LGA1/2 provide redundancy for the communication functions.

As the satellite remains pointed towards the Moon, the pointing of the high gain antenna may be performed using an electronically steerable antenna feed array. In this case, the reflector remains fixed but the antenna beam is electronically steered. Another possibility is to share pointing time between the observation of the Moon and the relay download (Figure 34).

6.2.5 Halo orbiter mass budgets

The estimated nominal mass of the relay satellite is about 350 kg (Table 4), including its 70 kg payload (which includes the specific TT&C subsystem of about 40 kg).

6.2.6 Current heritage and TRL

The relay satellite will be derived from the Myriade Evolution-class platform (mini-satellite jointly developed by CNES, Airbus Defense and Space and Thales Alenia Space). The first implementation of the new Myriades Evolution platform is MERLIN, a joint CNES-DLR mission that is scheduled for launch in 2019. The bus will thus be flight-proven for FARSIDE.

6.2.7 Relay satellite failure

The relay satellite will operate in a lunar halo orbit for 4 years. The radiation environment and the total dose in this environment are not significantly different from that encountered on geostationary

orbit. Even if COTS are used for the avionics, their flight record is sufficient to ensure a good confidence for a 4-year mission duration.

Table 4. Estimated satellite mass budgets (courtesy of Airbus Defense and Space).

Satellite	Mass budget		
	Current best estimate (kg)	Maturity / Margin (%)	Mass with margin (kg)
Total payload	17	20	20
Myriade platform	70	10	77
Propulsive subsystem	20	10	22
Power subsystem (battery+bus)	55	10	61
TTC (PAA type)	40	20	48
Harness	20	20	24
Communications	15	20	18
Command and Data Handling subsystem	20	10	22
AOCS / GNC	40	20	48
Thermal HW (heating)	10	15	12
Total satellite dry mass (kg)			351
Ergol TCM and Station keeping			12
Total satellite wet mass without transfer propulsion subsystem (kg)			363
Total satellite wet mass with transfer propulsion subsystem (kg)			483

If the relay satellite were to fail before the landing phase, the lander could be repositioned to land on the nearside hemisphere, allowing direct lander to Earth communications. Given that the relay satellite represents an unlikely single point of failure, a cheaper and smaller secondary relay satellite could be envisioned as a backup. A telecommunications backup could potentially be assured by a foreign lunar orbiter that is operational during the FAR SIDE mission. In the event of a lander failure, the relay satellite would still provide scientifically valuable data from the impact flash camera, magnetometers, and radio astronomy receiver.

6.3. Launch composite configuration

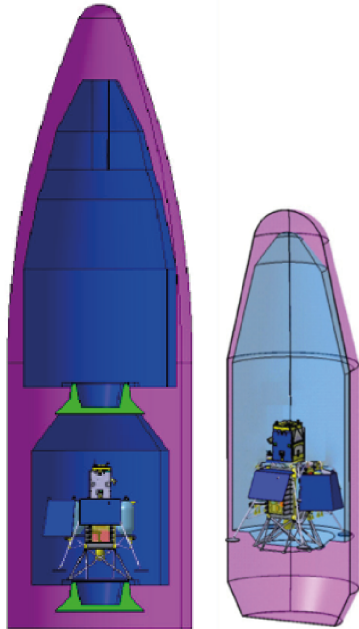


Figure 36. Ariane 5 (left) and Soyuz-Fregat (right) spacecraft accommodations. Images courtesy of Airbus Defense and Space.

The two elements of the space segment (the lander and the relay satellite) are stacked on the top of the Soyuz-Fregat stage. The small size of the lander is designed to be compatible with the Soyuz-

Fregat fairing, but is also compatible with a shared Ariane 5 commercial launch (Figure 36). To release the spacecraft composite, a pyro separation device is fired from the Soyuz-Fregat stage and preliminary separation is made by a spring. The lander and relay satellite are separated once they arrive in the LL2 orbit.

Table 2 provides the total mass budget using a system margin for the two elements of the space segment (lander and orbiter). The propellant mass budget computation is staged (transfer from GTO to LL2, separation of the orbiter, and landing) and a 300 s IPS is considered as a mix between high ISP main engine and 220 N thrusters. The proposed baseline (with 45 kg payload on lander and 70 kg payload on orbiter) is compatible with a Soyuz launch. The best staging option is the composite transfer instead of independent transfer. The current estimate gives a robust 8 % margin with respect to Soyuz capacity in GTO.

7. MANAGEMENT

7.1. Overall mission management structure

The proposed organization is based on previous mission organization schemes. Each space agency (ESA and possibly NASA) will have its own management office, including the program manager, the project manager and the project scientist. This core management team constitutes the FARSIDE program board. The science working team (SWT), managed by the project scientist, will be the assembly of all instrument PIs. Each instrument PI will be assisted by a deputy PI or instrument. In support of the science working team, three working groups will be assembled to support the (1) radio astronomy, (2) lunar interior structure, and (3) impact hazards science goals. All instruments will be under the responsibility of a payload manager of the spacecraft engineering team. The lead proposer will dedicate more than 20% of his time to support all phases of the FARSIDE project.

During the definition and preparatory phases (until late 2018), three meetings of the SWT will be held per year in order to refine the mission science requirements and to evaluate mission optimization scenarios. The utilization of shared spacecraft resources will be finalized, the exact number and length of the radio astronomy antennas will be decided upon, the feasibility of using the EMS electrodes for radio astronomy will be investigated, and various instrument deployment scenarios will be investigated. During the implementation phase, 1-2 meetings of the SWT will be held per year. These meetings will include preparations for scientific analysis, but will also develop the methods and techniques necessary for making synergistic measurements from Earth (such as with LOFAR and impact flash monitoring).

7.2. Proposed procurement approach

ESA will be responsible for procuring the lunar lander, relay satellite, and launch vehicle. The ESA member states (and NASA for the optional payload) will be responsible for procuring the scientific payload. The procurement approach for the European payloads will be made under the control and funding of national agencies (when existing), or will be followed by ESA/PRODEX. For US payloads, the funding will be requested via the SALMON process. The instrument deployment system (IDS) will either be part of the lander development, or provided as a contribution by a (not yet identified) partner.

7.3. Ground segment and operations

It is assumed that ESA will provide the mission ground segment (with the exception of the science facilities associated with instruments) and all operations of the mission with a contribution from the science teams for the instrument operations. A partner agency (CNES) may also take into account the nominal operations of the mission (and associated costs) two years into the mission, thanks to the reuse of the already developed SISMOC, the mission operation center developed for InSight.

7.4. Data archiving

All data from the FARSIDE lander and orbiter will be archived initially by ESA PSA, and the PSA will provide a FARSIDE Final Archive after the end of the mission. National agencies may also provide access to FARSIDE data through their own tools, when available. The FARSIDE team would have immediate access to the data for processing. ESA PSA will enable sharing the FARSIDE data products with NASA PDS relevant nodes every 6 months from the start of monitoring operations, using the standards developed in the frame of the IPDA. Seismic data will also be made available to the international seismic community through the European EPOS Seismic Data Management Center, with a copy sent to the US IRIS Data Management Center.

7.5. Relation to ESA's directorate of Human Spaceflight and Operations

With the cancelation of the ESA Lunar Lander, ESA's current plans for lunar exploration focus on a proposed collaboration with the Russian Luna 25, 26, and 27 missions, culminating in sample return from the south-polar region. However, these missions are predicated mostly on the study of polar volatiles, and would land on the nearside of the Moon. These missions will not address the geophysical, astronomical and impact hazard characterization objectives of this proposal. Rather the science of FARSIDE should be seen as complementary to this activity. The FARSIDE technology development will provide a route for ESA to develop independently planetary landing capability that the Russian collaboration will not provide.

8. MISSION COST AND PROGRAMMATICS

8.1. Mission cost analysis

Two scenarios impact the total mission cost. In one scenario, ESA provides a Soyuz-Fregat launch, and in the other, the launch is shared with a commercial flight on an Ariane 5. The Ariane 5 option is made possible by the commercial policy of Arianespace that charges a “kg in orbit price” regardless of the launcher used. For both options, the full science payload is possible.

A 20% participation to operation costs is assumed, and a dedicated outreach budget is included. The total mission cost is given in Table 5 as determined by Airbus Defense and Space. These costs are similar to an estimation obtained by a CNES phase 0 (PASO) study.

Table 5. Total mission cost (courtesy of Airbus Defense and Space).

	Cost (Current Best Estimate, M€) SOYOUZ Launch Scenario	Cost (Current Best Estimate, M€) Back up SHARED ARIANE V
Lander platform in 2015	158	158
1 platform (Myriade type)	15	15
Non Recurring costs	25	25
Total Satellite (M€)	40	40
Launch	70	75
ESA Internal Costs: 8 % of CaC (overhead + technical support)	36	36
Operations (landing,...): 20 %	90	90
Risk margin	35	35
FARSIDE Mission: Total Cost (M€)	429	434

8.2. Technology development requirements

This mission relies on a mature, low-risk approach with respect to technological developments. However, a specific set of actions should be undertaken.

- ESA TRP and CTP actions on critical components, including delta-qualification of ATV 250 N thrusters for GNC, thermal switch and parabolic radiator developments, and landing leg developments.
- Instrument R and T funded by national agencies/ESA in support of payload assessment studies.
- ESA internal studies on mission optimization.
- The possibility of using RHUs, which would simplify the lander thermal design.

8.3. Mission schedule and risk analysis

Technology developments are the first drivers in the mission development timeline, in particular RHU development if they are considered, and phasing with other required technologies (thermal hardware, robotic deployment arm). A possible mission schedule with a launch in a 2015/2026 timeframe is given in Figure 37.

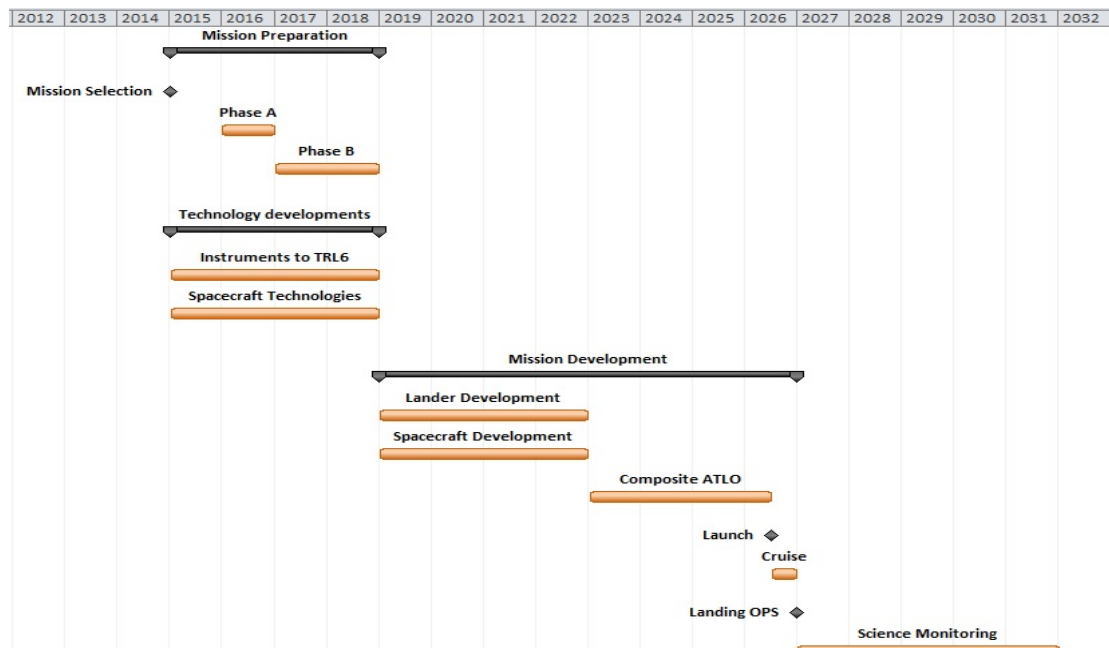


Figure 37. A possible mission schedule for a launch in early 2026 (courtesy of Airbus Defense and Space).

The main mission risks include an increase in the lander mass, lander technology readiness level, operational issues, lander loss and relay satellite failure (Figure 38).



Figure 38. Preliminary risk assessment matrix (courtesy of Airbus Defense and Space).

A. REFERENCES

- Alexander, J.K., M. L. Kaiser, J. C. Novaco, F. R. Grena, and R. R. Weber (1975). Scientific instrumentation of the Radio-Astronomy-Explorer-2 satellite, *Astron. Astrophys.*, **40**, 365-371.
- Baratoux, D., H. Chennaoui-Aoudjehane, F. Colas, Z. Benkhaldoun, A. Jambon, A. Leroy, P. Lognonné, O. Azagrouze, M. Ait Moulay Larbi, S. Bouley, A. Bounhir, M. Calvet, S. Chaabout, S. Chevrel, A. Daassou, R. Garcia, A. Habib, A. Jabiri, N. Larouci, P. Pinet, M. Sabil, and J. Vaubaillon (2012). A French-Morocco project for the study of impact processes on the Earth and Moon, *Lunar Planet. Sci. Conf.*, abstract 1667.
- Bely P.Y., R. J. Laurance, S. Volonte, R. R. Ambrosini, A. Ardenne, C. H. Barrow, J.-L. Bougeret, J. M. Marcaide, and G. Woan (1997). Very Low Frequency Array on the Lunar Far Side. *ESA report SCI(97)2*, European Space Agency.
- Bignami, G., P. Cargill, B. Schutz, and C. Turon (2005), Cosmic Vision, *BR-247*, ESA publications division, Noordwijk.
- Bottke, W.F., A. Morbidelli, R. Jedicke, J. M. Petit, H. F. Levison, P. Michel, T. S. Metcalfe (2002). Debiased orbital and absolute magnitude distribution of the near-Earth objects, *Icarus* **156**, 399–433 (2002)
- Bouley, S., D. Baratoux, J. Vaubaillon, A. Mocquet, M. Le Feuvre, F. Colas, Z. Benkhaldoun, A. Dassou, M. Sabil, and P. Lognonné (2012). Power and duration of impact flashes on the Moon: Implication for the cause of radiation, *Icarus*, **218**, 115-124.
- Bougeret, J.-L., et al. (2008). S/WAVES: The Radio and Plasma Wave Investigation on the STEREO Mission, *Space Sci. Rev.*, **136**, 487-528.
- Braden, S.E., J. D. Stopar, M. S. Robinson, S. J. Lawrence, C. H. van der Bogert and H. Hiesinger (2014). Evidence for basaltic volcanism on the Moon within the past 100 million years, *Nature*, doi: 10.1038/NGEO2252.
- Brown, P., R. E. Spalding, D. O. ReVelle, E. Tagliaferri and S. P. Worden (2002). The flux of small near-Earth objects colliding with the Earth, *Nature*, **420**, 294–296.
- Brown, P. G. and 32 coauthors (2013). A 500-kiloton airburst over Chelyabinsk and an enhanced hazard from small impactors, *Nature*, **503**, 238–241.
- Bruck, Yu., M., Ustimenko, and B. Yu (1976). Decametric radio emission from four pulsars, *Nature*, **260**, 766-767.
- Campbell-Brown, M. D. (2008). High resolution radiant distribution and orbits of sporadic radar meteoroids, *Icarus*, **196**, 144–163.
- Canup, R. (2012). Forming a Moon with an Earth-like composition via a giant impact, *Science*, **338**, 1052-1055.
- Cerman, A., P. Ripka, P. Kaspar, A. Tipek, A. Platil (2003). Precise Magnetic Sensors and Magnetometers for Military and Space Applications, *Sensors & Transducers Magazine*, **38**, pp.54-58.
- Cuk, M., and S. T. Stewart (2012). Making the Moon from a fast-spinning Earth: A giant impact followed by resonant despinning, *Science*, **338**, 1047-1052.
- Committee on the planetary science decadal survey (2010). Vision and Voyages for Planetary Science in the Decade 2013-2022, National Research Council, National Academies Press, Washington, DC.
- Daubar, I. J., A. S. McEwen, S. Byrne, C. M. Dundas, A. L. Keska, G. L. Amaya, M. Kennedy, and M. S. Robinson (2011). New Craters on Mars and the Moon, *Lunar and Planetary Science Conference*, **42**, abstract 2232.
- Dulk, G.A., W. C. Erickson, R. Manning, and J.-L. Bougeret (2010). Calibration of low-frequency radio telescopes using the galactic background radiation, *Astron. Astrophys.*, **365**, 294–300.
- Garcia, R. F., J. Gagnepain-Beyneix, S. Chevrot, and P. Lognonné (2011). Very preliminary reference Moon model, *Phys. Earth Planet. Inter.*, **188**, 96-113.
- Grimm, R.E., and Delory, G.T. (2012). Next-generation electromagnetic sounding of the Moon. *Adv. Space Res.*, **50**, doi:10.1016/j.asr.2011.12.014.
- Gritsevich, M., Koschny, D. (2011). Constraining the luminous efficiency of meteors, *Icarus*, **212**, 877–884.
- Grott, M., Knollenberg, J., Krause, C. (2010). Apollo lunar heat flow experiment revisited: a critical reassessment of the in situ thermal conductivity determination, *J. Geophys. Res.*, **115**, E11005.
- Grove, T. L., and M. J. Krawczynski (2009). Lunar mare volcanism: Where did the magmas come from? *The Elements*, **5**, 29-43.
- Gurnett, D. A., et al. (2004). The Cassini Radio and Plasma Wave Investigation, *Space Sci. Rev.*, **114**, 395-463.

- Haruyama, J., Ohtake, M., Matsunaga, T., Morota, T., Honda, C., Yokota, Y., Pieters, C.M., Hara, S., Hioki, K., Saiki, K., Miyamoto, H., Iwasaki, A., Abe, M., Ogawa, Y., Takeda, H., Shirao, M., Yamaji, A., Josset, J.-L. (2008). Lack of Exposed Ice Inside Lunar South Pole Shackleton Crater, *Science*, **322**, 938–939.
- Hess, S. L. G., and P. Zarka (2011). Modeling the radio signature of the orbital parameters, rotation, and magnetic field of exoplanets, *Astron. Astrophys.*, **531**, A29.
- Hiesinger, H., J. W. Head III, U. Wolf, R. Jaumann, and G. Neukum (2010). Ages and stratigraphy of lunar mare basalts in Mare Frigoris and other nearside maria based on crater size-frequency distribution measurements, *J. Geophys. Res.*, **115**, E03003, doi:10.1029/2009JE003380.
- Hood, L. L., F. Herbert, and C. P. Sonett (1982). The deep lunar electrical conductivity profile: Structural and thermal inferences, *J. Geophys. Res.*, **87**, 5311–5326.
- Hood, L.L. (1986). Geophysical constraints on the lunar interior. In: Hartmann, W.K., Phillips, R.J., Taylor, G.J. (eds.) *Origin of the Moon*, pp. 361–410. Lunar and Planetary Institute, Houston.
- Ivanov, B.A. (2006). Earth/Moon impact rate comparison: searching constraints for lunar secondary/primary cratering proportion, *Icarus*, **183**, 504–507.
- Jester, S., and H. Falcke (2009). Science with a lunar low-frequency array: From the dark ages of the Universe to nearby exoplanets, *New Astron. Rev.*, **53**, 1-26.
- Jolliff, B. L., J. J. Gillis, L. A. Haskin, R. L. Korotev, and M. A. Wieczorek (2000). Major lunar crustal terranes: Surface expressions and crust-mantle origins, *J. Geophys. Res.*, **105**, 4197–4216.
- Jolliff, B., M. Wieczorek, C. Shearer, and C. Neal (eds.), *New views of the Moon* (2006). *Rev. Mineral. Geochem.*, **60**, 721pp.
- Josset, J.-L., Beauvivre, S., Cerroni, P., De Sanctis, M. C., Pinet, P., Chevrel, S., Langevin, Y., Barucci, M. A., Plancke, P., Koschny, D., Almeida, M., Sodnik, Z., Mancuso, S., Hofmann, B. A., Muinonen, K., Shevchenko, V., Shkuratov, Yu., Ehrenfreund, P., Foing, B. H. (2006). Science objectives and first results from the SMART-1/AMIE multicolour micro-camera, *Adv. Space Res.*, **37**, 14–20.
- Khan, A., J. A. D. Connolly, A. Pommier, and J. Noir (2014). Geophysical evidence for melt in the deep lunar interior and implications for lunar evolution, *J. Geophys. Res. Planets*, **119**, 2197–2221, doi:10.1002/2014JE004661.
- Klein Wolt, M., A. Aminaei, P. Zarka, J.-R. Schrader, A.-J. Boonstra, H. Falcke (2012). Radio astronomy with the Lunar Lander: opening up the last unexplored frequency regime, *Planet. Space Sci.*, **74**, 167-178.
- Lamy, L. (2011). Variability of Southern and Northern SKR periodicities, in “*Planetary Radio Emissions VII*”, H. O. Rucker et al. eds., Austrian Acad. Sci. Press, Vienna, pp. 39-50.
- Langseth, M.G., Keihm, S.J. Peters, K. (1976). Revised lunar heat-flow values. In: Proc. Lunar Sci. Conf. 7th, 3143–3171.
- Laneuville, M., M. A. Wieczorek, D. Breuer, and N. Tosi (2013). Asymmetric thermal evolution of the Moon, *J. Geophys. Res. Planets*, **118**, 1435–1452, doi:10.1002/jgre.20103.
- Lawrence, D. J., W. C. Feldman, R. C. Elphic, R. C. Little, T. H. Prettyman, S. Maurice, P. G. Lucey, and A. B. Binder (2002). Iron abundances on the lunar surface as measured by the Lunar Prospector gamma-ray and neutron spectrometers, *J. Geophys. Res.*, **107**, 5130, doi:10.1029/2001JE001530.
- Lawrence, D. J., S. Maurice, and W. C. Feldman (2004). Gamma-ray measurements from Lunar Prospector: Time series data reduction from the gamma-ray spectrometer, *J. Geophys. Res.*, **109**, E07S05, doi:10.1029/2003JE002206.
- Le Feuvre, M., and M. A. Wieczorek (2011). Nonuniform cratering of the Moon and a revised crater chronology of the inner solar system, *Icarus*, **214**, 1-20.
- Lognonné, P., J. Gagnepain-Beyneix and H. Chenet (2003). A new seismic model of the Moon: implication in terms of structure, formation and evolution, *Earth Planet. Sci. Lett.*, **211**, 27-44.
- Lucey, P., Korotev, R.L., Gillis, J.J., Taylor, L.A., Lawrence, D., Campbell, B.A., Elphic, R., Feldman, B., Hood, L.L., Hunten, D., Mendillo, M., Noble, S., Papike, J.J., Reedy, R.C., Lawson, S., Prettyman, T., Gasnault, O., Maurice, S. (2006). Understanding the lunar surface and space–Moon interactions, *Rev. Mineral. Geochem.*, **60**, 83–219.
- Lognonné P., and C. L. Johnson (2007), Planetary seismology, *Treatise on Geophysics*, **10**, 69–122.
- Lognonné, P., M. Le Feuvre, C. L. Johnson, and R. C. Weber (2009). Moon meteoritic seismic hum: Steady state prediction, *J. Geophys. Res.*, **114**, E12003, doi:10.1029/2008JE003294.
- Mann, G., F. Jansen, R. J. MacDowall, M. L. Kaiser, and R. G. Stone (1999), A heliospheric density model and type III radio bursts, *Astron. Astrophys.*, **348**, 614-620.
- Meslin P.-Y., W. V. Boynton, J.-C. Sabroux, F. Forget, E. Chassefière, O. Gasnault, J.-F. Pineau, A.E. Metzger, B. Janes and the GRS team (2008). New evidence of the presence of radon in the Martian atmosphere and

- perspective of use as a geophysical tracer. Third International Workshop on the Mars Atmosphere: Modeling and Observations, held November 10-13, 2008 in Williamsburg, Virginia.
- Mimoun, D., M. A. Wieczorek, L. Alkalai, W. B. Banerdt, D. Baratoux, J.-L. Bougeret, S. Bouley, B. Ceconi, H. Falcke, J. Flohrer, R. F. Garcia, R. Grimm, M. Grott, L. Gurvits, R. Jaumann, C.L. Johnson, M. Knapmeyer, N. Kobayashi, A. Konovalenko, D. Lawrence, M. Le Feuvre, P. Lognonné, C. Neal, J. Oberst, N. Olsen, H. Röttgering, T. Spohn, S. Vennerstrom, G. Woan, and P. Zarka (2012). Farside Explorer: Unique science from a mission to the farside of the Moon, *Exp. Astron.*, **33**, 529-585.
- Morgan, T. and the International lunar network working group 1 (2009). International Lunar Network core instruments working group. <http://iln.arc.nasa.gov/>.
- Morosan, D. E., et al. (2014). LOFAR Tied-array Imaging of Type III Solar Radio Bursts, *Astron. Astrophys.*, **568**, A67.
- Nazaroff, W. W. (1992). Radon transport from soil to air, *Rev. Geophysics*, **30**, 137-160.
- Neal, C. (2012). The Moon 35 years after Apollo: What's left to learn? *Chemie der Erde, Geochem.*, **69**, 3-43.
- Nielsen, O.V., J. R. Petersen, F. Primdahl, P. Brauer, B. Hernando, A. Fernandez, J. M. G. Merayo, P. Ripka (1995). Development, construction and analysis of the "Oersted" fluxgate magnetometer, *Meas. Sci. Technol.*
- Oberst, J., Flohrer, J., Elgner, S., Maue, T., Margonis, A., Schroedter, R., Tost, W., Buhl, M., Ehrich, J., Christou, K., Koschny, D. (2011). The Smart Panoramic Optical Sensor Head (SPOSH)—a camera for observations of transient luminous events on planetary night sides, *Planet. Space Sci.*, **59**, 1-9.
- Ortiz J. L., F. J. Aceituno, J. A. Quesada, J. Aceituno, M. Fernandez, P. Santos-Sanz, J. M. Trigo-Rodriguez, J. Llorca, F. J. Martin-Torres, P. Montanes-Rodriguez, and E. Palle (2006). Detection of sporadic impact flashes on the Moon: Implications for the luminous efficiency of hypervelocity impacts and derived terrestrial impact rates, *Icarus*, **184**, 319-326.
- Papastefanou, C. (2006). Residence time of tropospheric aerosols in association with radioactive nuclides, *Applied Radiation and Isotopes*, **64**, 93-100.
- Peplowski, P. N. and D. J. Lawrence (2013). New insights into the global composition of the lunar surface from high-energy gamma rays measured by Lunar Prospector, *J. Geophys. Res.*, **118**, doi:10.1002/jgre.20063.
- Peplowski, P. N., D. Bazell, J. O. Goldsten, and D. J. Lawrence (2015). Hydrogen and major-element concentrations on 433 Eros: Evidence for an L- or LL-chondrite-like surface composition, *Meteorit. Planet. Sci.*, in press.
- Petrucha, V., P. Ripka, P. Kašpar, P. Merayo (2009). Automated system for the calibration of magnetometers, *J. App. Phys.*, **105**, 7.
- Prettyman, T. H., J. J. Hagerty, R. C. Elphic, W. C. Feldman, D. J. Lawrence, G. W. McKinney, D. T. Vaniman (2006). Elemental Composition of the Lunar Surface: Analysis of Gamma Ray Spectroscopy Data from Lunar Prospector, *J. Geophys. Res.*, **111**, E12007, doi:10.1029/2005JE002656.
- Pritchard, J. R., and A. Loeb (2012). 21 cm cosmology in the 21st century, *Rep. Prog. Phys.*, **75**, 086901.
- Popov, M. V., A. Kuz'min, O. Ul'yanov, A. Deshpande, A. Ershov, V. Zakharenko, V. I. Kondrat'ev, S. V. Kostyuk, B. Losovskii, and V. Soglasnov (2006). Instant radio spectra of giant pulses from the Crab pulsar from decimeter to decameter wavelengths, *Astron. Reports*, **50**, 562-568.
- Popova, O. P. and 58 collaborators (2013). Chelyabinsk Airburst, Damage Assessment, Meteorite Recovery, and Characterization. *Science*, **342**, 1069-1073.
- Pritchard, J. R., and A. Loeb (2010). Constraining the unexplored period between the dark ages and reionization with observations of the global 21 cm signal, *Phys. Rev. D*, **82**, 023006.
- Simpson, F., Bahr, K. (2005). Practical Magnetotellurics. Cambridge Univ. Press, 270 pp.
- Smith, D. E., M. T. Zuber, G. A. Neumann, F. G. Lemoine, E. Mazarico, M. H. Torrence, J. F. McGarry, D. D. Rowlands, J. W. Head III, T. H. Duxbury, O. Aharonson, P. G. Lucey, M. S. Robinson, O. S. Barnouin, J. F. Cavanaugh, X. Sun, P. Liiva, D.-d Mao, J. C. Smith, and A. E. Bartels (2010). Initial observations from the Lunar Orbiter Laser Altimeter (LOLA), *Geophys. Res. Lett.*, **37**, L18204, doi:10.1029/2010GL043751.
- Spohn, T.; M. Grott, J. Knollenberg, T. van Zoest, G. Kargl, S.E. Smrekar, W.B. Banerdt, T.L. Hudson and the HP3 Instrument Team (2012). INSIGHT: Measuring the Martian Heat Flow Using the Heat Flow and Physical Properties Package (HP3) (Poster). In: 43rd Lunar and Planetary Science Conference, 19-23 March 2012, The Woodlands, Texas.
- St-Laurent, F., J. S. Derr, F. T. Freund (2006). Earthquake lights and the stress-activation of positive hole charge carriers in rocks, *Phys. Chem. Earth*, **31**, 305-312.
- Suggs, R. M., D. E. Moser, W. J. Cooke, R. J. Suggs (2014). The flux of kilogram meteoroids from lunar impact monitoring, *Icarus*, **238**, 23-36.

- Suggs, R. M., W. J. Cooke, R. J. Suggs, W. R. Swift, and N. Hollon (2008). The NASA lunar impact monitoring program, *Earth Moon Planets*, **102**, 293-298.
- Tanner, A. B. (1980). Radon migration in the ground: A supplementary review. *Natural Radiation Environment III: U.S. Dept. Energy Rept. CONF-780422*, **1**, 5-56.
- Takahashi, Y. D. (2003). New astronomy from the Moon: A lunar based very low frequency array, M.Sc. thesis, University of Glasgow, 90pp.
- Vedantham, H. K., et al. (2015). Lunar occultation of the diffuse radio sky: LOFAR measurements between 35 and 80 MHz, *submitted to MNRAS* (<http://arxiv.org/abs/1407.4244>).
- Voytek, T. C., A. Natarajan, J. M. Jáuregui García, J. B. Peterson, and O. López-Cruz (2014). Probing the Dark Ages at $z \sim 20$: The SCI-HI 21 cm All-sky Spectrum Experiment, *Astrophys. J. Lett.*, **782**, L9.
- Yamada, R., R. F. Garcia, P. Lognonné, M. Le Feuvre, M. Calvet, J. Gagnepain-Beyneix (2011). Optimisation of seismic network design: Application to a geophysical international lunar network, *Planet. Space Sci.*, **59**, 343–354.
- Yamada, R., R. F. Garcia, P. Lognonné, N. Kobayashi, N. Takeuchi, T. Nébut, H. Shiraishi, M. Calvet, J. Ganepain-Beyneix (2013). On the possibility of lunar core phase detection using new seismometers for soft-landers in future lunar missions, *Planet. Space Sci.*, **81**, 18-31.
- Weber, R. C., P.-Y. Lin, E. J. Garnero, Q. Williams, and P. Lognonné (2011). Seismic detection of the lunar core, *Science*, **331**, 309-312.
- Weiss, B. P., and S. M. Tikoo (2014). The lunar dynamo, *Science*, **346**, 6241, doi: 10.1126/science.1246753.
- Werner, S.C., and S. Medvedev (2010). The Lunar rayed-crater population—Characteristics of the spatial distribution and ray retention, *Earth Planet. Sci. Lett.*, **295**, 147–158.
- Wieczorek, M. A., B. L. Jolliff, A. Khan, M. E. Pritchard, B. P. Weiss, J. G. Williams, L. L. Hood, K. Righter, C. R. Neal, C. K. Shearer, I. S. McCallum, S. Tompkins, B. R. Hawke, C. Peterson, J. J. Gillis, and B. Bussey (2006). The constitution and structure of the lunar interior, *Rev. Mineral. Geochem.*, **60**, 221-364.
- Wieczorek, M. A., G. A. Neumann, F. Nimmo, W. S. Kiefer, G. J. Taylor, H. J. Melosh, R. J. Phillips, S. C. Solomon, J. C. Andrews-Hanna, S. W. Asmar, A. S. Konopliv, F. G. Lemoine, D. E. Smith, M. M. Watkins, J. G. Williams, and M. T. Zuber (2013). The crust of the Moon as seen by GRAIL, *Science*, **6120**, 671-675.
- Woan, G. (2011). Radio astronomy from space, in “Radioastronomie Basses Fréquences”, Ecole thématique du CNRS, Goutelas (Loire), 4-8/6/2007, Edited by P. Zarka, M. Tagger, and B. Cecconi. Paris: Observatoire de Paris & SF2A, pp. 325-337, <http://www.lesia.obspm.fr/plasma/Goutelas2007/>.
- Zarka, P., J.-L. Bougeret, C. Briand, B. Cecconi, H. Falcke, J. Girard, J.-M. Griessmeier, S. Hess, M. Klein-Wolt, A. Konovalenko, L. Lamy, D. Mimoun, and A. Aminaei (2012). Planetary and exoplanetary low frequency radio observations from the Moon, *Planet. Space Sci.*, **74**, 156-166.
- Zarka, P., T. J. W. Lazio, G. Hallinan and the SKA “Cradle of Life” Working Group (2014). Magnetospheric Radio Emissions from Exoplanets with the SKA, PoS (SKA Science Book), in press.
- Zito, R. (1989). A new mechanism for transient lunar phenomena, *Icarus*, **82**, 419-422.

B. SCIENCE MEMBERS BY COUNTRY

Australia

Phil Bland *Curtin University, Perth, Australia*
Katarina Milkovic *Curtin University, Perth, Australia*

Belgium

Mikael Beuthe *Royal Observatory of Belgium, Belgium*
Véronique Dehant *Royal Observatory of Belgium, Belgium*
Ozgur Karatekin *Royal Observatory of Belgium, Belgium*
Tim Van Hoolst *Royal Observatory of Belgium, Belgium*

Canada

Catherine Johnson *University of British Columbia, Vancouver, British Columbia, Canada*
Gordon Osinski *University of Western Ontario, London, Ontario, Canada*

Czech Republic

Mattia Butta *Czech Technical University in Prague, Czech Republic*
Michal Janošek *Czech Technical University in Prague, Czech Republic*
Petr Kašpar *Czech Technical University in Prague, Czech Republic*
Gunther Kletetschka *Charles University, Prague, Czech Republic*
Jaroslav Laifr *Czech Technical University in Prague, Czech Republic*
Pavel Mlejnek *Czech Technical University in Prague, Czech Republic*
Vojtěch Petrucha *Czech Technical University in Prague, Czech Republic*
Antonin Platil *Czech Technical University in Prague, Czech Republic*
Michal Přibil *Czech Technical University in Prague, Czech Republic*
Pavel Ripka *Czech Technical University in Prague, Czech Republic*
Jan Vyhnanek *Czech Technical University in Prague, Czech Republic*
Ales Zikmund *Czech Technical University in Prague, Czech Republic*

Denmark

Nils Olsen *Technical University of Denmark, National Space Institute, Denmark*
Susanne Vennerstrom *Technical University of Denmark, National Space Institute, Denmark*

France

David Baratoux *University of Toulouse, Toulouse, France*
Jean-François Blanchette-Guerin *Institut de Physique du Globe de Paris, France*
Sylvain Bouley *Geosciences Paris Sud, Université Paris Sud, Orsay, France*
Jean-Louis Bougeret *LESIA, Observatoire de Paris-CNRS, Meudon, France*
Carine Briand *LESIA, Observatoire de Paris-CNRS, Meudon, France*
Valérie Ciarletti *LATMOS, Laboratoire Atmosphères, Milieux, Observations Spatiales, France*
Baptiste Cecconi *LESIA, Observatoire de Paris-CNRS, Meudon, France*
Sylvain Chaty *Université Paris Diderot, Institut Universitaire de France, Paris, France*
Serge Chevrel *University of Toulouse, Toulouse, France*
Anastasia Fialkov *Ecole Normale Supérieure, Paris, France*
Raphaël Garcia *Institut Supérieur de l'Aéronautique et de l'Espace (ISAE), Toulouse, France*
Olivier Gasnault *Institut de Recherche en Astrophysique et Planétologie, Toulouse, France*
Taichi Kawamura *Institut de Physique du Globe de Paris, France*
Laurent Lamy *LESIA, Observatoire de Paris-CNRS, Meudon, France*
Benoît Langlais *University of Nantes, Nantes, France*
Philippe Lognonné *Institut de Physique du Globe de Paris, Paris, France*
Antoine Mocquet *University of Nantes, Nantes, France*

Pierre-Yves Meslin	<i>Institut de Recherche en Astrophysique et Planétologie, Toulouse, France</i>
Chloé Michaut	<i>Institut de Physique du Globe de Paris, Paris, France</i>
David Mimoun	<i>Institut Supérieur de l'Aéronautique et de l'Espace (ISAE), Toulouse, France</i>
Patrick Pinet	<i>University of Toulouse, Toulouse, France</i>
François Poulet	<i>Institut d'Astrophysique Spatiale, Université Paris-Sud, Orsay, France</i>
Sébastien de Raucourt	<i>Institut de Physique du Globe de Paris, Paris, France</i>
Michel Tagger	<i>LPC2E, CNRS-Université d'Orléans, Orléans, France</i>
Mark Wieczorek	<i>Institut de Physique du Globe de Paris, France</i>
Philippe Zarka	<i>LESIA, Observatoire de Paris-CNRS, Meudon, France</i>

Germany

Vera Assis Fernandes	<i>Museum für Naturkunde, Berlin, Germany</i>
Jörg Fritz	<i>Museum für Naturkunde, Berlin, Germany</i>
Matthias Grott	<i>German Aerospace Center, Institute of Planetary Research, Berlin, Germany</i>
Harald Hiesinger	<i>Institut für Planetologie, Westfälische Wilhelms-Universität, Germany</i>
Ralf Jaumann	<i>German Aerospace Center, Institute of Planetary Research, Berlin, Germany</i>
Martin Knapmeyer	<i>German Aerospace Center, Institute of Planetary Research, Berlin, Germany</i>
Brigitte Knapmeyer-Endrun	<i>Max Planck Institute for Solar System Research, Göttingen, Germany</i>
Anastasios Margonis	<i>Technische Universität Berlin, Germany</i>
Jürgen Oberst	<i>German Aerospace Center, Institute of Planetary Research, Berlin, Germany</i>
Nicole Schmitz	<i>German Aerospace Center, Institute of Planetary Research, Berlin, Germany</i>
Tilman Spohn	<i>German Aerospace Center, Institute of Planetary Research, Berlin, Germany</i>
Kai Wünnemann	<i>Museum für Naturkunde Berlin, Germany</i>

Japan

Junichi Haruyama	<i>ISAS/JAXA, Sagamihara, Kanagawa, Japan</i>
Kazumasa Imai	<i>Kochi National College of Technology, Kochi, Japan</i>
Takahiro Iwata	<i>ISAS/JAXA, Sagamihara, Kanagawa, Japan</i>
Naoki Kobayashi	<i>ISAS/JAXA, Sagamihara, Kanagawa, Japan</i>
Koji Matsumoto	<i>National Astronomical Observatory of Japan, Japan</i>
Satoshi Tanaka	<i>ISAS/JAXA, Sagamihara, Kanagawa, Japan</i>

The Netherlands

Albert-Jan Boonstra	<i>ASTRON, Dwingeloo, The Netherlands</i>
James Carpenter	<i>ESA-ESTEC, The Netherlands</i>
Heino Falcke	<i>Radboud Universiteit Nijmegen, Nijmegen, The Netherlands</i>
Leonid Gurvits	<i>Joint Inst. for VLBI in Europe, Delft University of Technology, The Netherlands</i>
Marc Klein Wolt	<i>Radboud University Nijmegen, The Netherlands</i>
Leon Koopmans	<i>Kapteyn Astronomical Institute, University of Groningen, The Netherlands</i>
Huub Röttgering	<i>University of Leiden, Leiden, The Netherlands</i>
Wim van Westrenen	<i>VU University Amsterdam, Amsterdam, The Netherlands</i>

Norway

Svein-Erik Hamran	<i>University of Oslo, Oslo, Norway</i>
David Mota	<i>Institute of Theoretical Astrophysics, University of Oslo, Oslo, Norway</i>
Stephanie Werner	<i>SCW, Centre of Earth Evolution and Dynamics, University of Oslo, Norway</i>

Poland

Marek Banaszkiewicz	<i>Space Research Center, Polish Academy of Sciences, Poland</i>
Jerzy Grygorczuk	<i>Space Research Center, Polish Academy of Sciences, Poland</i>
Daniel Mège	<i>Polish Academy of Sciences, Institute of Geological Sciences, Poland</i>
Hanna Rothkaehl	<i>Space Research Center, Polish Academy of Sciences, Poland</i>

Russia

Tamara Gudkova
Boris Ivanov

*Schmidt Institute of Physics of the Earth, Moscow, Russia
Russian Academy of Sciences, Moscow, Russia*

Sweden

Jan Bergman

Swedish Institute of Space Physics, Uppsala, Sweden

Switzerland

James Connolly
Domenico Giardini
Beda Hofmann
Jean-Luc Josset
Marie Josset
Amir Khan
Johann Robertsson
Max Schmidt
Audrey Souchon
Paul Tackley

*ETH Zürich, Switzerland
ETH Zürich, Switzerland
Naturhistorisches Museum Bern, Switzerland
Space Exploration Institute, Neuchâtel, Switzerland
Space Exploration Institute, Neuchâtel, Switzerland
ETH Zürich, Switzerland
ETH Zürich, Switzerland
ETH Zürich, Switzerland
Space Exploration Institute, Neuchâtel, Switzerland
ETH Zürich, Switzerland*

United Kingdom

Richard Ambrosi
Mahesh Anand
Neil Bowles
Gareth Collins
Anthony Cook
Ian Crawford
Kerri Donaldson Hanna
Graeme Hansford
Katherine Joy
Thomas Pike
Sara Russel
Mark Sims
Alan Smith
Graham Woan

*University of Leicester, United Kingdom
Open University, United Kingdom
Oxford University, United Kingdom
Imperial College London, London, United Kingdom
Aberystwyth University, Aberystwyth, United Kingdom
Birkbeck College London, London, United Kingdom
Oxford University, United Kingdom
University of Leicester, United Kingdom
University of Manchester, Manchester, United Kingdom
Imperial College London, London, United Kingdom
National History Museum, United Kingdom
University of Leicester, United Kingdom
Mullard Space Science Laboratory, United Kingdom
Glasgow University, Glasgow, United Kingdom*

United States

Bruce Banerdt
Greg Delory
Robert Grimm
David Lawrence
Clive Neal
Renee Weber

*Jet Propulsion Laboratory, Pasadena, California, USA
University of California, Berkeley, USA
Southwest Research Institute, Boulder, Colorado, USA
Johns Hopkins University, Applied Physics Laboratory, Maryland, USA
University of Notre Dame, Indiana, USA
Marshall Space Flight Center, NASA, Huntsville, USA*

Ukraine

Alexander Konovalenko

Institute of Radio Astronomy, Kharkov, Ukraine

C. LETTERS OF COMMITMENT

Instrument	PI	Country	Organization
Radio astronomy receiver	Philippe Zarka	France	CNES
Radio astronomy antennas ¹	Hanna Rothkaehl	Poland	Polish Ministry
Seismometer (SEIS)	Philippe Lognonné	France	CNES
Radon and polonium detector (DORN)	Pierre-Yves Meslin	France	CNES
Heat flow and physical properties package (HP ³)	Matthias Grott	Germany	DLR
Heat flow and physical properties package (HP ³) ¹	Jerzy Grygorczuk	Poland	Polish Ministry
Impact flash camera (SPOSH)	Jürgen Oberst	Germany	DLR
Acquisition and central electronics (FACE)	Domenico Giardini	Switzerland	Swiss Delegation
Context cameras (CoCam)	Jean-Luc Josset	Switzerland	Swiss Delegation
Magnetometer (MAG)	Pavel Ripka	Czech Republic	Czech Technical Univ. in Prague
Gamma-ray spectrometer (GRS)	David Lawrence	USA	NASA
Electromagnetic sounder (EMS)	Robert Grimm	USA	NASA

¹Sent by email only.

Direction de la Prospective, de la Stratégie, des Programmes
de la Valorisation et des Relations Internationales
Programme Sciences de l'Univers, Microgravité et Exploration
Sent by Email: M4support@cosmos.esa.int

Prof. Alvaro Giménez Cañete

Director of the ESA Science and Robotic Exploration
Program
8-10 Rue Mario Nikis, 75338 Paris Cedex 15

Paris, January 10th, 2015
Réf : DSP/SME – 2015.0000220

Subject: Endorsement of a French contribution to the FAR SIDE proposal in response to the M4 call

Dear Prof Gimenez,

The Centre National d'Etudes Spatiales (CNES) is aware of the contribution of the French scientists in the **FAR SIDE** proposal submitted in response to the call for the fourth medium size mission of Cosmic Vision.

The French component that the consortium intends to provide, beyond the science contribution, is:

- A radio receiver for low frequency astronomy studies under the responsibility of LESIA
- A 3 axis VBB (very broad band) seismometer under the responsibility of IPGP (the electronic being provided by ETHZ (Switzerland);
- Instruments for the detection of Radon and the studies of the lunar exosphere and outgassing under the responsibility of IRAP.

Should this proposal be selected by ESA and the French involvement corresponding to the final proposal successfully checked by CNES (before mid-February), CNES intends to support the activities of the French members of the consortium throughout the study phase.

Should this mission be selected as the 4th medium size mission of Cosmic Vision, CNES will do its best efforts to secure the funding for the development and implementation of the proposed nationally provided elements. The level of support is being subject to the availability of funds within the CNES budget for Science.

Sincerely,



Christian Sirmain
Acting Head of Space Science,
Microgravity and Exploration Office

DLR e. V. Space Administration
Postfach 30 03 64, 53183 Bonn, Germany

Your reference

Your letter

Our reference

Prof. Alvaro Giménez Cañete
European Space Agency

Your correspondent

Dr. Frings

Headquarters
8-10 rue Mario Nikis
75738 Paris Cedex 15, France

Telephone +49 228 447-

Telefax +49 228 447-

E-mail

wolfgang.frings@dlr.de

12 January 2015

ESA call for a medium-size mission opportunity (M4)

Participation of Prof. Oberst and Dr. Grott in the mission proposal FAR SIDE

Dear Prof. Giménez,

Prof. J. Oberst, *Technische Universität, Berlin*, and Dr. M. Grott, *DLR-Institut für Planetenforschung, Berlin*, intend to participate in the FAR SIDE mission proposal to be submitted by Prof. Mark Wieczorek (*Institut de Physique du Globe de Paris*).

Prof. Oberst intends to provide a camera for the research of meteoritic impacts on the Moon.
Dr. Grott intends to provide the Heat Flow Probe (Heat Flow and Physical Properties Package, HP³).

We take note of their proposals and will consider the support of their work in the study phase in case FAR SIDE will be selected.

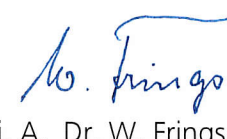
It is understood that the support during the study phase is subject to the relevant DLR funding procedures.

Therefore, at present time this letter does not constitute any obligation to provide financial support.

Sincerely



i. V. Dr. Th. Galinski



i. A. Dr. W. Frings

cc: Prof. Wieczorek, Prof. Oberst, Dr. M. Grott



Schweizerische Eidgenossenschaft
Confédération suisse
Confederazione Svizzera
Confederaziun svizra

Swiss Confederation

Federal Departement of Economic Affairs,
Education and Research EAER

State Secretariat for Education,
Research and Innovation SERI
Swiss Space Office

CH-3003 Bern, SERI

European Space Agency,
Director of Science And Robotic Exploration,
by email to "M4support@cosmos.esa.int"

Ihr Zeichen: D/SRE/29102
Referenz/Aktenzeichen: D632.13
Unser Zeichen:
Sachbearbeiter/in: Andreas Werthmueller
Bern, 12.01.2015

Letter of Endorsement

**Potential Swiss science experiment and hardware contribution to FARSIDE in the context of
ESA's M4 selection procedure**

Dear Prof. A. Giménez Cañete

On behalf of the Swiss Delegation to ESA and related to the "Call for a Medium-size mission opportunity in ESA's Science Programme for a launch in 2025 (M4)" published on 19 August 2014 I wish to inform you that Prof. Dr. Domenico Giardini at Eidgenössische Technische Hochschule Zürich participates in the preparation of the FARSIDE mission.

The Swiss Space Office expresses herewith its readiness to fund the Swiss member of the FARSIDE Consortia throughout the study phase, and to undertake the necessary action to secure funding for the development and implementation of the nationally provided mission elements falling under its responsibility, contingent on the successful achievement of all the goals of the selection reviews, and to the consolidation of the cost figures for all nationally funded mission elements subject to corresponding budget allocations on the Federal level as well as the positive outcomes of national reviews on scientific, technical and cost aspects.

I remain at your disposal should you have questions or wish to receive additional information.

Yours sincerely

Swiss Space Office

Dr. Andreas Werthmueller
Space Sciences and Instruments

Copy to: Prof. Dr. Domenico Giardini, Eidgenössische Technische Hochschule Zürich

State Secretariat for Education
Research and Innovation SERI
Andreas Werthmueller
Einsteinstrasse 2, 3005 Berne
Phone +41 58 463 35 95, Fax +41 58 464 96 14
andreas.werthmueller@sbfi.admin.ch
www.sbfi.admin.ch



Schweizerische Eidgenossenschaft
Confédération suisse
Confederazione Svizzera
Confederaziun svizra

Swiss Confederation

Federal Departement of Economic Affairs,
Education and Research EAER

State Secretariat for Education,
Research and Innovation SERI
Swiss Space Office

CH-3003 Bern, SERI

European Space Agency,
Director of Science And Robotic Exploration,
by email to "M4support@cosmos.esa.int"

Ihr Zeichen: D/SRE/29102
Referenz/Aktenzeichen: D632.13
Unser Zeichen:
Sachbearbeiter/in: Andreas Werthmueller
Bern, 07.01.2015

Letter of Endorsement

**Potential Swiss science experiment and hardware contribution to FAR SIDE in the context of
ESA's M4 selection procedure**

Dear Prof. A. Giménez Cañete

On behalf of the Swiss Delegation to ESA and related to the "Call for a Medium-size mission opportunity in ESA's Science Programme for a launch in 2025 (M4)" published on 19 August 2014 I wish to inform you that Prof. Dr Jean-Luc Josset at Space Exploration Institute participates in the preparation of the FAR SIDE mission.

The Swiss Space Office expresses herewith its readiness to fund the Swiss member of the FAR SIDE Consortia throughout the study phase, and to undertake the necessary action to secure funding for the development and implementation of the nationally provided mission elements falling under its responsibility, contingent on the successful achievement of all the goals of the selection reviews, and to the consolidation of the cost figures for all nationally funded mission elements subject to corresponding budget allocations on the Federal level as well as the positive outcomes of national reviews on scientific, technical and cost aspects.

I remain at your disposal should you have questions or wish to receive additional information.

Yours sincerely

Swiss Space Office

Dr. Andreas Werthmueller
Space Sciences and Instruments

Copy to: Prof. Dr Jean-Luc Josset, Space Exploration Institute

State Secretariat for Education
Research and Innovation SERI
Andreas Werthmueller
Einsteinstrasse 2, 3005 Berne
Phone +41 58 463 35 95, Fax +41 58 464 96 14
andreas.werthmueller@sbfi.admin.ch
www.sbfi.admin.ch



CZECH TECHNICAL UNIVERSITY IN PRAGUE
prof. Ing. Petr Konvalinka, CSc.
rector

Prague, January 14, 2015
Ref. No.15/13911/15-FEL/ORO-V

Subject: Letter of Endorsement for the M4 mission candidate FARSIDE

Dear Dr. Gimenez,

Scientists from the Czech Technical University in Prague (CTU) have participated in the preparation of the proposal for the FARSIDE mission led by Dr. Mark Wieczorek, Directeur de Recherche, CNRS, in response to the announcement of opportunity for a medium-size mission in ESA's Science Programme, M4.

The Czech Technical University in Prague strongly supports the Czech participation in FARSIDE, as described in the proposal.

Teams from Czech Technical University in Prague are willing to join the project as contributors to its scientific content as well as to the development of hardware and software systems and components necessary for the mission, with focus on contribution to the 3-axis fluxgate magnetometer for the lander that will be located on the farside of the Moon, as well as to two 3-axis fluxgate magnetometers for the relay satellite that will be located at the Earth-Moon L2 Lagrange point.

The Czech Technical University in Prague will support activity of research and development teams involved in the project.

Best regards,

Dr Alvaro Gimenez
Director of Science and Robotic Exploration
European Space Agency
8-10 rue Mario Nikis
F-75738 Paris Cedex 15 - France
e-mail: M4support@cosmos.esa.int

National Aeronautics and Space Administration

Headquarters

Washington, DC 20546-0001



Reply to Attn of:

SMD/Planetary Science Division

January 9, 2015

NASA has received a description of the following mission, which has been identified as a mission that will be proposed to the European Space Agency (ESA) for consideration as a Cosmic Vision M4 mission, as well as a description of the mission's science objectives.

Mission: FARSIDE

Letter requested by: Dr. David J. Lawrence, Johns Hopkins University Applied Physics Laboratory

NASA is aware of this proposal and acknowledges that its planetary science objectives are aligned with the 2014 *Science Plan* for NASA's Science Mission Directorate (available at <http://science.nasa.gov/about-us/science-strategy/>) and the Planetary Science Decadal Survey, *Vision and Voyages*.

This letter may be included in the proposal that is submitted to ESA. NASA has not provided ESA with a copy of this letter. NASA will enter into discussions with ESA about support of selected proposals at an appropriate time.

Sincerely,

A handwritten signature in black ink. The signature appears to read "James L. Green".

James L. Green
Director, Planetary Science Division
Science Mission Directorate